SLAC-PUB-1314
(T/E)
October 1973

DIFFRACTIVE PROCESSES*

K. C. Moffeit

Stanford Linear Accelerator Center
Stanford University, Stanford, California 94305

Rapporteur talk presented at the International Symposium on
Electron and Photon Interactions at High Energies

Bonn

August 27-31, 1973

*Work supported by the U.S. Atomic Energy Commission.

I. Introduction

In this talk I will try to summarize our present knowledge of the diffractive process. Before showing any data, I would first like to review the properties and characteristics of diffractive scattering. The classical picture shows a wave scattering from a black or grey disk giving rise to a sharp peak in the angular distribution. The amount of scattering is independent of energy. In the Regge picture we think of scattering in terms of t-channel exchanges and diffraction corresponds to a separate Pomeron trajectory. Whatever the picture, three basic properties have been used to signify diffractive scattering: i) a cross section which is independent of energy or at most has a ln s dependence; ii) peaked angular distributions at $\theta = 0^\circ$ and iii) mainly imaginary amplitudes. In terms of $d\sigma/dt$ we expect to find exponential t-distributions whose slope is related to the transverse size of the target and beam particle. Over the years additional properties have been suggested:

i) the angular distribution becomes more peaked with increasing energy (shrinkage). In the Regge picture shrinkage results from a Pomeron exchange with trajectory $\alpha = \alpha_o + \alpha' t$ with $\alpha' > 0$.

ii) the scattering process is s-channel helicity conserving (SCHC).

iii) in the t-channel the quantum numbers of the vacuum ($I = 0$ and $C = 1$) are exchanged.

iv) the change in parity of the beam or target particle in the scattering process follows the natural spin-parity series $(-1)^J$ or $p_f = p_i(-1)^{\Delta J}$ where ΔJ = spin change and p_f and p_i are the intrinsic parities of the outgoing and incoming particles (the Morrison-Gribov rule).

These and other properties such as equivalence of particle and anti-particle cross section and factorization of the upper and lower vertices of the Pomeron coupling have been discussed in recent reviews by David Leith[1].

Today I shall concentrate primarily on data of photoproduction and electroproduction of vector mesons. Photoproduction and more recently electroproduction has been an extremely useful tool in the study of diffractive production. The advantages are due to the strong coupling of the vector mesons to the $J^P = 1^-$ photon whose initial spin characteristics can be controlled experimentally. This allows us to study the production characteristics using the decay angular distributions of the vector meson decay as an analyzer. The following topics will be covered:

i) higher mass vector mesons

ii) $\pi^+\pi^-$ line shape in dipion photoproduction on complex nuclei

iii) energy dependence of the t-distribution for the diffractive photoproduction of vector mesons

iv) diffractive vector meson electroproduction.

II. Higher Mass Vector Mesons

Many theories and phenomenological analyses have suggested the existence of additional vector-meson states[(2)] apart from the well-known ρ^o, ω^o, and φ mesons. For example, the failure of the simple vector dominance model to explain photoproduction by coupling only to ρ^o, ω, and φ could be remedied by adding higher mass vector mesons.

In analogy to ρ^o, ω and φ production it is natural to look for higher mass vector mesons in diffractive photoproduction as well as the direct production of the $J^{PC} = 1^{--}$ system in e^+e^- annihilation through one-photon exchange. The production of an $I^{CG} = 1^{-+}$ vector meson state, the ρ' (1600), has been reported by several groups by the time of the 1972 XVI International Conference on High Energy Physics at Chicago. Its resonance interpretation has been confirmed since. In the following I give a summary of the ρ' (1600) situation. In addition, diffractive photoproduction of an $I^{CG} = 1^{-+}$ $\omega\pi^0$ state at a mass of ~ 1250 MeV has been reported to this conference.

A. Evidence for ρ' (1600) production.

The $\pi^+\pi^-$ mass distribution of the reaction

$$\gamma N \rightarrow \pi^+\pi^- N \tag{1}$$

has been examined for the production of higher mass vector mesons in bubble chamber and electronic experiments [3-10]. No distinct higher mass vector mesons were found. However, a broad structure as seen in Fig. 1 was observed in the experiments on complex nuclei [9-10]. These experiments were hard to analyze since the ρ^0 tail is not well understood and coherent nuclear production is suppressed at high mass.

The SLAC streamer chamber group [11] has reported a wide enhancement in the 4π invariant mass near 1.6 GeV in the reaction

$$\gamma p \rightarrow \pi^+\pi^-\pi^+\pi^- p \tag{2}$$

Their complete data are given in Fig. 2 for photon energies 6-18 GeV and show a clear enhancement which is emphasized when the Δ^{++} signal is excluded and a ρ^0 is required to be in the 4π combination (Fig. 2c).

The cross section for the e^+e^- annihilation [13,14,15] into $4\pi^{\pm}$ also shows a broad peak centered at 1.6 GeV (see Fig. 3), looking quite similar to the photoproduction enhancement. The Ceradini et al. [15] results consist of 23 events in the energy range 1.5-1.7 GeV. Note, that the peak ρ' cross section is now about 10 nb lower than the earlier published results of the $\mu\pi$ group[14].

In order to connect the $4\pi^{\pm}$ enhancements (hereafter referred to as the ρ') found in photoproduction and e^+e^- annihilation, the photoproduced ρ' should have the quantum numbers $J^{PC} = 1^{--}$. The $4\pi^{\pm}$ mass enhancement in reaction (2) has the following production properties:

i) peripheral production $\frac{d\sigma}{dt} \propto e^{\sim 6t}$ as seen in Fig. 4.

ii) approximately energy independent cross section of 1 to 1.6 μb

iii) dominance of the $\rho^o \pi^+\pi^-$ final state.

These characteristics are consistent with diffractive production of the ρ' and suggest the above quantum number assignment. The SLAC-Berkeley (SB) collaboration [16] presented evidence that the ρ' indeed had quantum numbers $J^P = 1^-$ and $I^G = 1^+$ ($C = -1$ from $G = C(-1)^I$) using the decay angular distribution of the ρ' and the branching ratio into $\pi^+\pi^-\pi^o\pi^o$. I shall briefly present some of the arguments and data supporting these conclusions. For further details the reviews by M. Davier[17] and G. Wolf[18] and the original papers[11,12,16] are suggested.

i) As seen in Fig. 2 a ρ^o is usually found in the $4\pi^{\pm}$ system. However, the other $\pi^+\pi^-$ pair could have isospin 0, 1, and 2. Isospin 1 is ruled out by the lack of the $\rho^o\rho^o$ decay and the experimental ratio of $(\rho' \to \rho^o\pi^o\pi^o)$ to $(\rho' \to \rho^o\pi^+\pi^-) \approx 0.5$ supports $I = 0$ instead of $I = 2$.

ii) For an isovector-vector ρ' decaying to $\rho^o\pi^+\pi^-$ we would expect a decay matrix element using Bose symmetry together with the assumptions of lowest angular momentum and the absence of final state interactions

$$M = \vec{\epsilon} \cdot \vec{Q}$$

where $\vec{\epsilon}$ is the ρ' polarization and $\vec{Q}$ is the decay analyzer. The problem is to find a vector which can be used as an anlyzer for the decay. It can be shown[16] that for not too large 4π masses the vector

$$\vec{Q} = \vec{P}_{\pi_1^+} + \vec{P}_{\pi_2^+}$$

is reasonably efficient, where $\vec{P}_{\pi^+_{1,2}}$ are momentum vectors of the 2 π^+ in the 4π center of mass.

Figure 5 (top) gives the distributions of the angles θ, ψ of the vector $\vec{Q}$ in the helicity system which show an approximate $\sin^2\theta$ and $\cos^2\psi$ behavior for the ρ' mass region similar to that found for elastic ρ^0 decay[4]. The amount of $\sin^2\theta \cos^2\psi$ component in the 4π angular distribution, and consequently the number of s-channel helicity-conserving $J^P = 1^-$ 4π events can be determined from

$$\Pi = \frac{1}{P_\gamma}\sqrt{\frac{40\pi}{3}} \sum_{i=1}^{N} \mathrm{Re}\, Y_2^2\, (\theta_i\ ,\ \psi_i) \tag{3}$$

and is shown in Fig. 5(bottom). The quantity Π peaks near 1.5 GeV and has a FWHM of ~ 500 MeV(Note that Π has not been corrected for the efficiency of the analyzer which decreases with increasing mass). This means that the decay angular distribution for the ρ' (1600) is consistent with $J^P = 1^-$ and rules out the $J^P = 0^\pm$ states.

iii) The spin-parity analysis was made assuming the ρ' (1600) is produced via s-channel helicity conservation, natural parity exchange in the t-channel and decays predominantly into ρ^0 ϵ (ϵ is an s-wave iso-scaler $\pi\pi$ state). The e^+e^- annihilation data of Ceradini <u>et al</u>. also give evidence for a $\rho^o\epsilon$ decay[15]. The SB authors[16] calculate the decay angular distributions of the analyzer Q for the J^P states $1^\pm$, $2^\pm$ and 3^- assuming lowest allowed angular momentum between the ρ^o and ϵ. Only the $J^P = 1^-$ state is found to agree with the decay angular distribution of Fig. 5. Hence the quantum number assignment found in photoproduction

$$J^{PC} = 1^{--}$$

is identical with that of e^+e^- annihilation into ρ' through one photon exchange. Therefore, it is natural to treat the ρ' found in photoproduction and e^+e^- annihilation as being the same state. This conclusion is further reinforced when one calculates the expected $e^+e^- \to \rho'$ $\hookrightarrow 4\pi^\pm$ cross section. To accomplish this we use the relationship between the $\gamma\to\rho'$ coupling constant $\frac{\gamma_{\rho'}^2}{4\pi}$ and the $\gamma\to\rho^o$ coupling $\frac{\gamma_\rho^2}{4\pi}$,

$$\frac{\sigma(\gamma p \to \rho p)}{\sigma(\gamma p \to \rho' p)_{\hookrightarrow 4\pi^\pm}} = \left(\frac{\gamma_{\rho'}}{\gamma_\rho}\right)^2 \frac{\Gamma_{\rho'}}{\Gamma\,(\rho' \to 4\pi^\pm)} \tag{4}$$

assuming the amplitude for ρ' production via an intermediate ρ^o is small and that the amplitudes for ρp and $\rho' p$ elastic scattering are comparable. Analogously, the peak cross sections for $e^+e^- \to \rho^o$ and ρ are related by

$$\left[\frac{\sigma(e^+e^- \to \rho)}{\sigma(e^+e^- \to \rho')_{\hookrightarrow 4\pi^\pm}}\right]_{peak} = \left(\frac{\gamma_{\rho'}}{\gamma_\rho}\right)^2 \frac{\Gamma_{\rho'}^2}{\Gamma_\rho\,\Gamma(\rho' \to 4\pi^\pm)} \frac{M_{\rho'}}{M_\rho} \tag{5}$$

Using the measured photoproduction cross section $\sigma(\rho) = 14.0 \pm 0.9\mu b$[4]

and $\sigma(\rho' \to 4\pi^{\pm}) = 1.6 \pm 0.4\ \mu b$[16], the ρ' width $300 < \Gamma_{\rho'} < 600$ MeV, $M_{\rho'} = 1.6$ GeV, and $\sigma(e^+e^- \to \rho)_{peak} = 1.00 \pm 0.13\ \mu b$[19] eqs. (4) and (5) would predict:

$$12 < \sigma_{peak}\ (e^+e^- \to \rho' \hookrightarrow 4\pi^{\pm}) < 25 \text{ nb}$$

consistent with the measured value of (16 ± 5) nb[15] .

As discussed above the $\pi^+\pi^-$ decay mode seems to be quite suppressed, although two experiments[9,10] have shown some indication for a structure in $M(\pi^+\pi^-)$ near 1.5 GeV in photoproduction on complex nuclei as shown in Fig. 1. When kinematical effects are taken into account, one obtains[17]:

$$\frac{\rho' \to \pi^+\pi^-}{\rho' \to 4\pi^{\pm}} \lesssim 0.14$$

consistent with the upper limit of 0.20 found in the SLAC-Berkeley-Tufts bubble chamber data[3,4].

B. Non-Resonance Explanation of the ρ'

Two proposals have been put forward to explain the 4π enhancement without identifying the above described state with a resonant ρ' vector meson:

i) An explanation equally applicable to photoproduction and e^+e^- annihilation is the effect of the opening of quasi-two-body decay modes of the ρ^o which produce bumps just after their threshold e.g. $\rho^o \to \rho^o\ \epsilon$.[20,21,22] While this naively explains the decay angular distributions, the normalized mass distributions shown in Fig. 6 (data divided by by 5 body $\rho^o\pi^+\pi^-p$ phase space) do not follow the expected ρ^o Breit-Wigner shape[23]. However, Renard has suggested the ρ propagator has a cusp at the masses of the coupled channels which affect the ρ^o high mass tail.[22] He obtains qualitative agreement with the $\gamma A \to \pi^+\pi^- A$ and $e^+e^- \to 4\pi + X^o$ data. We would expect from this hypothesis similar behavior in hadronic interactions, i.e.

$$\frac{\sigma(\gamma p \to p\, \rho^o \pi^+ \pi^-)}{\sigma(\gamma p \to p\, \rho^o)} = \frac{\sigma(\pi^+ p \to \Delta^{++}\, \rho^o \pi^+ \pi^-)}{\sigma(\pi^+ p \to \Delta^{++}\, \rho^o)}$$

The data of Y. Eisenberg et al.[24] on $\pi^+ p \to \Delta^{++} \rho(\rho')$ sets limits on ρ' production which are in disagreement with the ρ/ρ' ratio of 10:1 found in γp experiments. However, as pointed out by D. H. Miller[25], the problem with the analysis of the $\pi^+ p$ experiment is probably that at such a low momentum and high t one-pion exchange is no longer valid, the minimum t at the ρ' mass is 0.3 GeV^2 at 5 GeV/c for $\pi^+ p \to \Delta^{++} \rho'$.

ii) Ferbel and Slattery have suggested that the ρ' might be just another kinematic enhancement similar to the A_1 and Q found in πp and K p scattering[26]. While their naive reggeized Deck calculation satisfactorily describes the observed mass and momentum transfer dependence (Fig. 7) it also predicts forward-backward peaking of the $\pi^\pm$ not found in the data[23]. In addition, this model fails to explain the ρ' signal seen in e^+e^- annihilation. See also comments by Rapporteur Ph. Salin.

C. Resonance Behavior in $\pi^+\pi^-$ Phase Shift for $M_{\pi\pi} \sim 1600$ MeV

The non-resonance explanations of the ρ' were motivated by the absence of a decay mode into two pseudoscalar mesons. The CERN-MÜNCHEN collaboration[27] has performed an energy dependent and an energy independent analysis of elastic $\pi\pi$ scattering using the data of the reaction $\pi^- p \rightarrow \pi^+\pi^- n$ at 17.2 GeV/c. The $\pi\pi$ energy covers the range from 600 to 1900 MeV. Apart from the well-known resonances ρ, f, and g they find a strong s-wave in the ρ and in the f-meson region. A P-wave resonance occurs in both analyses at ~ 1600 MeV with a total width of 180 MeV and an elasticity of 0.25, which could be identified with the 2π decay of the ρ' meson (see Fig. 8a,b).

Note that the energy independent phase shifts have been parameterized in terms of the K-matrix formalism using Breit-Wigner forms for the resonances plus background. This representation is shown in the Argand diagrams of Fig. 8b. If the ρ' were related to the $\rho^0 \rightarrow \rho^0\, \epsilon$ decay the Argand diagram would not show a loop but rather a departure from the circle (see Fig. 6 of Ref. 22). The effect of the ρ' on the angular distributions is seen in Fig. 9 where the $< Y_\ell^m >$ moments are given for $1.4 < M_{\pi\pi} < 1.8$ GeV. In particular the moments $< Y_0^0 >$ and $< Y_2^0 >$ are not described unless a second resonance is included in the P-wave. The resonance mass of 1590 ± 20 MeV is consistent with that found in photoproduction. However, the γp experiments and e^+e^- annihilation show a much broader ρ' (300 - 600 MeV compared to 180 ± 50 MeV).

The upper limit of $R = \dfrac{\rho' \rightarrow 2\pi^\pm}{\rho' \rightarrow 4\pi^\pm} < 0.14$ in the photoproduction data on complex nuclei and $R < 0.2$ from the SBT bubble chamber data would give an upper limit on the elasticity $\eta < 0.11$ for $\rho' \rightarrow \pi^+\pi^-$ (assuming $(\rho' \rightarrow \rho^0\pi^0\pi^0)/(\rho' \rightarrow \rho^0\pi^+\pi^-) = 0.5$ and no other decay channels) compared with the measured elasticity of 0.25 ± 0.05 by the CERN-MÜNCHEN group. Perhaps, some non-resonant background from processes as discussed above is contributing to the ρ' mass region in photoproduction.

D. γ - ρ' Coupling Constant

Using Eqn. (4) and accounting for $\rho' \to \pi^+\pi^-$ and $\rho' \to \pi^+\pi^-\pi^0\pi^0$ one finds[11,16] that

$$4 \lesssim \left(\frac{\gamma_{\rho'}}{\gamma_\rho}\right)^2 \lesssim 8$$

Thus the ρ' contributes ~ 10% to the Compton sum rule at t=0[18]

$$\sqrt{\frac{d\sigma}{dt}(\gamma p \to \gamma p)} = \sqrt{\frac{\alpha}{4}} \left\{ \sum_{V=\rho,\omega,\varphi,\rho'} \left[\left(\frac{\gamma_V^2}{4\pi}\right)^{-1} \frac{d\sigma}{dt} (\gamma p \to V_T p) \right]^{\frac{1}{2}} \right\} \qquad (6)$$

$$\underset{\gamma p \to \gamma p}{\underline{0.87 \pm 0.2}} = \underset{\substack{\gamma p \to \rho^0 p \\ =0.71\pm 0.05}}{\underline{0.52 \pm 0.04}} + \underset{\substack{\gamma p \to \omega p \\ (\mu b/GeV^2)^{\frac{1}{2}}}}{\underline{0.066 \pm 0.014}} + \underset{\gamma p \to \varphi p}{\underline{0.043 \pm 0.004}} + \underset{\gamma p \to \rho' p}{\underline{0.084 \pm 0.03}}$$

neglecting possible real parts and using the input values listed in Table I. D. R. Yennie has pointed out that one should also include a non-resonant $\pi^+\pi^-$ production in the Compton sum rule which could contribute to Eqn. 6 as much as 10 to 20% of the ρ^0 contribution[31] and would be almost sufficient to saturate the Compton Sum-Rule.

In summary, we have seen ρ' production in three different production processes: e^+e^- annihilation into the ρ' in a $J^{PC} = 1^{--}$ state through one-photon exchange, photoproduction of the ρ' (1600) shown by the SLAC-Berkeley collaboration to have quantum numbers $J^P = 1^-$, $I^G = 1^+$, and evidence for a p-wave (I = 1) resonance in the analysis of elastic $\pi^+\pi^-$ scattering at ~ 1600 MeV with an elasticity of 0.25. A summary of the ρ' properties for these experiments is found in Table II. Criticisms can be made of each technique but as a whole they give good evidence for a resonance behavior.

E. Other Higher Mass Vector Mesons

As discussed above the ρ' is found at 1.6 GeV. However, we were supposed to find the ρ' at 1.2 - 1.4 GeV and a ρ'' at 1.6 - 1.8 GeV[2]. Thus the ρ' (1600) is closest to the ρ'' mass region and no enhancement was observed at $1.2 < M_{4\pi^\pm} < 1.4$ GeV. Perhaps the ρ' (1250) does not couple strongly to $\pi^+\pi^-$ or $4\pi^\pm$.

The SLAC-Berkeley (S-B) collaboration[32] have investigated other channels for higher mass vector mesons. They observe a strong enhancement as seen in Fig. 10 in the channel

$$\gamma \, p \rightarrow p \, \pi^+\pi^- \, MM \tag{7}$$

at $M(\pi^+\pi^- MM)$ near 1.25 GeV at the three energies 2.8, 4.7, and 9.3 GeV. Here MM signifies two or more neutrals. The selection $MM^2 > 0.1$ GeV^2 which is applied to the sample of Fig. 10 eliminates most of the events from the channel $\gamma p \rightarrow p \, \pi^+\pi^-\pi^o$. An enhancement at 1240 MeV in the meson's mass recoiling off the proton in the reaction $\gamma p \rightarrow p$ + anything was first reported by Anderson et al.[33] Since no comparable enhancement has been observed in any other photoproduction final state[32], the enhancement in the S-B data and the SLAC MM experiment are most likely due to the same effect. A similar peak was also observed in the DESY streamer chamber experiment[34].

The S-B collaboration finds that the enhancement is strongly associated with $\pi^+\pi^-$ pairs in the mass region $0.32 < M_{\pi^+\pi^-} < 0.6$ GeV (shaded portion of Fig. 10). From this and from a study of other final states they conclude that $\omega \, \pi^o$ is the dominant decay mode. However, sizeable contributions from a $\rho^+\rho^-$ decay cannot be ruled out.

Note that any $\omega \, \pi^o$ system has the quantum numbers $I^{CG} = 1^{-+}$ and hence can be photoproduced diffractively.

The enhancement is produced peripherally as can be seen from the t distribution in Fig. 11 and from the lack of signal in the bottom part of Fig. 10. The production cross section is shown in Fig. 12 together with a point derived from the data of Anderson et al. The cross section is roughly independent of the photon energy at a level of 1 μb. It should be noted however, that the cross section of Fig. 12 was obtained by fitting a Breit-Wigner distribution of fixed width (150 MeV) and assuming a sizeable $\omega\pi$ background under the peak. If both assumptions are relaxed twice as large a cross section can be obtained.

The above observations suggest that the $\omega\pi$ enhancement is produced diffractively. The unimportance of non-diffractive contributions is supported by the lack of an $\omega\pi^-$ enhancement at 1240 MeV in $\gamma n \rightarrow p\,\omega\,\pi^-$.[36] An analysis of the decay correlations observed in the S-B experiment shows that both a $J^P = 1^-$ and 1^+ assignment are compatible with the data.

The SLAC-Berkeley authors conclude that the enhancement is primarily due to one or a mixture of the following processes[37]:

i) a non-resonant Deck effect $\gamma p \rightarrow p\,\omega\,\pi^0$ according to the diagrams of Fig.13. From rough calculations of non-reggeized and reggeized Deck processes[32] one expects contributions from diagrams of Fig.13 in the order of 2 μb, which peak at masses of 1.2 GeV. The peak is rather broad ($\Gamma \gtrsim 300$ MeV). The uncertainty of its detailed shape makes a further analysis difficult.

ii) Production of the B(1235).

The B meson is the only established particle which has a dominant $\omega\pi$ decay compatible with the data. The B can be photoproduced diffractively via an orbital momentum $\ell = 1$ exchange since the B belongs to the unnatural spin-parity series with $J^P = 1^+$ favored[39]. (This process would violate the Morrison-Gribov rule).

iii) Production of a ρ' (1250)

The enhancement might as well be due to the diffractive production of the long sought ρ' (1250) observed in its dominant $\omega\pi^0$ decay mode.

The SLAC-Berkeley data also show a ρ' (1600) signal in the channel $\gamma p \rightarrow p\,\pi^+\pi^-$ MM at 9.3 GeV which is compatible with a $\rho^0\,\epsilon$ decay of the ρ'[40]. This is seen in Fig. 14 where a ρ^0 selection has been made in the $\pi^+\pi^-$ mass. Data are shown only for low $|t| < 0.5$ GeV^2.

In contrast to the $\rho^0\,\pi^+\pi^-$ channel (see Fig. 2) figure 14 shows a broad maximum between 1.6 and 2 GeV. The maximum peaks at higher masses than expected from the $\rho' \rightarrow \rho^0\pi^+\pi^-$ final state. Hence some presently unidentified background or resonance contributions must be present between masses of 1.8 and 2.1 GeV[40].

III. $\pi^+\pi^-$ Line Shape in Dipion Photoproduction on Complex Nuclei

In photoproduction on hydrogen the skewing of the rho mass shape has been interpreted as an interference of the ρ Breit-Wigner amplitude with a P-wave Drell background commonly referred to as the Söding model. This model describes well[3,4] the P-wave $\pi^+\pi^-$ amplitude of the reaction

$$\gamma p \rightarrow \pi^+\pi^- p\,.$$

Bauer[41] has suggested that when the production takes place on complex nuclei one must consider in addition to the single scattering diagram, the scattering of both pions from the nucleons. The Drell amplitudes are then significantly smaller resulting in a $\pi^+\pi^-$ line shape which is less skewed on heavier nuclei. In the SLAC $\pi^+\pi^-$ spectrometer experiment on complex nuclei, photoproduction of the ρ^0 at 5, 7, 9 GeV was studied on Be, C, Al, Cu and Pb. The results of the study on the γ-ρ coupling constant and the rho-nucleon cross section have been reported.[42] The analysis of the $\pi^+\pi^-$ line shape in terms of the Söding model shows a decreasing contribution of the Drell amplitude relative to the ρ^0 with increasing A consistent with the theoretical predictions of Bauer.[43]

In a contribution to this conference the DESY streamer chamber group study photoproduction of dipion pairs on Carbon[44]. The events originate from a scintillation counter used to trigger the streamer chamber. Nearly the full angular distribution of the $\rho^0 \to \pi^+\pi^-$ decay was detected. The events were separated from other channels by a 1C kinematic fit to

$$\gamma\ C \to \pi^+\pi^-\ C \qquad (8)$$

using the measurement of the photon energy in the tagging system. Incoherent events on the nucleus were reduced by excluding the events with signature of a nuclear breakup.

Figure 15 shows the $\pi^+\pi^-$ mass distribution for the 2 higher energy intervals. A strong ρ^0 is observed with little background. The rho region has an exponential t-dependence of slope $\sim 60\ \mathrm{GeV}^{-2}$ reflecting the coherent production.

The t-dependence of the rho shape was studied using the parameterization procedure, i.e. multiplying the p-wave Breit-Wigner shape for the rho by $(M_\rho/M_{\pi\pi})^{n(t)}$. In Fig. 16 n is given as a function of t. For comparison the photoproduction data of the streamer chamber on hydrogen[34] is given along with the SLAC-Berkeley-Tufts[3] results for n. For Carbons the exponent n decreases with t much faster than for hydrogen, i.e.

the mass skewing is gone at a smaller t. In addition, the value of n at $t = 0$ is approximately 1 unit lower for Carbon than for hydrogen which agrees qualitatively with the SLAC complex nuclei data and the prediction of Bauer. However, the approach to a pure Breit-Wigner form at lower t values on Carbon is not well understood.

IV. Energy Dependence of the Momentum Transfer Distribution

In the classical picture of diffractive scattering, a plane wave on a black disk yields an energy independent differential cross section. However, the lower energy experimental data on pp scattering showed a strong increase in the exponential slope of the t-distribution. In the Regge picture the data suggested a Pomeron trajectory $\alpha(t) = \alpha(0) + \alpha' t$ with $\alpha' > 0$. In other reactions, e.g. $\pi^{\pm} p \rightarrow \pi^{\pm} p$, little or no energy dependence is observed. It has been suggested that meson exchange contributes to $\pi^{\pm}p$ elastic scattering and interferes with the Pomeron exchange yielding an energy independent exponential slope parameter. In photoproduction, the reaction $\gamma p \rightarrow \rho^{o} p$ corresponds to the $\pi^{\pm}p \rightarrow \pi^{\pm}p$ behavior while the reaction $\gamma p \rightarrow \Phi p$ is throught to proceed only via Pomeron exchange. In this section I discuss the energy dependence of the t-distributions of the quasi-elastic ρ^{o} and Φ photoproduction.

A. The Reaction $\gamma p \rightarrow \rho^{o} p$

In Fig. 17 we show the differential cross section for the high energy SLAC data > 10 GeV on the reaction $\gamma p \rightarrow \rho^{o} p$(45). The forward $\pi^{+}\pi^{-}$ are detected in a spectrometer from the production of a bremsstrahlung photon beam on a hydrogen target. The data have been corrected for an inelastic rho contribution which varied from 2.5% for their 14 - 16 GeV selection to 25% for the 10 - 12 GeV interval in their 16 GeV endpoint run. The spectrometer had a reasonable acceptance for most of the decay angular distributions and the data are consistent with s-channel helicity conservation. These data occur for $-t < 0.2\ \mathrm{GeV}^2$ and show an exponential decreasing behavior with t. Cross section values have been determined by the "standard method" suggested by Yennie(46):

$$\frac{d\sigma}{dt} = \frac{d^2\sigma}{dm\,dt}\bigg|_{m=m_\rho} \cdot \frac{\pi\,\Gamma_\rho}{2} \qquad (9)$$

This method avoids some of the problems associated with comparing experimental data, namely:

i) the line shape of the $\pi\pi$ mass spectrum in photoproduction need not be specified over a wide range. The broad width of the ρ^o, $\Gamma \sim 140$ MeV, leads to uncertainties in the high mass intensity of the ρ^o Breit-Wigner shape.

ii) Models such as that of Söding result in artificially reducing the ρ^o forward differential cross section due to the Chew-Low kinematical boundary limiting the contribution from the high mass tail at small t.(3,4)

iii) Since the incoherent background varies between different experimental techniques and energies, accounting for this background is a more difficult problem over the entire mass range than only in the region of the rho mass.

iv) Different experimenters use grossly varying forms for the Söding model. While on the surface one would think that the "Söding" results obtained by different experiments can be compared, in actuality the results for the rho cross sections vary a great deal due to detailed assumptions chosen for the model even for the same raw data[47].

However, some problems remain associated with obtaining the ρ^o signal at M_ρ and thereby obtaining the ρ^o cross section via Eqn. 9.

i) Different experimenters use different values for M_ρ thus evaluating $d\sigma/d\,M_{\pi\pi}$ at different points on a curve falling rapidly with increasing mass. In addition, the experimental mass determination between experiments may be systematically wrong by as much as 1%.

ii) Subtraction of incoherent background is still a problem. This is relatively easy, but not always done, in bubble chamber experiments where the $\pi^+\pi^-p$ channel is easily separated by a kinematical fit and the $\Delta^{++}\pi^-$ and phase space contributions can be subtracted. In experiments where only the $\pi^+\pi^-$ line shape is observed, a more difficult problem is encountered.

iii) The matrix element for the ρ^o and coherent $\pi\pi$ background can also be important e.g. ignoring the ρ^o-ω interference can result in ~ 10% difference in the rho cross section.

iv) Obviously from Eqn. 9, the width used is very important. While Γ may vary in obtaining $d\sigma/dt/_{M=M\rho}$ from the line shape, it should remain fixed in determining the rho cross sections via Eqn. 9. Comparisons should use the same $\Gamma\rho$.

The differential cross section of Fig. 17 has been fit to the form

$$\frac{d\sigma}{dt} = \frac{d\sigma}{dt}\bigg|_{t=0} e^{At}$$

resulting in the slopes A plotted as a function of energy in Fig. 18.

The bubble chamber data of SLAC-Weizmann-Tel Aviv collaboration (SWT)[48], of the SLAC-Berkeley-Tufts collaboration (SBT)[4], and the spectrometer data of the Cornell group[29] using the standard method are also given. The SWT data include an incoherent background in the $\pi^+\pi^-p$ channel which is important at low E_γ. One should note the different t ranges used for extracting the ρ slope, which are relevant if $d\sigma/dt$ is not a pure exponential. In pp elastic scattering the slope for $|t| < 0.15$ is 1 to 2 units larger than for $0.15 < |t| < 0.3$ GeV^2. The importance of the t-range can be seen in Fig. 19 where $d\sigma/dt$ is given for the SB 9.3 GeV data and the SLAC forward $\pi^+\pi^-$ spectrometer data. The results for $d\sigma/dt$ are in agreement. However, the slopes as seen in Fig. 18 differ by 2.5 units. The data show little s-dependence of the exponential slope and are consistent with the energy variation of the average of the $\pi^{\pm}p$ elastic scattering slopes in the region $0.1 < |t| < 0.4$ GeV^2 shown as a dashed curve on Fig. 18, although the photoproduction slope is on the average ~ 1 unit smaller. For comparison, the s-dependence of other elastic hadron-hadron slopes are given in Fig. 20[1,49]. We see that pp and K^+p elastic scattering show strong shrinkage (slope increases with increasing energy) while their anti-particle counterparts show no shrinkage ($\bar{p}p$ shows anti-shrinkage).

The recent literature contains attempts to reconcile the energy dependence of the differential cross section for different reactions. In terms of the dual absorption model (DAM) the differences arise from the different allowable meson exchange amplitudes interfering with the Pomeron exchange.

M. Davier[50] for πp elastic scattering and Chadwick et al.[51] for

Compton scattering and "elastic" ρ^o photoproduction have carried out an amplitude analysis to extract the Pomeron and meson exchange amplitudes. They assumed that only the Pomeron and the f^o meson contribute to the isoscalar exchanges in the t-channel (other exchanges are expected to be negligible or are specifically excluded, e.g., $I \neq 0$ exchanges[52]). Following the ideas of H. Harari[53] they parameterized the imaginary part of f exchange by a peripheral amplitude

$$\mathrm{Im}\, f(t) = \frac{A_f}{\sqrt{s}} \cdot e^{B_f t} \cdot J_o\,(R\,\sqrt{-t}) \tag{10}$$

and the Pomeron by a central collision process $iA_p e^{B_p t}$. They describe the t-dependence of the differential ρ^o cross section well as seen in Fig. 21. The results for the energy dependence of the exponential slopes of the Pomeron, B_p, and f-exchange, B_f, amplitudes are given in Fig. 21. Within the assumptions of the dual absorption model the data indicate

i) the Pomeron amplitude shrinks with increasing energy

ii) the f-exchange slope is consistent with a linear increase in ln s.

Thus we see that a small non-diffractive amplitude can make a large effect in the energy dependence of the differential cross section.

The SBT data show a small but significant s-channel helicity flip amplitude in $\gamma p \to \pi^+\pi^- p$ with $M_{\pi^+\pi^-} \sim M_{\rho^o}$ associated with natural parity exchange in the t-channel[4]. The ratio of helicity single-flip to non-flip amplitudes at the γ-ρ^o vertex is comparable in magnitude to that found in πp elastic scattering[54] where nucleon helicity flip is measured.In Fig. 22 the ratio of single-flip to nonflip amplitudes for πp elastic scattering is shown along with 2 Re ρ^N_{10} for $\gamma p \to \pi^+\pi^- p(M_{\pi^+\pi^-} \sim M_{\rho^o})$

($2\,\mathrm{Re}\,\rho^N_{10} \simeq (\mathrm{Im}\,T^N_{01}/T^N_{11})$, where N refers to the natural parity exchange component). The flip amplitudes do not show zeros at $-t = 0.2$ and $0.6\ \mathrm{GeV}^2$, which would be expected, if most of the s-channel helicity flip were due to f exchange and the f amplitude has the peripheral character of Eqn.10. Thus in terms of the dual absorption model the SCHC violation is most likely associated with the Pomeron exchange or with background in the case of $\gamma p \to \rho^o p$.

B. <u>The Reaction $\gamma p \to \varphi p$</u>

At this point we thought we understood the s-dependence of the differential cross section and why different reactions display different behavior. However, the results of the SLAC-Wisconsin group(30) and the recent Bonn results(55) on elastic φ photoproduction have thrown into disarray once again our understanding of diffractive processes. Freund(56), and more recently Barger and Cline(57), have pointed out on very general grounds that φp elastic scattering should proceed only by Pomeron exchange. This follows directly from the quark model with the φ made up of two strange quarks and is supported by experimental evidence showing the φ to be decoupled from nonstrange hadrons. Therefore, a measurement of φp elastic scattering would more unequivocally determine the parameters of the Pomeron trajectory than other elastic scattering processes involving additional exchange contributions.

Since the φ meson has the same quantum numbers as the photon, the φ photoproduction cross section should be directly related to elastic scattering of transversely polarized φ mesons on the proton, i.e.,

$$\frac{d\sigma}{dt}\ (\gamma p \to \varphi p) = \frac{\alpha}{4}\left(\frac{\gamma_\varphi^2}{4\pi}\right)^{-1} \frac{d\sigma}{dt}\ (\varphi_T\, p \to \varphi_T\, p). \tag{11}$$

Thus, measurements of the photoproduction of φ mesons should determine the energy dependence of the differential cross section for the elastic scattering of φ mesons and hence for the Pomeron.

C. Properties of $\gamma p \to \varphi p$

Before presenting the cross section measurements, let us first look at the data on other properties of φ photoproduction. The Wisconsin-SLAC group[58] measured the asymmetry parameter at a photon energy of 8.14 GeV and $|t| = 0.2$ GeV^2 in a setup which detects the proton and the K^+K^- pair and obtained

$$\Sigma = 0.985 \pm 0.12$$

in excellent agreement with the predictions from pure Pomeron exchange. This result is different from that of an earlier Cornell measurement[59], possibly due to a contamination from inelastic φ in the Cornell data. In fact, Berger et al.[29] who measure the recoil proton and the K^+K^- of the φ decay, point out that if the inelastic component in the McClellan et al.[59] data is polarized oppositely to the elastic, the large asymmetry (0.55 ± 0.13) reported by McClellan et al. can be understood without invoking non-diffractive behavior in the elastic production.

The Wisconsin-SLAC data are supported by the SLAC-Berkeley-Tufts experiment[4]. They have studied φ-photoproduction with smaller statistics in the bubble chamber using a linearly polarized photon beam and find that the φ decay density matrix elements and measured asymmetry at 2.8/4.7 and 9.3 GeV are consistent with SCHC and pure natural parity exchange. In Fig. 23 their $\cos\theta$ and ψ dependence shows the familiar $\sin^2\theta \cos^2\psi$ decay distribution in the helicity system expected for s-channel helicity conservation.

The Cornell experiment of McClellan <u>et al</u>.[60] also measures φ production on deuterium and find the deuterium-to-hydrogen ratio, extrapolated to $t = 0$, to be $R(o) = 3.6 \pm 0.6$ although no inelastic contributions have been subtracted. The predicted ratio, assuming no isospin exchange, is $R(o) = 3.89$. The data are thus consistent with the pure Pomeron exchange hypothesis.

The DESY/MIT group studied φ photoproduction from a carbon target at about 7 GeV[61]. They observed copious coherent production of the φ, an analysis of the decay distribution is again consistent with s-channel helicity conservation.

However, there is some indication that the forward $\gamma p \to \varphi p$ may not be purely imaginary as one would have expected for pure Pomeron exchange. The DESY/MIT group have measured the real part of the $\gamma p \to \varphi p$ process[62] by observing the interference between the resonant φ production and the Bethe-Heitler process in $\gamma C \to \varphi C$, with $\varphi \to e^+e^-$ at 7 GeV. They report that the φ amplitude differs from being purely imaginary by $25^\circ \pm 15^\circ$ or, in other terms, $\frac{\mathrm{Re}A\varphi}{\mathrm{Im}A\varphi} = (-\,0.48\,{}^{+0.33}_{-0.45})$. This may be an indication that the $\gamma \to \varphi$ process is not purely due to Pomeron exchange. Unfortunately, this is a difficult experiment and the errors are not small enough to draw firm conclusions.

D. <u>t-Distribution of φ Production</u>

The differential cross section for φ production is displayed in Fig. 24,25 for three energy-regions. The data from various experimental techniques are consistent with one another. Some evidence is seen at large $|t|$ for a deviation from a pure $\exp(At)$ dependence in the spectrometer data of Anderson et al.[30]. The recent Bonn data [55] at E_γ = 2 GeV shows a sharp falloff in t consistent with a pure exponential dependence. The s-dependence of the φ differential cross section at t = -0.6 GeV^2 is given in Fig. 26. Little or no s-dependence is observed.

This conclusion can also be reached for the entire $|t|$ range ≥ 0.3 GeV^2 as seen in Fig. 27 where the high statistic counter data for $d\sigma/dt$ are plotted. However, the low t point of Bonn is significantly lower by 23% (or 4SD) than the higher energy data (anti-shrinkage) where one would have expected the 2 GeV data to be larger, if anything, if s-channel effects are important. In addition, the flux factor relating the cross section to the amplitude would give a slightly larger low energy cross section assuming that the amplitude is energy independent.

Perhaps the lack of shrinkage is associated with only the intermediate t region. To test this hypothesis the t = -0.6 GeV^2 differential cross section[63] is given in Fig. 28 for the K^+p and pp elastic scattering which show strong shrinkage. While a strong energy dependence is observed below s = 10 -15 GeV^2 the data show little energy dependence between s = 10 - 40 GeV^2 [64]. In contrast, the φ data are consistent with no energy dependence from s = 4 $\rightarrow$ 40 GeV^2 at t = -0.6 GeV^2.

All the SLAC-Wisconsin data were taken with almost identical spectrometer settings. They detect only the proton and consequently the complete decay angular distribution and all decay modes are included. The proton momentum is measured in a MM spectrometer and is identified by pulse height. Pions are rejected by a Lucite Čerenkov counter. The $\gamma p \rightarrow \varphi p$ cross sections were obtained by analyzing the missing mass distribution against the proton in the vicinity of the φ mass. Accordingly the cross section ratios are unaffected by systematic uncertainties in the spectrometer efficiencies.

The Bonn point at 2 GeV was obtained in a spectrometer experiment where the K^+K^- and p were measured and identified by time of flight. They assume s-channel helicity conserving φ production to take into account their geometrical cutoff in the K^+K^- acceptance. Only φ's with

$$\cos\theta_H = 0 \pm 0.39 \; (\theta_H = 90 \pm 23^\circ)$$

$$\varphi = 90 \pm 12^\circ$$

are detected. The SCHC assumption was checked at $t = -0.457\ \mathrm{GeV}^2$ with the apparatus sensitive to φ's at

$$\cos\theta_H = 0.47 \pm 0.18 \; (\theta_H = 62 \pm 12^\circ)$$

$$\varphi = 90 \pm 12^\circ$$

and was found to be consistent with the expected $\sin^2\theta_H$ dependence. Corrections are also made for K decays in flight and unseen decay modes for φ decay. Included in the error is a systematic uncertainty of $\lesssim 10\%$.

Analysis of the SLAC-Wisconsin missing mass results alone at $t = -0.6\ \mathrm{GeV}^2$ in terms of

$$\frac{d\sigma}{dt} \sim s^{2(\alpha_{eff}-1)}$$

gave a value of $\alpha_{eff} = 1.02 \pm 0.08$. If $\alpha_{eff}(t)$ is expressed as $\alpha_{eff}(t) = 1 + \alpha' t$, the $\alpha' = -0.03 \pm 0.13$ i.e. no shrinkage. When the actual slope measurements are combined, a similiar behavior is found in the s-dependence of the exponential slope as seen in Fig. 29 and Table III. The slope A and $\frac{d\sigma}{dt}\Big|_{t=0}$ are shown for the photoproduction data by fitting the measurements for $|t| < 1$ GeV^2 to the form

$$\frac{d\sigma}{dt} = \frac{d\sigma}{dt}\Big|_{t=0} \cdot e^{At}$$

with $\frac{d\sigma}{dt}\Big|_{t=0}$ and A as parameters. The smooth curve in Fig. 29 is a fit of the form $A = A_o + 2\alpha' \ln s$ with

$$A_o \approx 4.0 \quad \mathrm{GeV}^{-2}$$

$$\alpha' = 0.14 \pm 0.09 \ \mathrm{GeV}^{-2}$$

which is in fact compatible with the missing mass results at $t = -0.6$ GeV^2.

Let us now accept the smaller α' as representing the true φ. Then α' for $\gamma p \rightarrow \varphi p$ is similar to that found in pp elastic scattering[1,49] for the t-region $0.15 < |t| < 0.3$ GeV^2 and s-region $30 < s < 4000$ GeV^2

$$A_o = 9.2 \pm 0.9 \ \mathrm{GeV}^{-2}$$

$$\alpha' = 0.10 \pm 0.06 \ \mathrm{GeV}^{-2}$$

However, as seen in Fig. 30, this is only true for high s: the s-dependence is very strong for $s < 30$ GeV^2. Perhaps the interpretation one can place on these results is that φ photoproduction may have only Pomeron exchange and thus reflects the behavior of high energy pp scattering at a much lower energy. Assuming this is true, the larger value for A_o in pp scattering over that for $\gamma p \rightarrow \varphi p$ means the φ acts as if the φ-nucleon interaction radius is smaller than the nucleon-nucleon, pion-nucleon and rho-nucleon interaction radii. A similar conclusion can be reached by comparing $\sigma(\varphi N) = 9.8 {+2.9 \atop -3.3}$ mb from the DESY experiment[61] to $\sigma(pp) \approx$

40 - 45 mb[1].

Note that the conclusions reached on the s-dependence of "elastic" φ production essentially come from the three high statistics experiments of Bonn, Cornell and SLAC-Wisconsin. However, as we have noted above the assumption of s-channel helicity conservation is crucial to the extraction of the differential cross section in the 2 GeV Bonn data. Because the s-channel helicity flip amplitudes are necessarily zero for forward produced φ's, a contribution to $\gamma p \to \varphi p$ from s-channel helicity flip amplitudes can also affect the slope determination as well as the normalization in the differential cross section. At such a low energy the assumption of SCHC may not be valid, although, at 2.8 and 4.7 GeV the SBT data are consistent with SCHC[4] within rather large errors.

E. Non-Peripheral f-Exchange Amplitude

The result for the Pomeron exchange amplitude from φ photoproduction is in contradiction to the dual absorption model extraction of the Pomeron exchange amplitude as seen by the dashed curve of Fig. 29. Barger, Geer and Halzen[65] address this problem. In contrast to the approach of Davier[50] and Chadwick et al.[51] they extract the f-exchange ampli- at each value of α'. They find for $\alpha' < 0.4$ (which is required for the Pomeron from the φ results) a non-peripheral t-distribution is obtained for the (A_2, f, K_T^*) tensor exchanges, i.e., the amplitude is not of the form of Eqn. 10. In this case, as Chadwick et al.[51] point out the s-channel helicity flip amplitude found in the $\pi^+\pi^-$ mass region near the rho, which does not show a peripheral character, can then come from the Pomeron, the f-exchange amplitudes, or the background under the ρ^0.

V. Diffractive Vector Meson Electroproduction

The recent data on electroproduction of vector mesons allows us to investigate diffractive ρ^0-production as the "mass$^2 \leftrightarrow Q^2$" of the incident particle is altered. This enables us in principle to study vector meson production and decay from longitudinal photons which do not necessarily behave like those from the transverse component. In addition, the Q^2-dependence of both the transverse and longitudinal components may be studied.

(A) ρ^0 Mass Distributions

The track chamber and wide aperture spectrometer experiments[66,67,68] isolate the channel

$$\gamma_V p \rightarrow \pi^+\pi^- p \tag{12}$$

by kinematic fits and consequently obtain a relatively clean sample of "elastic" rho events. Fig. 31 shows the $\pi^+\pi^-$ mass distributions; one observes a distinct ρ^0 signal on a background of $\lesssim 20\%$. For three Q^2-intervals of the SLAC bubble chamber data the $\pi^+\pi^-$ mass projections are given in Fig. 32 and show a distinct ρ^0 signal in each Q^2-interval. The background contribution in the region of the rho mass can further be reduced by fitting the Dalitz plot density allowing for contributions from $\rho^0 p$, $\Delta^{++}\pi^-$, $\Delta^0\pi^+$ and phase space. The resulting ρ^0 contribution to the total cross section is given in Fig. 33 and shows that the relative importance of ρ^0 production decreases with Q^2 for $2 < W < 5$ GeV.

However, the fractional decrease of $\sigma(\rho^0)/\sigma_{TOT}$ differs between the experiments. Relative to the SLAC WAS data the DESY STC result falls ~ 1.5 times faster with Q^2 while the SLAC HBC result has about a factor 1.5 less Q^2 dependence. These experiments are found to be roughly in agreement with the predictions of the vector dominance model of Sakurai and Schildknecht [69], i.e., the ρ^o cross section decreases as the ρ^o propagator squared

$$\frac{1}{\left(1 + \frac{Q^2}{m_\rho^2}\right)^2} \tag{13}$$

This agreement is more clearly seen in Fig. 34 where the cross section for $\gamma_V p \to \rho^o p$ is given as a function of Q^2. The cross section data do not require a longitudinal component. However, as we shall see, the angular decay distribution require a longitudinal component if we assume s-channel helicity is conserved in electroproduction.

(B) ρ^o Decay Distributions

In all the present experiments the longitudinal and transverse components are not separated. To do so requires the Q^2-dependence of a particular W interval to be studied with different incident energy lepton beams, i.e., for different ϵ (the ratio of the longitudinal to transverse photon flux). For the description of the ρ^o decay in electroproduction, the usual density matrix representation [72] must be expanded to include production by longitudinal photons [73]. If θ and φ are the polar and azimuthal angles of the π^+ in the ρ^o rest system (with the z axis along the CMS ρ^o direction, the x axis in the hadron production plane, and Φ the azimuth of the scattered lepton with respect to the hadron production plane in the hadronic CMS), then the angular distribution of ρ decay is

$$\begin{aligned}W(\cos\theta,\varphi,\Phi)\frac{3}{4\pi}\Big[&\tfrac{1}{2}(1-r^{04}_{00})+\tfrac{1}{2}(3r^{04}_{00}-1)\cos^2\theta-\sqrt{2}\ \mathrm{Re}\ r^{04}_{10}\sin2\theta\cos\varphi-r^{04}_{1-1}\sin^2\theta\cos2\varphi\\ &-\epsilon\ \cos2\Phi(r^1_{11}\sin^2\theta+r^1_{00}\cos^2\theta-\sqrt{2}\ \mathrm{Re}\ r^1_{10}\sin2\theta\cos\varphi-r^1_{1-1}\sin^2\theta\cos2\varphi)\\ &-\epsilon\ \sin2\Phi(\sqrt{2}\ \mathrm{Im}\ r^2_{10}\sin2\theta\sin\varphi+\mathrm{Im}\ r^2_{1-1}\sin^2\theta\sin2\varphi) \qquad (14)\\ &+\sqrt{2\epsilon(1+\epsilon+\Delta)}\ \cos\Phi(r^5_{11}\sin^2\theta+r^5_{00}\cos^2\theta-\sqrt{2}\ \mathrm{Re}\ r^5_{10}\sin2\theta\cos\varphi-r^5_{1-1}\sin^2\theta\cos2\varphi)\\ &+\sqrt{2\epsilon(1+\epsilon+\Delta)}\sin\Phi(\sqrt{2}\ \mathrm{Im}\ r^6_{10}\sin2\theta\sin\varphi+\ \mathrm{Im}\ r^6_{1-1}\sin^2\theta\sin2\varphi)\Big]\end{aligned}$$

where the polarization parameter

$$\epsilon = \frac{1}{1+\dfrac{2(Q^2+\nu^2)\ \tan^2\Theta/2}{Q^2\ (1-Q^2_{min}/Q^2)^2}}$$

and $Q^2_{min} = 2(EE' - |\vec{p}||\vec{p}\,'| - M^2_\ell)$, $\nu = E - E'$, and Θ is the lepton polar scattering angle.

The density matrix elements r^α_{ij} are the same as for polarized real photons except

$$r^{04}_{ik} = \frac{\rho^{OT}_{ik} + (\epsilon+\Delta)R\ \rho^{OL}_{ik}}{1+(\epsilon+\Delta)R}\ , \quad r^\alpha_{ik} \quad \alpha = 1,2 \quad \frac{\rho^\alpha_{ik}}{1+(\epsilon+\Delta)R}$$

where T and L refer to production by transverse and longitudinal photons respectively and Δ is defined as $\Delta = \frac{2M_\ell^2}{Q^2}(1 - \epsilon) \ll 1$. It is clear that ρ^{oT} and ρ^{oS} can only be separated by varying $\epsilon + \Delta$ at fixed W and Q^2; for the present data no separation is possible because the experiments have fixed incident lepton energies.

The ρ^o decay distribution may be simplified if we use the angle $\Psi = \varphi - \Phi$ which is defined in Fig. 35 for forward produced rhos. As a reminder, Fig. 36 shows the distribution of $\cos\theta_H$ and Ψ for ρ^o mesons produced with linearly polarized real photons[4]. An almost pure $\sin^2\theta \cos^2\Psi$ distribution due to s-channel helicity conservation is observed. Assuming that SCHC and natural parity exchange in the t-channel holds for $Q^2 > 0$ we would expect similar behavior for the transverse rho electroproduction. In electroproduction the transverse photons are linearly polarized with the degree of polarization equal to ϵ (≈ 0.9 for present experiments) and the polarization vector is in the scattering plane. If the longitudinal photons produce rhos then the longitudinal rho decay distribution will be isotropic around the ρ^o direction of flight with respect to the electron scattering plane, i.e. $W(\Psi_H) = \text{const}$ and assuming SCHC then $W(\cos\theta) = \cos^2\theta_H$.

The angular distributions for the SLAC bubble chamber[66] $\gamma_V p \to \rho^o p$ data are shown in Fig. 37a. The data of Dakin et al[67] and the DESY streamer chamber[68] experiment show similar behavior as seen in Fig. 37b, c. The anisotropic Ψ distribution can only arise from production by transverse photons. The strong $\cos^2\Psi$ component indicates that the ρ^o mesons are produced predominantly by transverse photons. The rather flat $\cos\theta$ distribution indicates a $\cos^2\theta$ component from the longitudinal photon or s-channel helicity flip amplitudes of the transverse rho component.

In the scatter plot of Fig. 37a, the effect of interference between longitudinal and transverse ρ^o can be seen as enhanced $\Psi = 0^o$ (360^o) production for $\cos\theta_H < 0$ and enhanced $\Psi = 180^o$ production for $\cos\theta_H > 0$.

The SLAC bubble chamber group[66] and the DESY streamer chamber group[68] analyze the ρ^o decay angular distribution of Eqn. 14 in terms of the ρ^o density matrix in the helicity system from moment analyses for events in the ρ^o mass region and $|t| < 0.6$ GeV^2. This procedure allows a small background component from phase space and $\Delta^{++}\pi^-$ events to be included ($\lesssim 5\%$ of the rho for $|t| < 0.6$ GeV). The values for all parameters are given in Table IV along with the expected results if s-channel helicity is conserved. Within one to two standard deviations the density matrix elements of Table IV are consistent with SCHC with the exception of r^1_{00} which shows a 2 - 3 standard deviation effect from the expected zero in the SLAC data. The DESY experiment finds a value for r^1_{00} consistent with SCHC. If $r^1_{00} > 0$, it would imply a contribution from single flip helicity amplitudes to transverse rho production; however, in photoproduction

ρ^1_{00} is consistent with zero[4]. Note, that the s-channel helicity flip terms are necessarily zero at t = 0 and the data are weighted to small t values by an exponential t-dependence (see Rapporteur talk by R. Talman). Thus the low t data may be washing out a helicity flip amplitude contribution for $t \gtrsim 0.2\ \mathrm{GeV}^2$. However, the DESY STC group[74] have checked their decay angular distributions for $0.2 < t < 0.6\ \mathrm{GeV}^2$ and find the density matrix elements to be consistent with SCHC.

With this warning, we now assume SCHC holds in electroproduction as it approximately does in photoproduction and also only natural parity exchange occurs in the t-channel. Then the decay angular distribution of Eqn. 14 reduces to

$$W(\theta,\psi) = \frac{3}{8\pi^2(1+\epsilon R)} \Big\{\epsilon R \cos^2\theta + \frac{1}{2}\sin^2\theta(1 + \epsilon \cos 2\psi) - (\epsilon R(1+\epsilon)/2)^{\frac{1}{2}} \cos \delta \sin 2\theta \cos \psi\Big\} \qquad (15)$$

The two free parameters, R and $\cos\delta$, are then determined in maximum likelihood fits accounting for $\pi^- \Delta^{++}$ and phase space contributions. R measures the ratio of longitudinal to transverse ρ^o production cross sections and $\cos\delta$ measures the phase between the production amplitudes for longitudinal and transverse photons. In Fig. 38 the parameters R and $\cos\delta$ are given for the data of the DESY streamer chamber[68], SLAC bubble chamber[66] and the SLAC wide aperture spectrometer experiments[67]. Within errors the experiments agree and show a large contribution from longitudinally polarized rhos which interfere strongly with the transverse component. Vector dominance models[69, 75] suggest

$$R = \xi^2 \frac{Q^2}{M_\rho^2} \tag{16}$$

where ξ gives the ratio of $\sigma_L(\rho^o p \to \rho^o p)$ to $\sigma_T(\rho^o p \to \rho^o p)$. The measurements (Fig. 38) fall between the two cases: i) $\xi = 1$ with $\sigma_L = \sigma_T$[75] and ii) $\xi \lesssim 0.35$ suggested by Sakurai and Schildknecht[69]. However, Sakurai[76] has pointed out that the new results from the MIT experiment in Riordan's thesis[77] for $R = \sigma^L_{TOT}/\sigma^T_{TOT}$ at high ω result in a value for $R = \sigma^L_\rho/\sigma^T_\rho$ between $(0.25 \to 0.56)\ Q^2/m_\rho^2$ in their model.

In fact, the combination of the three experiments suggest R = constant is also possible (ϵ is essentially independent of Q^2 for these data see Fig. 3 or ref. 78).

(C) $\pi^+\pi^-$ Line Shape

Two groups have presented results on the $\pi^+\pi^-$ line shape[66, 67]. In their fits to the Dalitz plot density of reaction (12) the rho Breit-Wigner form is multiplied by the mass skewing factor $(M_\rho/M_{\pi^+\pi^-})^n$ and n is determined in the fit. The results are plotted in Fig. 39. The SLAC HBC data show no Q^2 variation while the SLAC WAS results indicate the $\pi^+\pi^-$ line shape becomes more like a p-wave Breit-Wigner form. Within errors the experiments agree. The diffraction disociation model of Kramer and Quinn[79] suggest the skewing goes away with Q^2 as $(m_\rho^2+Q^2-t)^2/(m_{\pi\pi}^2+Q^2-t)^2$.

(D) ω^o- Electroproduction

Two groups[66, 68] measured ω-electroproduction in the channel

$$\gamma_V p \to \pi^+\pi^-\pi^o p \ . \tag{17}$$

The $\pi^+\pi^-\pi^o$ mass distributions are shown in Fig. 40 and show a strong ω peak. The shaded events occur for $0.5 < Q^2 \lesssim 2.5$ GeV^2 in the SLAC-HBC data and show a significant ω signal.

The ω contribution to the total cross section is given in Fig. 41a together with the photoproduction results for the same W interval. The data points agree with the photoproduction value, but do not exclude the Q^2 variation found for $\sigma(\rho)/\sigma_{TOT}$. A similar conclusion was found in the DESY data. Their Q^2 dependence for $\gamma_V p \to \omega\, p$ is seen in Fig. 41b. However, we do not expect σ_ω to behave like σ_ρ at low energies because of the large one-pion exchange contribution to σ_ω observed at $Q^2 = 0$[4, 80].

VI. Conclusions

1. The ρ' has been observed in three different experimental techniques:

a) ρ'-photoproduction shows a diffractive behavior and from an analysis of the decay angular distributions one finds a $J^P = 1^-$ $I^G = 1^+$ system decaying into $\rho^o\epsilon^o_{\hookrightarrow\pi^+\pi^-}$

b) e^+e^- annihilation into a $J^{PC} = 1^{--}$ $\rho' \rightarrow \rho^o \epsilon^o$
$\qquad\qquad\qquad\qquad\qquad\qquad\qquad\qquad\qquad\qquad\qquad \hookrightarrow \pi^+\pi^-$

c) $\pi^- p \rightarrow \pi^+\pi^- n$ shows a resonance structure in the p-wave $\pi^+\pi^-$ phase shift at 1590 MeV which is associated with the $\rho' \rightarrow \pi^+\pi^-$ decay.

2. The t-distribution of $\gamma p \rightarrow \varphi p$ shows little energy dependence between 2 and 20 GeV photon energies assuming that s-channel helicity flip contributions can be neglected at 2 GeV. Since only the Pomeron trajectory is thought to contribute to $\gamma p \rightarrow \varphi p$ the φ results imply a flat Regge trajectory for the Pomeron.

3. The study of ρ^o-electroproduction has shown:

a) The relative contribution of the "elastic" ρ^o electroproduction cross section to σ_{TOT} decreases with Q^2 over the W range 2 - 5 GeV^2. The Q^2 dependence of $\gamma_v p \rightarrow \rho^o p$ falls roughly as the ρ^o propagator $1/(1 + Q^2/M_\rho^2)^2$.

b) The decay angular distribution of the ρ^o are consistent with SCHC and natural parity exchange in the t-channel. If these properties are assumed to hold exactly for ρ^o electroproduction, a significant longitudinal ρ^o contribution which interferes strongly with the transverse ρ^o amplitude is observed.

Acknowledgements

I wish to thank Dr. H. Besch and Dr. U. Trinks for their assistance as scientific secretaries. Their tireless efforts allowed this report to be ready on time. My special thanks go to Dr. Hans Besch who made my stay at Bonn particularly enjoyable. Discussions with Professor J. Ballam, Professor H. Bingham, Dr. G. Chadwick, Professor S. Drell, Professor E. Eisenberg, Dr. H. Meyer, Professor H. Spitzer, Professor I. Skillicorn, Dr. Günter Wolf and Professor D. Yennie are gratefully acknowledged. I want to thank Professor W. Paul, the organizing committee and the Staff of the Physikalisches Institut at Universität Bonn for the hospitality extended me.

References

1. David W. G. S. Leith, SLAC-PUB-1263 (1973); and Proceedings of the XVI International Conference on High Energy Physics, National Accelerator Laboratory, Chicago, Vol. 3, 321 (1972).

2. G. Veneziano, NC 57A, 190 (1968); V. Barger and D. Cline, PR 182, 1849 (1969).

3. SLAC-Berkeley-Tufts Collaboration, PR D5, 545 (1972).

4. SLAC-Berkeley Collaboration, PR D7, 3150 (1973).

5. J. Park, M. Davier, I. Derado, D.C. Fries, F.F. Liu, R.F. Mozley, A.C. Odian, W.P. Swanson, F. Villa, and D. Yount, NP B36, 404 (1972).

6. Eisenberg et al., PR D5, 15 (1972).

7. N.Hicks, A. Eisner, G. Feldman, L. Litt, W. Lockeretz, F.M. Pipkin, J.K. Randolph, and K.C. Stanfield, PL 29B, 602 (1969).

8. G. McClellan, N. Mistry, P. Mostek, H. Ogren, A.Osborne, A. Silverman, J. Swartz, R. Talman, and G. Diambrini-Palazzi, PRL 23, 718 (1969).

9. F. Bulos, W. Busza, R. Giese, E. E. Kluge, R. R. Larsen, D.W.G.S. Leith, B. Richter, S.H. Williams, B. Kehoe, M. Beniston, and A. Stetz, PRL 26, 149 (1971).

10. H. Alvensleben, U. J. Becker, William K. Bertram, M. Chen, K. J. Cohen, R. T. Edwards, T.M. Knasel, R. Marshall, D.J. Quinn, M. Rohde, G. H. Sanders, H. Schubel, and Samuel C. C. Ting, PRL 26, 273 (1971).

11. M. Davier, I. Derado, D. C. Fries, F. F. Liu, R. F. Mozley, A. Odian, J. Park, W. P. Swanson, F. Villa, and D. Yount, SLAC-PUB-666 (1969), and contribution to the 4th International Conference on Electron and Photon Interactions of High Energy, Liverpool (1969);

M. Davier, I. Derado, D. E. C. Fries, F. F. Liu, R. F. Mozley, A. Odian, J. Park, W. P. Swanson, F. Villa, and D. Yount, SLAC-PUB-1205 (1973). For a recent analysis of the SLAC streamer chamber data, see Ref. 12.

12. P. Schacht, I. Derado, D. C. Fries, J. Park, and D. Yount, Max-Planck-Institut für Physik und Astrophysik, München, paper No. 291.

13. B. Bartoli, B. Coluzzi, F. Felicetti, V. Silvestrini, G. Goggi, D. Scannicchio, G. Marini, F. Massa, and F. Vanoli, NC 70, 615 (1970); and B. Bartoli et al., PR D6, 2374 (1972).

14. G. Barbarino, M. Grilli, E. Iarocci, P. Spillantini, V. Valente, R. Visentin, F. Ceradini, M. Conversi, L. Paoluzi, R. Santonico, M.Nigro, L. Trasatti, and G. T. Zorn, NCL 3, 689 (1972); M. Grilli et al., NC 13A, 593 (1973).

15. F. Ceradini et al., PL 433, 341 (1973).

16. SLAC-Berkeley Collaboration , LBL-991 (1972); and 3rd International Conference on Meson Spectroscopy, Philadelphia (1972).

H. H. Bingham, W. B. Fretter, W. J. Podolsky, M. S. Rabin, A.H. Rosenfeld, G. Smadja, G.P. Yost, J. Ballam, G. B. Chadwick, Y. Eisenberg, E. Kogan, K. C. Moffeit, P. Seyboth, I. O. Skillicorn, H. Spitzer, and G. Wolf, PL 41B, 635 (1972).

17. M. Davier, Proceedings of the XVI International Conference on High Energy Physics, National Accelerator Laboratory, Vol. 1, 104 (1972).

18. G. Wolf, DESY 72/61 (1972).

19. G. Parrour, doctoral dissertation, Université de Paris, LAL-1257 Orsay (1971).

20. D. Mortara, University of Illinois Preprint (October 1972).

21. G. Kramer and T. Walsh, DESY 72-46 (1972);
G. Kramer, Grado Lectures, CERN-Report 72-17 (1972);
A. C. Hirshfeld and G. Kramer, paper No. 19.

22. F. Renard, Montepellier preprint PM/73/3 (1973) Cedex, France.

23. SLAC-Berkeley-Tufts, private communication H. H. Bingham, A. Rosenfeld, and George Yost.

24. Y. Eisenberg et al., PL 43B, 149 (1973); Eisenberg et al. also look for $\rho' \to \pi^+\pi^-$ in a 5 GeV/c π^+p experiment and find a null signal. However, the $\pi^+\pi^-$ phase space in the region of the $\rho'(1600)$ is severely reduced. Presumably, this is also why they do not observe a g(1680) signal in their $\pi^+\pi^-$ mass distribution.

25. D. H. Miller, CERN/D. Ph. II/Phys. 73-22 (1973).

26. T. Ferbel and P. Slattery, University of Rochester, Preprint COO-3065-40 (1973).

27. B. Hyams, C. Jones, and P. Weilhammer, Max-Planck-Institut für Physik und Astrophysik, München, Preprint 28 (1973) and Paper No. 162.

28. Proceedings, 1971 International Symposium on Electron and Photon Interactions at High Energies, Cornell University, ed. by N. Mistry.

29. C. Berger, N. Mistry, L. Roberts, R. Talman, and P. Walstrom, PL 39B, 659 (1972).

30. R. L. Anderson, B. Gottschalk, D. B. Gustavson, D. M. Ritson, G. A. Weitsch, B. H. Wiik, H. J. Halpern, R. Prepost, and D. H. Tompkins, PRL 30, 149 (1973).

31. D. R. Yennie, paper No 128.

32. SLAC-Berkeley Collaboration, paper No. 293, and SBT Collaboration, contribution to Kiev Conference on High Energy Physics, 1970.

33. R. Anderson, D. Gustavson, J. Johnson, D. Ritson, B. H. Wiik, W. G. Jones, D. Kreinick, F. Murphy, and R. Weinstein, PR D1, 27 (1970), and D. Kreinick Ph.D. Thesis, California Institute of Technology, Pasadena (1970) (unpublished).

34. E. Rabe, Internal Report DESY F1-71/2 (1971) (Diploma Thesis, unpublished).

35. Note that any $\omega\pi^0$ system has the quantum numbers $I^{GC} = 1^{+-}$ and can be diffractively produced by a photon (see Ref. 32).

36. Aachen-Bonn-Hamburg-Heidelberg-Munchen Collaboration, private communication (1973).

37. One might also interpret the enhancement as the onset of the $\omega\pi^0$ or $\rho^+\rho^-$ decay of the $\rho^0(760)$. However, G. Kramer (Ref. 38) has calculated the process $\gamma p \to \rho^0 p$, $\rho^0 \to \omega\pi^0$ and predicts a peak at $M_{\pi^+\pi^-MM} = 1.1$ GeV and a cross section of 0.1 μb in the region $1.15 < M_{\pi^+\pi^-MM} < 1.35$ GeV. Both results are unable to explain the bulk of the observed enhancement.

38. G. Kramer, private communication to SBT collaboration (1972).

39. As reported by J. Lynch at Division of Particle and Fields, Berkeley, California, August 1973.

40. SLAC-Berkeley Collaboration, private communication I. Skillicorn and H. Spitzer.

41. T. Bauer, PR D3, 2671 (1971).

42. F. Bulos, W. Busza, R. Giese, R. R. Larsen, D. W. G. S. Leith, B. Richter, V. Perez-Mendez, A. Stetz, S. H. Williams, M. Beniston, and J. Rettberg, PRL 22, 490(1969).

43. S. H. Williams, (Ph.D. Thesis, unpublished) (1973).

44. AHHM Collaboration, paper No. 294.

45. F. Bulos, R. K. Carnegie, G. E. Fischer, E. E. Kluge, D.W.G.S. Leith, H. L. Lynch, B. Ratcliff, B. Richter, H. H. Williams, and S. H. Williams, paper 343 submitted to the XVI International Conference on High Energy Physics, Chicago-Batavia (1972); B. Giese, Stanford University, Thesis.

46. D. R. Yennie (private communication), and R. Spital and D. R. Yennie, paper No. 67.

47. G. E. Gladding, J. J. Russell, M. J. Tannenbaum, J. M. Weiss, and G. B. Thomson, Harvard Report No. COO-2232-8 Ex and paper No. 244.

48. Y. Eisenberg, B. Haber, E. E. Ronat, A. Shapira, Y. Stahl, G. Yekutieli, J. Ballam, G. B. Chadwick, M. M. Menke, P. Seyboth, S. Dagan, and A. Levy, PR D5, 15 (1972).

49. U.S.S.R.-U.S.A. collaboration, V. Bartenev et al., NAL-PUB-73/54 (1973).

50. M. Davier, PL 40B, 369 (1972).

51. G. Chadwick, Y. Eisenberg, and E. Kogan, SLAC-PUB-1093 (1972).

52. Y. Eisenberg, B. Haber, U. Karshon, E. Kogan, E. E. Ronat, D. Salzman, A. Shapira, Y. Stahl, and G. Yekutieli, paper No. 80.

53. H. Harari, Ann. Phys. (N.Y.), 63, 432 (1971).

54. A. DeLesquen, B. Amblard, R. Beurtey, G. Cozzika, J. Bystricky, J. Deregel, Y. Ducros, J. M. Fontaine, A. Gaidot, M. Hansroul, F. Lehar, J. P. Merlo, S. Miyashita, J. Moychet, and L. van Rossum, PL 40B, 277 (1972).

G. Cozzika, Y. Ducros, A. Gaidot, A. de Lesquen, J. P. Merlo, and L. van Rossum, PL 40B, 281 (1972).

55. H. J. Besch, G. Hartmann, R. Kose, F. Krautschneider, W. Paul, and U. Trinks, paper No. 193. (Page 11 line 6 should read $\epsilon = \Gamma(\phi \to K^+K^-)/\Gamma(\phi \to \text{all}) = 0.491$, private communication).

56. P. G. Freund, NC 48A, 541 (1967).

57. V. Barger and D. Cline, PRL 24, 1313 (1970).

58. H. J. Halpern, R. Prepost, D. H. Tompkins, R. L. Anderson, B. Gottschalk, D. B. Gustavson, D. M. Ritson, G. A. Weitsch, and B. H. Wiik, PRL 29, 1425 (1972).

59. G. McClellan, N. Mistry, B. Sandler, J. Swartz, R. Talman, P. Walstrom, and G. Diambrini-Palazzi, PRL 26, 1597 (1971).

60. G. McClellan, N. Mistry, P. Mostek, H. Ogren, A. Osborne, J. Swartz, R. Talman, and G. Diambrini-Palazzi, PRL 26, 1593 (1971).

61. H. Alvensleben, U. Becker, P. Biggs, M. Binkley, W. Busza, M. Chen, K. H. Cohen, E. Coleman, R. T. Edwards, P. M. Mantsch, R. Marshall, T. Nash, D. J. Quinn, M. Rohde, H. F. W. Sadrozinski, G. H. Sanders, H. Schubel, S.C.C. Ting, and S.L. Wu, PRL 28, 66 (1972).

62. H. Alvensleben, U. Becker, W. Busza, M Chen, K. J. Cohen, R. T. Edwards, P. M. Mantsch, R. Marshall, T. Nash, M. Rohde, H. F. W. Sadrozinski, G. H. Sanders, H. Schubel, S. C. C. Ting, and S. L. Wu, PRL 27, 444 (1971).

63. Particle Data Group, UCRL 20 000 Kp and 20 000 NN

64. A similar conclusion was reached by Y. Eisenberg using vector dominance and the quark model to relate $\gamma p \to \rho p$ to K^+p, K^-p and π^-p elastic scattering (see Y. Eisenberg, paper No. 82).

65. V. Barger, K. Geer, and F. Halzen, NP B49, 302 (1972).

66. J. Ballam, E. D. Bloom, J. T. Carroll, G. B. Chadwick, R.L.A. Cottrell, M. Della Negra, H. DeStaebler, L.K. Gershwin, L.P. Keller, M. D. Mestayer, K. C. Moffeit, C. Y. Prescott, S. Stein, SLAC-PUB-1163 (1972). J. Ballam, et al., paper No. 292.

67. J. T. Dakin, G. J. Feldman, W. L. Lakin, F. Martin, M. L. Perl, E. W. Petraske, and W. T. Toner, PRL 30, 142 (1973).

68. V. Eckardt, H. J. Gebauer, P. Joos, H. Meyer, B. Naroska, D. Notz, W. J. Podolsky, G. Wolf, S. Yellin, H. Dau, G. Drews, D. Greubel, W. Meincke, H. Nagel, and E. Rabe, NP B55, 45 (1973); V. Eckardt et al., paper No. 59.

69. J. J. Sakurai, and D. Schildknecht, PL 40B, 121 (1972).

70. L. Ahrens, K. Berkelman, G. S. Brown, D. G. Cassel, W.R Francis, P. H. Garbincius, D. Harding, D. L. Hartill, J.L. Hartmann, R. L. Loveless, R. C. Rohlfs, and D. H. White, PRL 31, 131 (1973).

71. S. Attenberger, J. Eickmeyer, S. Michalowski, N. Mistry, L. Roberts, J. Storer, R. Talman, and C. Berger, paper No. 232.

72. K. Schilling, P. Seyboth and G. Wolf, NP B15, 397 (1970) and NP B18, 332 (E) (1970).

73. K. Schilling and G. Wolf, DESY-73/13 (1973).

74. S. Yellin, private communication.

75. H. Fraas and D. Schildknecht, NP B14, 543 (1969).

76. J. J. Sakurai, private communication.

77. Riordan, MIT Thesis (1973) (unpublished).

78. J. Ballam, E.D. Bloom, J. T. Carroll, G.D. Chadwick, R.L.A. Cottrell, M. Della Negra, H. DeStaebler, L.K. Gershwin, L.P. Keller, M. D. Mestayer, K.C. Moffeit, C.Y. Prescott and S. Stein, paper No. 286.

79. A. Kramer and H. Quinn, NP B55, 222 (1973).

80. ABBHHM-Collaboration, PR 175,1669 (1968).

Table I: Input Values for the Compton Sum Rule [a] at $E_\gamma = 9.3$ GeV.

Vector Meson	$\gamma_V^2/4\pi$	$\left.\frac{d\sigma}{dt}\right\|_{t=0}$ $(\gamma p \to V p)(\mu b/GeV^2)$
ρ	0.64 ± 0.05 [b]	100 ± 15 [c]
ω	4.8 ± 0.5 [b]	11.4 ± 2.1 [d]
φ	2.8 ± 0.2 [b]	2.85 ± 0.2 [e]
ρ'	3.9 ± 1.3 [f]	15 ± 5 [f]

a) G. Wolf, Ref. 18

b) J. le Francois, Ref. 28

c) G. Wolf, Ref. 28

d) SB , Ref. 4

e) Ref. 29, 30

f) SB , Ref. 16

Table II: Summary of ρ' Properties

Procedure	J^P	I^G	M (MeV)	Γ (MeV)	$\sigma(\rho^0\pi^+\pi^-)$	$\gamma^2_{\rho'}/4\pi$ [d]
$\gamma p \to \rho' p$, $\rho' \to \rho^0\pi^+\pi^-$ [a]	1^-	1^+	≈ 1500	≈ 600	$1.6 \pm 0.4\,\mu b$	3.9 ± 1.3
$e^+e^- \to \rho'$, $\rho' \to \rho^0\pi^+\pi^-$ [b]	1^-	1^+	≈ 1600	300-400	16 ± 5 nb	4.2 ± 1.3
$\pi^- p \to \underbrace{\pi^+\pi^-}_{\rho'} n$ [c]	1	1	1590 ± 20	180 ± 50	$\frac{\Gamma(\rho' \to \pi^+\pi^-)}{\Gamma(\rho' \to \text{all})} = 0.25 \pm 0.05$	

a) SB Ref. 16 and streamer chamber Ref. 11

b) Ref. 14

c) CERN-Munchen Ref. 27

c) Assuming only $\rho' \to \rho^0\pi^+\pi^-$ and $(\rho' \to \rho^0\pi^0\pi^0) = 1/2(\rho' \to \rho^0\pi^+\pi^-)$

Reaction $\gamma p \to \phi p$

Table III: Results of Fits to $\frac{d\sigma}{dt} = \left.\frac{d\sigma}{dt}\right|_{t=0} e^{At}$ for all t and for $|t| < 0.75$ GeV^2

E (GeV)	Group	all t: $d\sigma/dt_{t=0}$ ($\mu b/GeV^2$)	all t: A(GeV^{-2})	all t: $\chi^2/^\circ f$	$\|t\|<0.75$: $d\sigma/dt_{t=0}$ ($\frac{\mu b}{GeV}$)	$\|t\|<0.75$: A(GeV^{-2})	$\|t\|<0.75$: $\chi^2/^\circ f$
2	Bonn Ref. 55	1.47 $\pm$ 0.156	4.06 $\pm$ 0.24	8.1/3	same		
2.8/4.7	SBT Ref. 4	1.74 $\pm$ 0.48	4.2 $\pm$ 1.1	2.7/2	same		
8.5	Cornell Ref. 29	2.63 $\pm$ 0.34	5.45 $\pm$ 0.53	1.2/2	same		
9.3	SBT Ref. 4	2.32 $\pm$ 0.58	4.26 $\pm$ 0.88	0.33/2	same		
12	SLAC-Wisconsin Ref. 30	1.99 $\pm$ 0.37	4.43 $\pm$ 0.27	3.3/4	2.70 $\pm$ 0.72	5.13 $\pm$ 0.53	0.3/1
6.5	SLAC 1970 Ref. 33	1.88 $\pm$ 0.65	3.50 $\pm$ 0.55	6.6/6	1.58 $\pm$ 0.76	3.15 $\pm$ 0.83	6.0/4
11.5	"	1.71 $\pm$ 0.78	4.31 $\pm$ 0.75	1.0/2	1.95 $\pm$ 1.29	4.58 $\pm$ 1.22	0.9/1
13.0	"	1.61 $\pm$ 0.38	4.22 $\pm$ 0.41	9.3/8	1.79 $\pm$ 0.57	4.45 $\pm$ 0.65	7.6/6
14.5	"	1.43 $\pm$ 0.35	4.09 $\pm$ 0.46	7.5/7	1.40 $\pm$ 0.41	4.05 $\pm$ 0.57	7.5/6
16.0	"	0.60 $\pm$ 0.22	3.16 $\pm$ 0.44	2.3/5	0.89 $\pm$ 0.54	3.91 $\pm$ 1.13	0.08/2

Table IV: ρ^o- density matrix elements in the helicity system from events of the reaction $\gamma_v\, p \to \pi^+\pi^-\, p$ in the ρ^o region $0.6 < M_{\pi\pi} < 0.9$ GeV for $|t| < 0.6$ GeV^2 [a]

	DESY[b]: $2.2 < W < 2.8$ GeV $0.3 < Q^2 < 1.5$ GeV^2	SLAC[c]: $2.5 < W < 5$ GeV $0.2 < Q^2 < 2.5$ GeV^2	Prediction from SCHC[e]
r^{04}_{00}	0.215 ± 0.039 [d]	0.330 ± 0.093	$\epsilon R/(1+\epsilon R)$
Re r^{04}_{10}	0.047 ± 0.040	0.041 ± 0.057	0
r^{04}_{1-1}	-0.050 ± 0.061	-0.091 ± 0.083	0
r^{1}_{00}	0.082 ± 0.108	0.383 ± 0.160	0
r^{1}_{11}	-0.066 ± 0.077	-0.033 ± 0.100	0
Re r^{1}_{10}	0.076 ± 0.062	0.200 ± 0.093	0
r^{1}_{1-1}	0.333 ± 0.098	0.31 ± 0.13	$0.5/(1+\epsilon R)$
Im r^{2}_{10}	-0.014 ± 0.059	-0.095 ± 0.088	0
Im r^{2}_{1-1}	-0.247 ± 0.093	-0.37 ± 0.12	$-0.5/(1+\epsilon R)$
r^{5}_{00}	-0.000 ± 0.052	0.068 ± 0.065	0
r^{5}_{11}	-0.020 ± 0.036	-0.081 ± 0.047	0
Re r^{5}_{10}	0.080 ± 0.032	0.127 ± 0.039	$\frac{\sqrt{R/8}}{(1+\epsilon R)} \cos\delta$
r^{5}_{1-1}	-0.006 ± 0.049	0.120 ± 0.067	0
Im r^{6}_{10}	-0.089 ± 0.031	-0.139 ± 0.048	$-\frac{\sqrt{R/8}}{(1+\epsilon R)} \cos\delta$
Im r^{6}_{1-1}	0.032 ± 0.047	0.00 ± 0.06	0

a) For the DESY data $0.6 < M_{\pi\pi} < 0.85$ GeV and $|t| < 0.5$ GeV^2 was used.

b) DESY Streamer chamber Ref. 68.

c) SLAC Bubble chamber Ref. 66.

d) Determined by a maximum likelihood fit to the Dalitz plot density.

e) $R = \sigma_L/\sigma_T$: actually ϵ should be replaced by $(\epsilon + \Delta)$ where $\Delta = 2M_\rho^2(1-\epsilon)/Q^2 \ll 1$.

Figure Captions

1. The mass spectrum of $\pi^+\pi^-$ pairs photoproduced on carbon. Figure taken from Ref. 10.

2. Four-pion invariant mass distribution from the SLAC streamer chamber experiment on the reaction $\gamma p \longrightarrow \pi^+\pi^-\pi^+\pi^- p$. Figure taken from Ref. 11.
   (a) All events
   (b) Events not containing a Δ^{++}
   (c) Events not containing a Δ^{++} but including a ρ^0

3. Cross section for the reaction $e^+e^- \longrightarrow 4\pi^\pm$. Data taken from Ref. 13, 15.

4. Reaction $\gamma p \longrightarrow \pi^+\pi^-\pi^+\pi^- p$: Differential cross section versus momentum-transfer ($t' = t - t_{min}$) for $6 < E_\gamma < 18$ GeV for events in the ρ' region. Data of the SLAC streamer chamber group. Figure taken from Ref. 11.

5. Reaction $\gamma p \longrightarrow \pi^+\pi^-\pi^+\pi^- p$: Top, distribution of the angles θ and ψ for $M_{4\pi} < 1.7$ GeV; bottom, Π uncorrected for analyzer efficiency. Data of SB. Figure taken from Ref. 16.

6. Reaction $\gamma p \longrightarrow \pi^+\pi^-\pi^+\pi^- p$: $4\pi^\pm$ mass distribution divided by 5-body phase space weighted by the ρ^0 Breit-Wigner to account for $(\rho^0\pi^+\pi^-)p$ phase space. Curve gives the shape of the ρ^0 Breit-Wigner.

7. Reaction $\gamma p \longrightarrow \pi^+\pi^-\pi^+\pi^- p$: Top, model for the ρ' in terms of a Deck effect; below, comparison of t and mass spectra for the data with the prediction of Deck effect model. Figure taken from Ref. 26.

8. Reaction $\pi^- p \longrightarrow \pi^-\pi^+ n$ at 17.2 GeV/c. Data of CERN-MÜNCHEN Collaboration.
   (a) $\pi\pi$ phase shift δ_1^1 and elasticity η_1^1 in the energy range $600 \leq M_{\pi\pi} < 1900$ MeV for isospin 1, P-wave
   (b) Argand diagrams (Im T^I versus Re T^I) for the partial wave amplitudes from the energy-dependent fit. Numbers indicate the $\pi\pi$ energy. Figure taken from Ref. 27.

9. Reaction $\pi^- p \to \pi^- \pi^+ n$: Data of CERN-MÜNCHEN Collaboration. $\pi\pi$ angular distribution moments in the region between $M_{\pi\pi} = 1400$ and 1800 MeV, and comparison of two mass-dependent fits. The full line includes a second resonance in the P-wave. The broken line is the result without including a second resonance in the P-wave; this fit is seen not to reproduce well the Y_0^0, Y_1^0, and Y_2^0 moments. The dots are reconstructed from the energy independent analysis and follow closely the drop at 1450 MeV. Figure taken from Ref. 27.

10. Reaction $\gamma p \to p\pi^+\pi^-$ + neutrals at 2.8, 4.7, and 9.3 GeV. $\pi^+\pi^-$ MM mass distribution for

    (a) $|t| < 0.5$ GeV^2.

    (b) $0.5 < |t| < 1$ GeV^2. Events with $0.32 < M_{\pi^+\pi^-} < 0.6$ GeV (ω^0 like) are shaded. Figure taken from Ref. 32.

11. Reaction $\gamma p \to p\pi^+\pi^-$ MM at 9.3 GeV. Differential cross section $d\sigma/dt$ for events in the "B" region. Figure taken from Ref. 32.

12. Reaction $\gamma p \to p$"B". The point labelled "SLAC-Berkeley" comes from the SLAC-Berkeley experiment and has been obtained from a fit with a "B" width of 150 MeV and an $\omega\pi^0$ background, according to an OPE calculation of G. Wolf. The cross sections have been corrected for the decays $\omega \to$ neutrals. The point labelled "SLAC spectrometer $\Gamma = 100$ MeV" has been extrapolated from differential cross sections given in Ref. 33. The point labeled "$\Gamma = 150$ MeV" was obtained by scaling the above point by a factor 1.5. Figure taken from Ref. 32.

13. Reaction $\gamma p \to p\omega\pi^0$: Diagrams for a non-resonant Deck effect.

14. Reaction $\gamma p \to p\pi^+\pi^-$MM at 9.3 GeV. $\pi^+\pi^-$MM mass distribution for $|t| <$ 0.5 GeV with $0.6 < M_{\pi^+\pi^-} < 0.9$ GeV (ρ^0 MM like).

15. Reaction $\gamma C \rightarrow \pi^+\pi^-C$: The $\pi^+\pi^-$ mass distribution at the two indicated energy intervals. Figure taken from Ref. 44.

16. Reaction $\gamma A \rightarrow \rho^0 A$ for $A = H_2$ and Carbon: $\pi^+\pi^-$ mass skewing parameter n as a function of momentum transfer. Data of Ref. 3, 34, 44.

17. Reaction $\gamma p \rightarrow \rho^0 p$: The differential cross section, $d\sigma/dt$, for $0.5 < M_{\pi\pi} < 1.0$ GeV. The solid line is the result of a Söding fit (a) - (d) for the indicated photon energy intervals. Figure taken from Ref. 45.

18. Reaction $\gamma p \rightarrow \rho^0 p$: Energy dependence of the exponential slope. Rho differential cross section obtained from the standard method suggested by Yennie. Data from Ref. 48 (SWT), 4 (SB), 29 (Cornell), and 45 (SLAC).

19. Reaction $\gamma p \rightarrow \rho^0 p$: Differential cross section for $|t| < 0.15$ GeV. Comparison of SB data and the SLAC-$\pi^+\pi^-$ spectrometer data for photon energies ~ 9.3 GeV. Data taken from Ref. 4 and 45.

20. Energy dependence of the slope of elastic $\pi^\pm$, $K^\pm$, $p^\pm$ scattering in hydrogen. Figure taken from Ref. 1.

21. (a) Fits of $d\sigma/dt$ of ρ^0 photoproduction to sum of P and f exchange, utilizing the dual absorptive model.

    (b, c) Pomeron and f exchange amplitude slopes as obtained from fits of $d\sigma/dt$. Dash curve shows the results obtained by Davier from πp elastic scattering. Figure taken from Ref. 51.

22. Helicity amplitudes for $\gamma p \rightarrow \pi^+\pi^- p$ $(M_{\pi^+\pi^-} \sim M_\rho)$ $\left(2\, \mathrm{Re}_{10}^{N}\right)$ and $\pi N\left(|F_{+-}^{0}|/|F_{++}^{0}|\right)$ scattering. Figure taken from Ref. 51.

23. Reaction $\gamma p \rightarrow \phi p$ at 2.8, 4.7, 9.3 GeV. Decay angular distribution of $K\bar{K}$ pairs in the helicity system in the ϕ mass region and $0.02 < |t| < 0.8$ GeV^2. The curves are calculated for an s-channel helicity conserving production amplitude. Figure taken from Ref. 4.

24. Reaction $\gamma p \to \phi p$: Bonn data at 2 GeV together with the bubble chamber data of ABBHHM Collaboration, 1.8 - 2.5 GeV (Ref. 55).

25. Reaction $\gamma p \to \phi p$ differential cross section.

(a) 2.8 + 4.7 GeV of SBT, ABBHHM from 2.5 - 5.8 GeV and DESY-MIT, 6.2 GeV.

(b) 9.3 GeV SB, Cornell at 8.5 GeV and SLAC-Wisconsin spectrometer experiment at ~ 12 GeV.

Figure taken from Ref. 4.

26. Reaction $\gamma p \to \phi p$. s-dependence of $d\sigma/dt$ at $t = -0.6$ GeV. Data of SLAC-Wisconsin[30] and Bonn.[55]

27. Reaction $\gamma p \to \phi p$. Differential cross section for the high statistic counter data. Data of Ref. 29, 30, 55, and 61.

28. Reaction $K^{\pm}p \to K^{\pm}p$ and $pp \to pp$: Differential cross section for $t = -0.6$ GeV^2.

29. Reaction $\gamma p \to \phi p$. s-dependence of

(a) exponential slope A.

(b) $d\sigma/dt$ at $t = 0$.

Full curve is a fit to $A = A_0 + 2\alpha' \ln(s/s^0)$. The dashed curve is the result of Chadwick et al.[51] for the s-dependence of the Pomeron amplitude (times factor 2) of Fig. 21.

30. Reaction $pp \to pp$: Experimental slope parameter A (denoted b on figure) as a function of the center of mass energy s. Figure taken from Ref. 49.

31. Reaction $\gamma_V p \to \pi^+\pi^- p$: $\pi^+\pi^-$ mass distribution data from Ref. 66, 67, and 68.

32. Reaction $\gamma_V p \to \pi^+\pi^- p$: $\pi^+\pi^-$ mass distributions for the three indicated Q^2 intervals. Figure taken from Ref. 66 (SLAC bubble chamber data).

33. Reaction $\gamma_V p \to \rho^o p$: Q^2-dependence of $\sigma(\gamma_V p \to \rho^o p)/\sigma_{total}$ data of Ref. 66, 67, and 68.

34. Reaction $\gamma_V p \to \rho^o p$: Q^2-dependence of $\sigma(\gamma_V p \to \rho^o p)$ for two energy intervals. The curves were calculated using the given expressions. The factor $p^*(0)/p^*(Q^2)$ enters because of the difference in photon flux (see Ref. 68). Data of Ref. 67, 68, 70, and 71. $\sigma(\rho)_{Q^2=0} = 13.3 \pm 0.5\,\mu b$ for the higher energy data of Dakin et al.

35. Reaction $ep \to ep\rho^o$: Definition of decay angles θ_H, ψ_H in the helicity system for forward ρ^o production. Figure taken from Ref. 18.

36. Reaction $\gamma p \to \pi^+\pi^- p$: Decay angular distributions in the helicity system for events in the ρ region. Figure taken from Ref. 4.

37. Reaction $\gamma_V p \to \pi^+\pi^- p$: Decay angular distributions in the helicity system for events in the ρ region.

    (a) Figure taken from Ref. 66, SLAC bubble chamber data.

    (b) Figure taken from Ref. 68, DESY streamer chamber data.

    (c) Scatter plots of the data as a function of ψ and $\cos\theta$. The top plot is of the raw data and the bottom plot is of data approximately corrected for geometrical acceptance. Figure taken from Ref. 67, SLAC WAS.

38. Reaction $\gamma_V p \to \rho^o p$: $R = \sigma_L/\sigma_T$ and $\cos\delta$ the longitudinal (L)-transverse (T) phase difference assuming s-channel helicity conservation. The curves show predictions from vector dominance models with $\sigma_L = \sigma_T$ (----) and $\sigma_L = 0.35\,\sigma_T$ (-.-.) for the $\rho^o p \to \rho^o p$ cross section. Data taken from Ref. 66, 67, 68. Note: $\cos\delta$ determined by the method of moments for DESY result.

39. Reaction $\gamma p \to \pi^+\pi^- p$: Mass skewing parameter n from $BW_\rho\left(\frac{m_\rho}{m_{\pi\pi}}\right)^n$ as a function of Q^2. Figure taken from Ref. 66.

40. Reaction $\gamma_V p \rightarrow \pi^+\pi^-\pi^o p$: $M_{\pi^+\pi^-\pi^o}$ mass distribution for $Q^2 > 0$. Data of Ref. 66 and 68.

41. Reaction $\gamma_V p \rightarrow \omega p$.

    (a) $\sigma(\gamma_V p \rightarrow \omega p)/\sigma_{TOT}$ versus Q^2 for the SLAC-HBC data. Figure taken from Ref. 66.

    (b) $\sigma(\gamma_V p \rightarrow \omega p)$ versus Q^2 for the DEST STC data. Figure taken from Ref. 68.

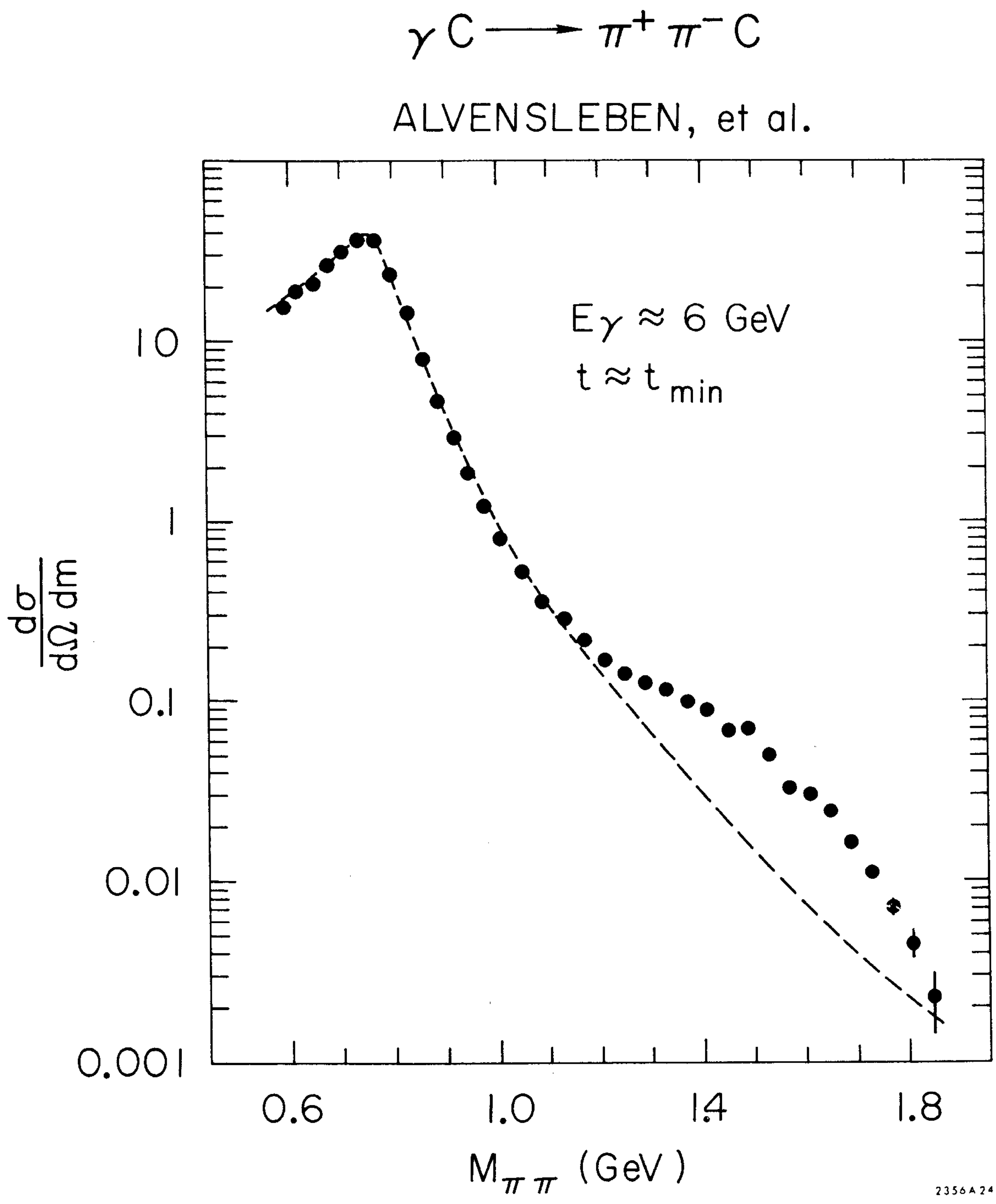

$\gamma C \longrightarrow \pi^+ \pi^- C$
ALVENSLEBEN, et al.
$E\gamma \approx 6$ GeV
$t \approx t_{min}$
10
1
0.1
0.01
0.001
$\frac{d\sigma}{d\Omega\, dm}$
0.6
1.0
1.4
1.8
$M_{\pi\pi}$ (GeV)
2356A24

Fig. 1

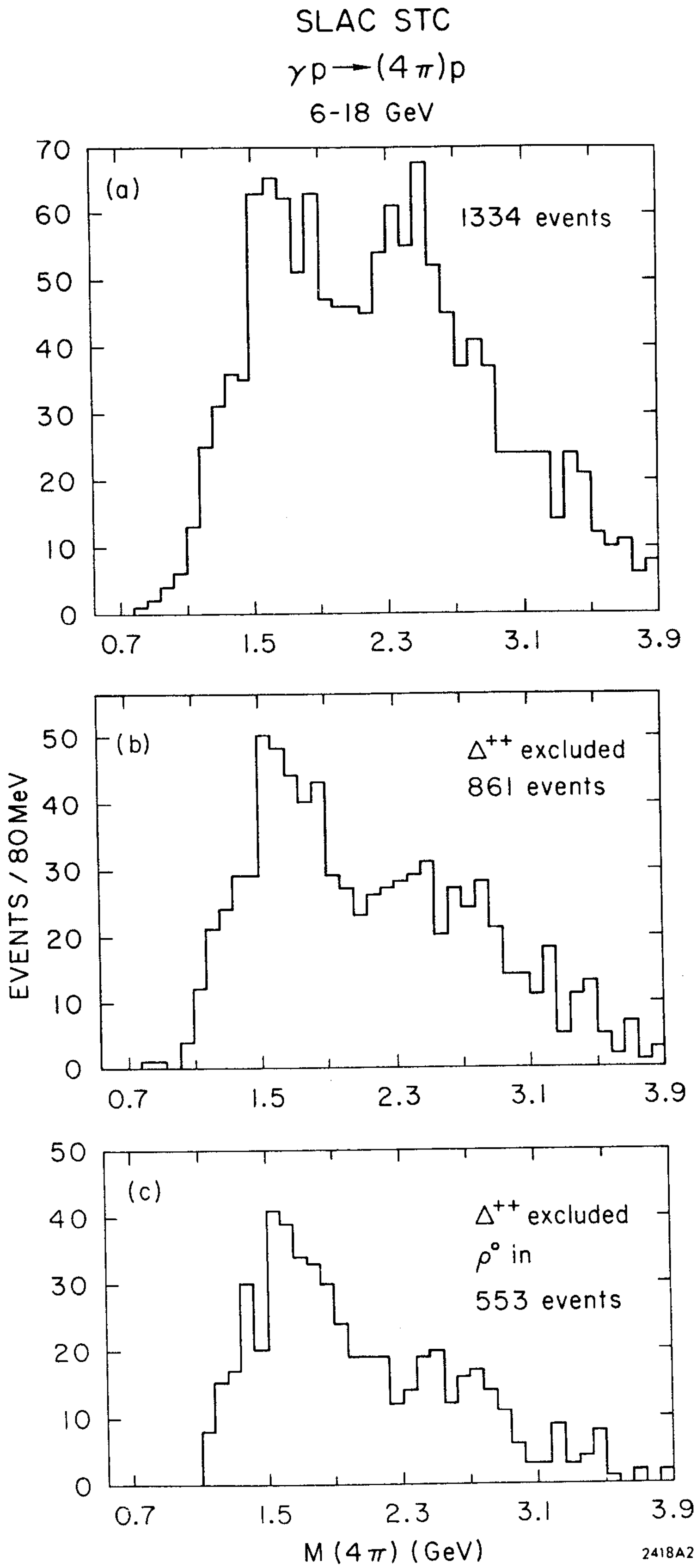

SLAC STC
γp → (4π)p
6-18 GeV
(a)
1334 events
(b)
Δ++ excluded
861 events
EVENTS / 80 MeV
(c)
Δ++ excluded
ρ° in
553 events
M (4π) (GeV)
2418A2

Fig. 2

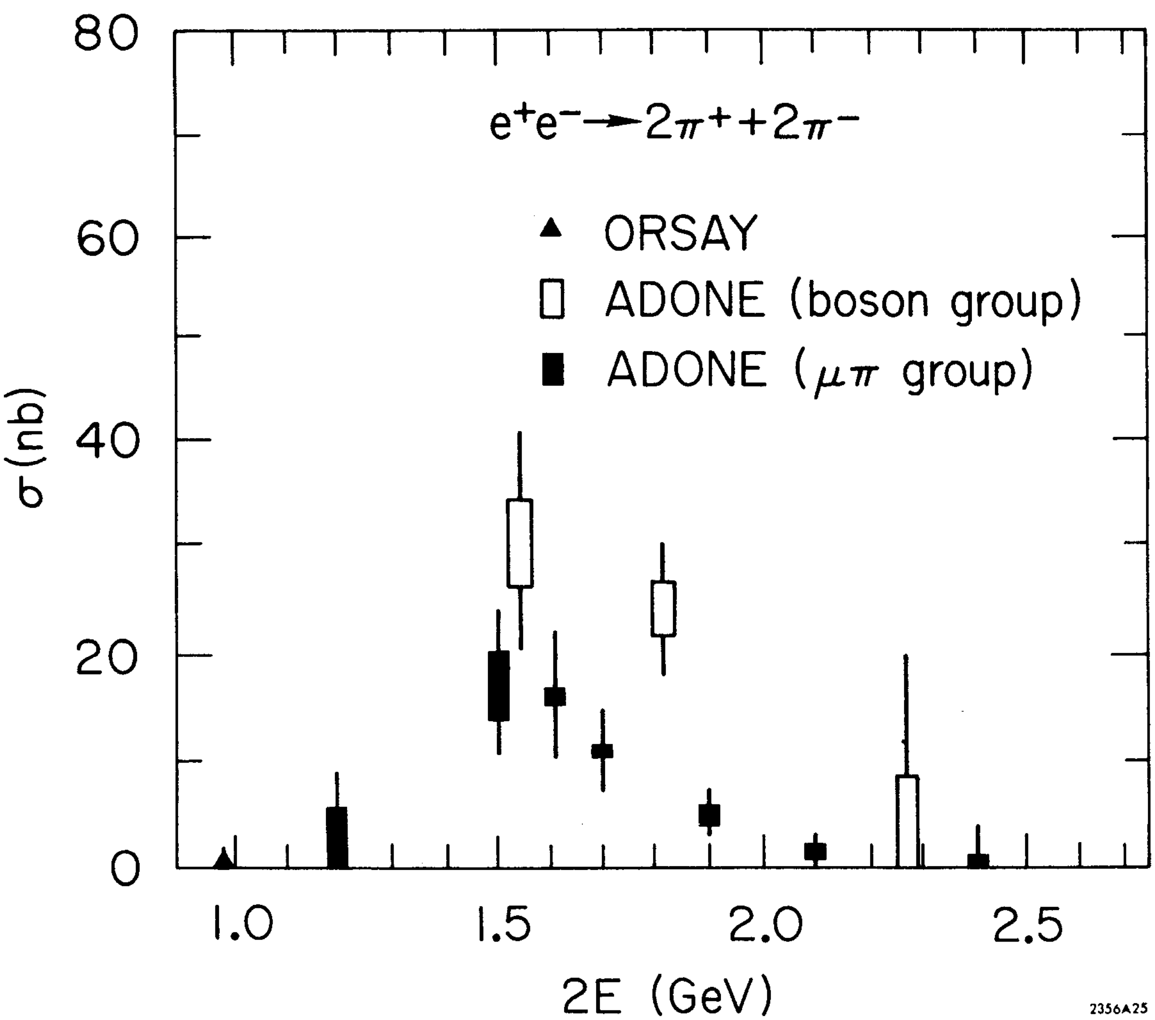

80
60
40
20
0
σ (nb)
$e^+e^- \to 2\pi^+ + 2\pi^-$
ORSAY
ADONE (boson group)
ADONE ($\mu\pi$ group)
1.0
1.5
2.0
2.5
2E (GeV)
2356A25

Fig. 3

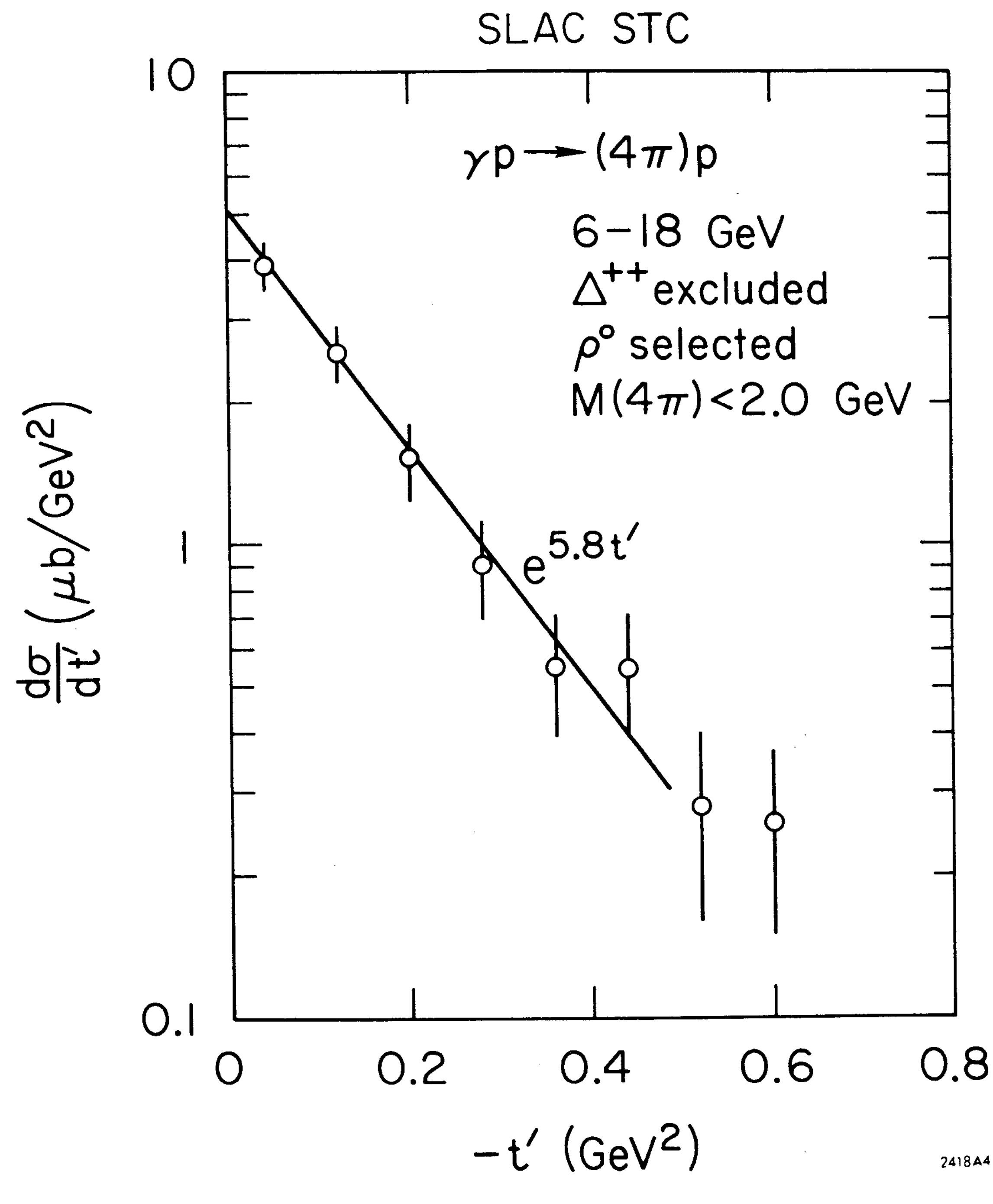

SLAC STC
10
1
0.1
$\gamma p \rightarrow (4\pi)p$
6–18 GeV
Δ^{++} excluded
ρ^{o} selected
$M(4\pi)<2.0$ GeV
$e^{5.8t'}$
$\frac{d\sigma}{dt'}$ (μb/GeV^2)
0
0.2
0.4
0.6
0.8
$-t'$ (GeV^2)
2418A4

Fig. 4

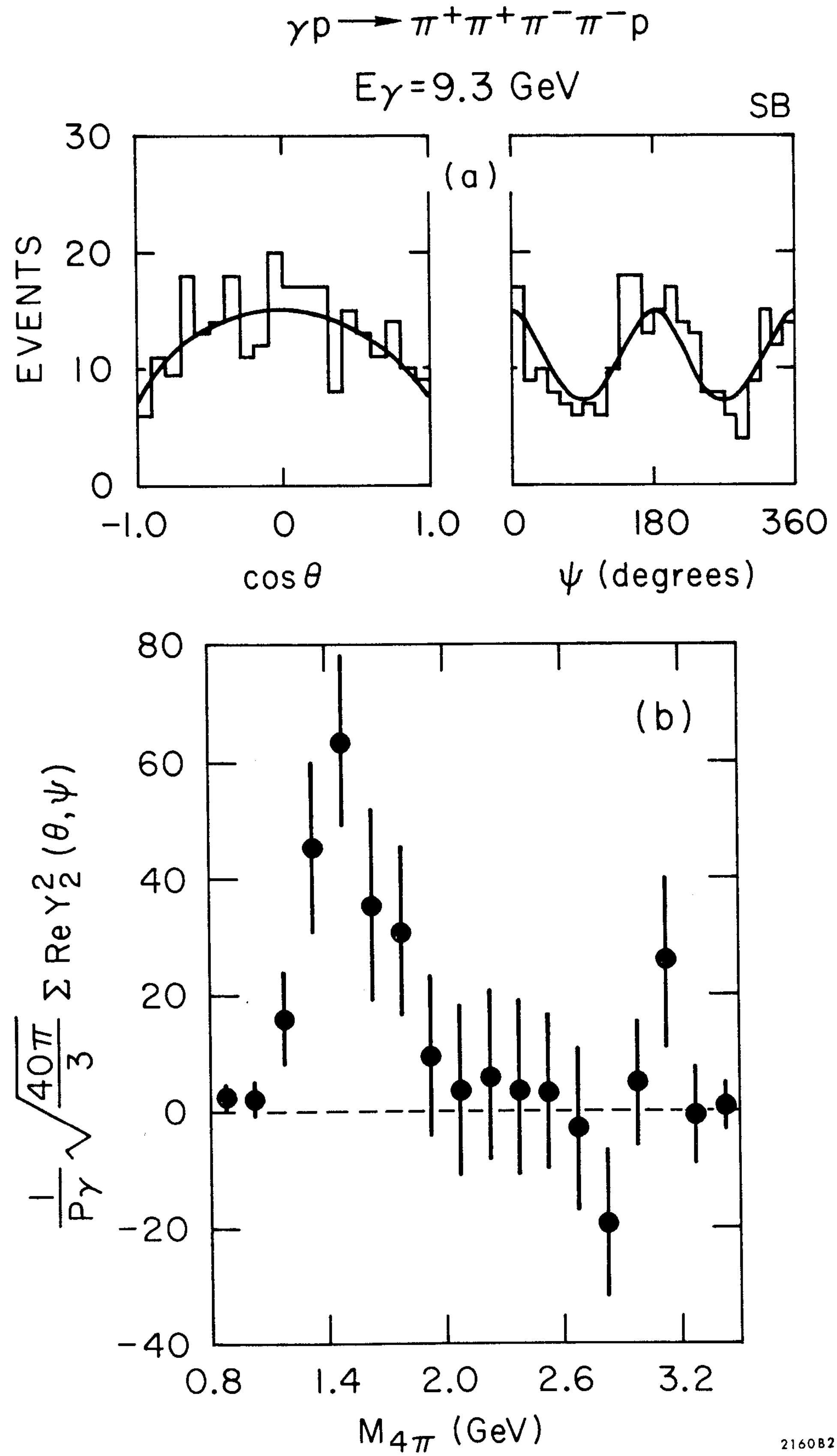

γp → π⁺π⁺π⁻π⁻p
Eγ = 9.3 GeV
SB
(a)
EVENTS
30
20
10
0
-1.0
0
1.0
cos θ
0
180
360
ψ (degrees)
(b)
80
60
40
20
0
-20
-40
0.8
1.4
2.0
2.6
3.2
M4π (GeV)
216082

Fig. 5

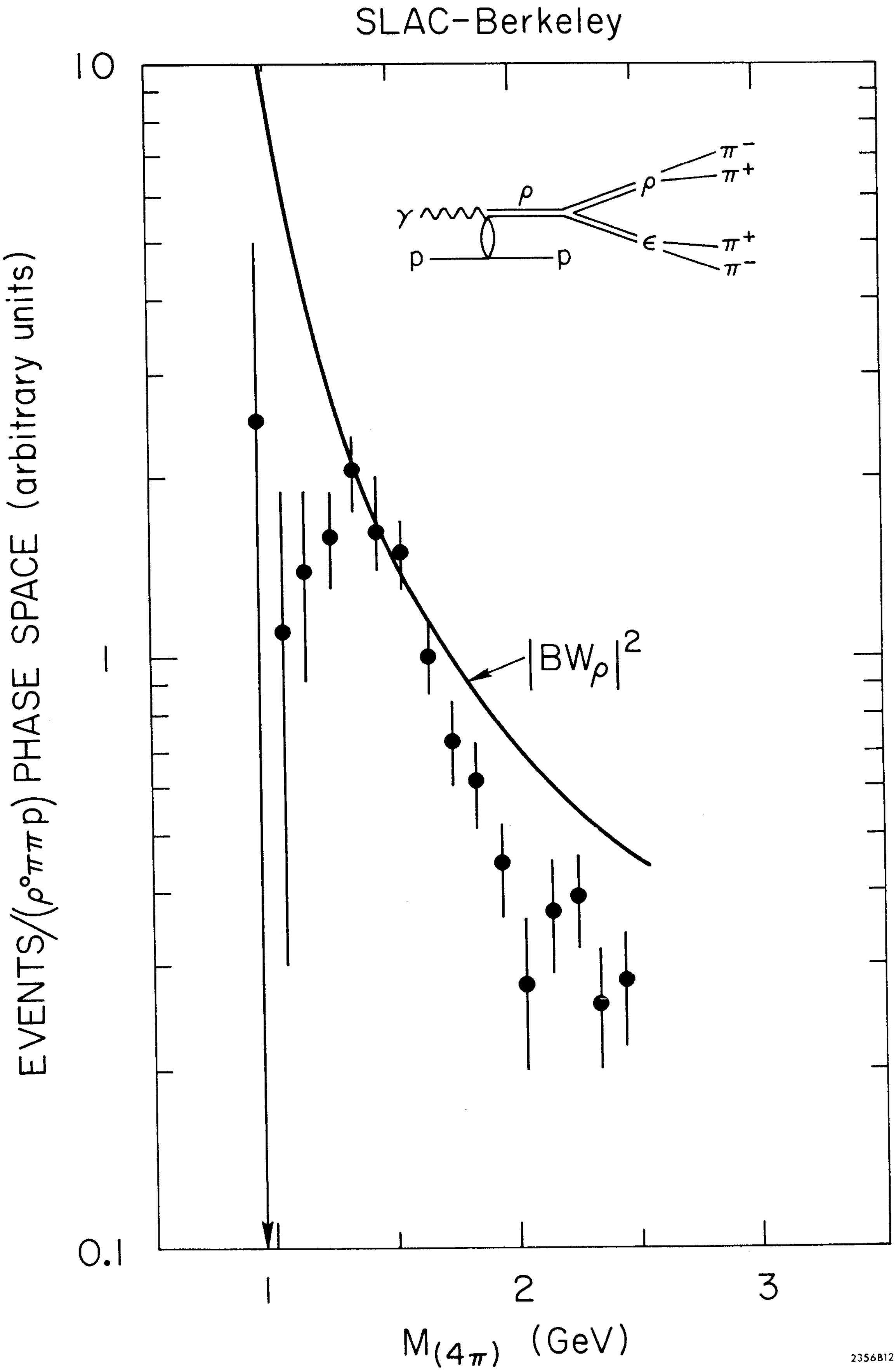

SLAC-Berkeley
10
1
0.1
EVENTS/($\rho^\circ\pi\pi$p) PHASE SPACE (arbitrary units)
γ
p
ρ
p
ρ
π^-
π^+
ϵ
π^+
π^-
$|BW_\rho|^2$
1
2
3
$M_{(4\pi)}$ (GeV)
2356B12

Fig. 6

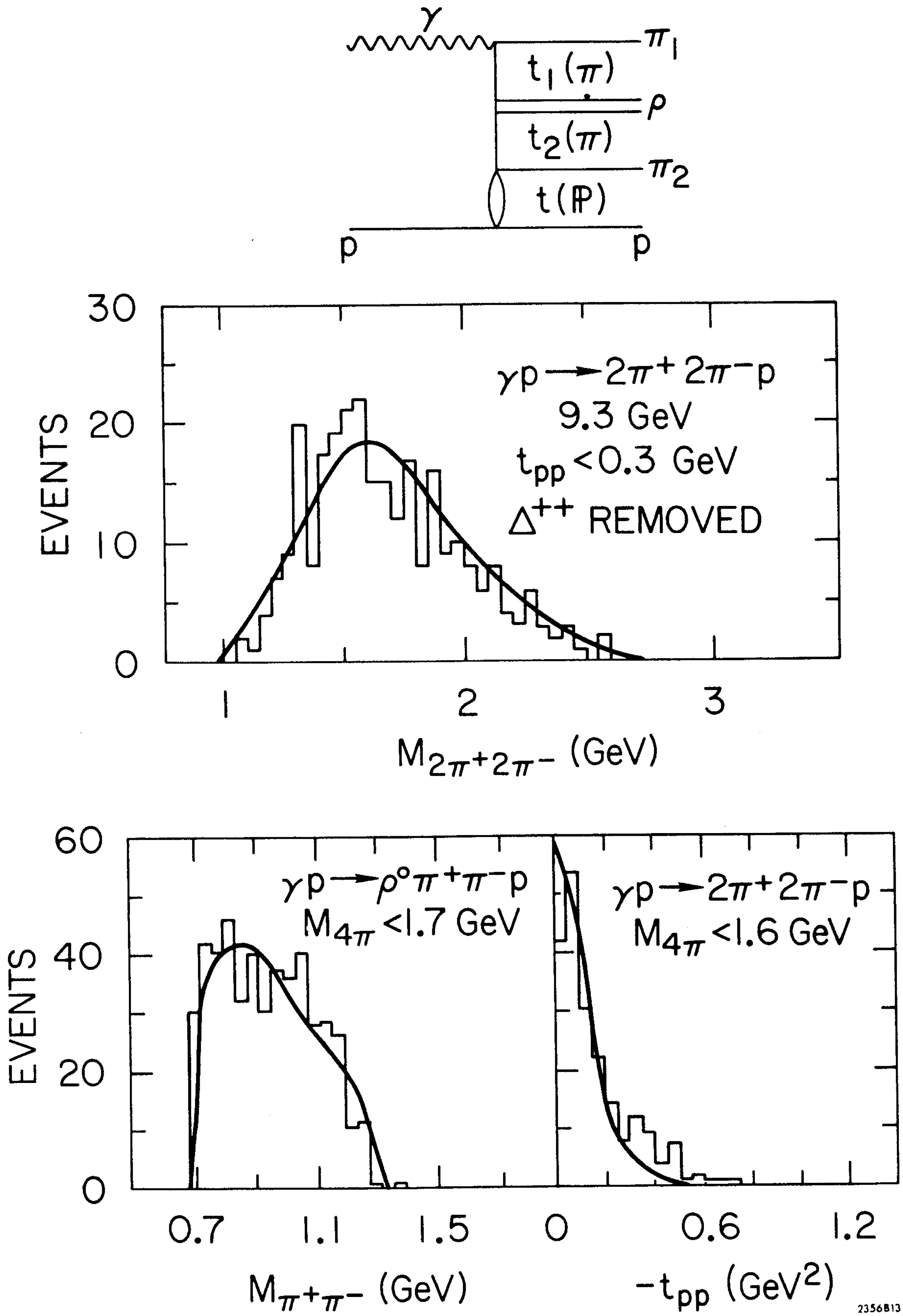

γ
π1
t1(π)
ρ
t2(π)
π2
t(IP)
p
p
γp → 2π+2π−p
9.3 GeV
tpp <0.3 GeV
Δ++ REMOVED
EVENTS
M2π+2π− (GeV)
γp → ρ°π+π−p
M4π <1.7 GeV
γp → 2π+2π−p
M4π <1.6 GeV
EVENTS
Mπ+π− (GeV)
−tpp (GeV2)
2356B13

Fig. 7

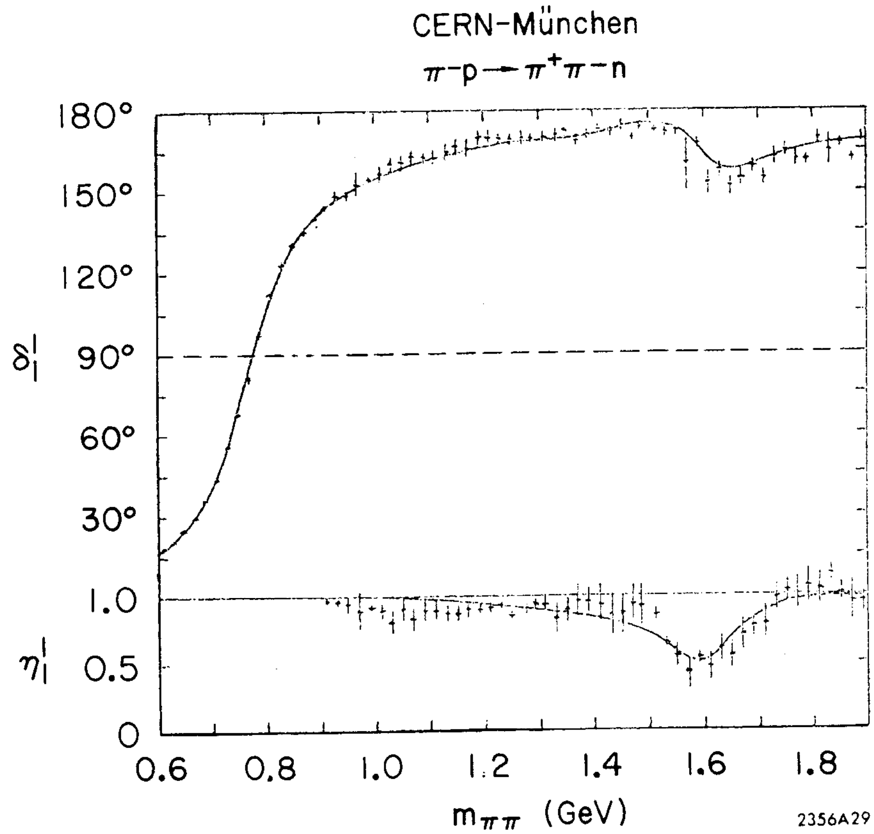

CERN-München
$\pi^- p \rightarrow \pi^+ \pi^- n$
180°
150°
120°
δ_1^1
90°
60°
30°
1.0
η_1^1
0.5
0
0.6
0.8
1.0
1.2
1.4
1.6
1.8
$m_{\pi\pi}$ (GeV)
2356A29

Fig. 8a

CERN-München

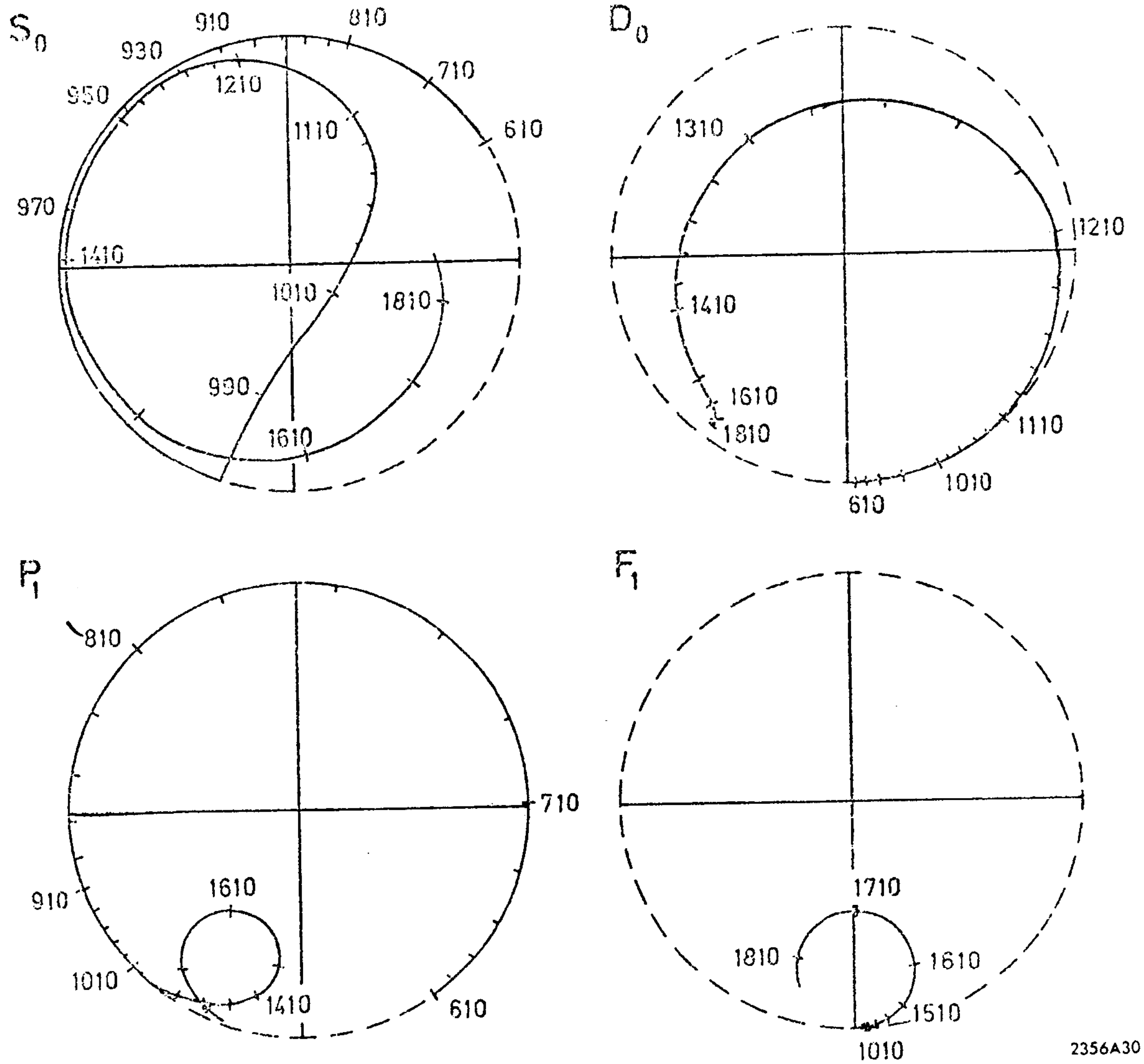

Fig. 8b

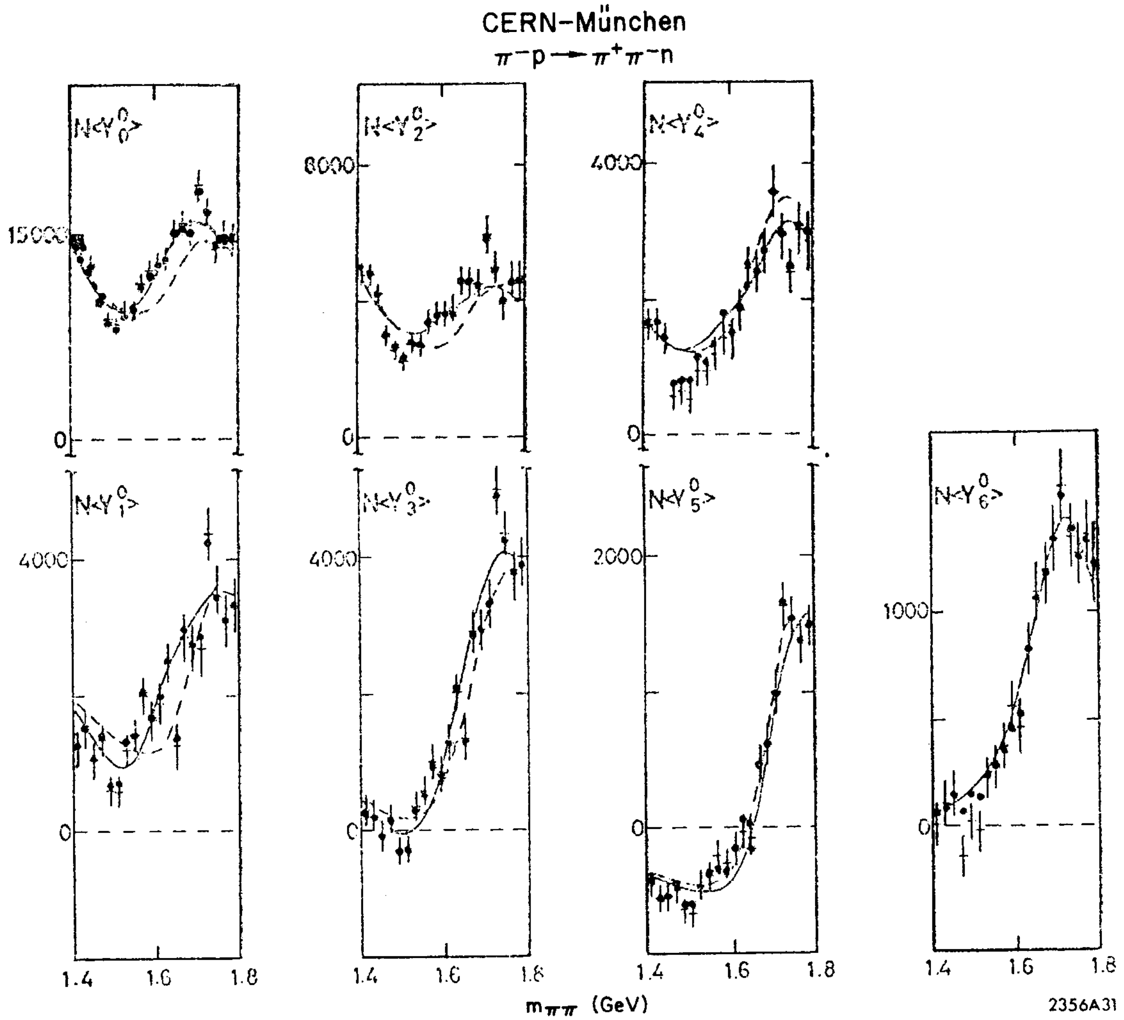

CERN–München
$\pi^- p \to \pi^+ \pi^- n$
$N\langle Y_0^0\rangle$
15000
0
$N\langle Y_2^0\rangle$
8000
0
$N\langle Y_4^0\rangle$
4000
0
$N\langle Y_1^0\rangle$
4000
0
$N\langle Y_3^0\rangle$
4000
0
$N\langle Y_5^0\rangle$
2000
0
$N\langle Y_6^0\rangle$
1000
0
1.4
1.6
1.8
$m_{\pi\pi}$ (GeV)
2356A31

Fig. 9

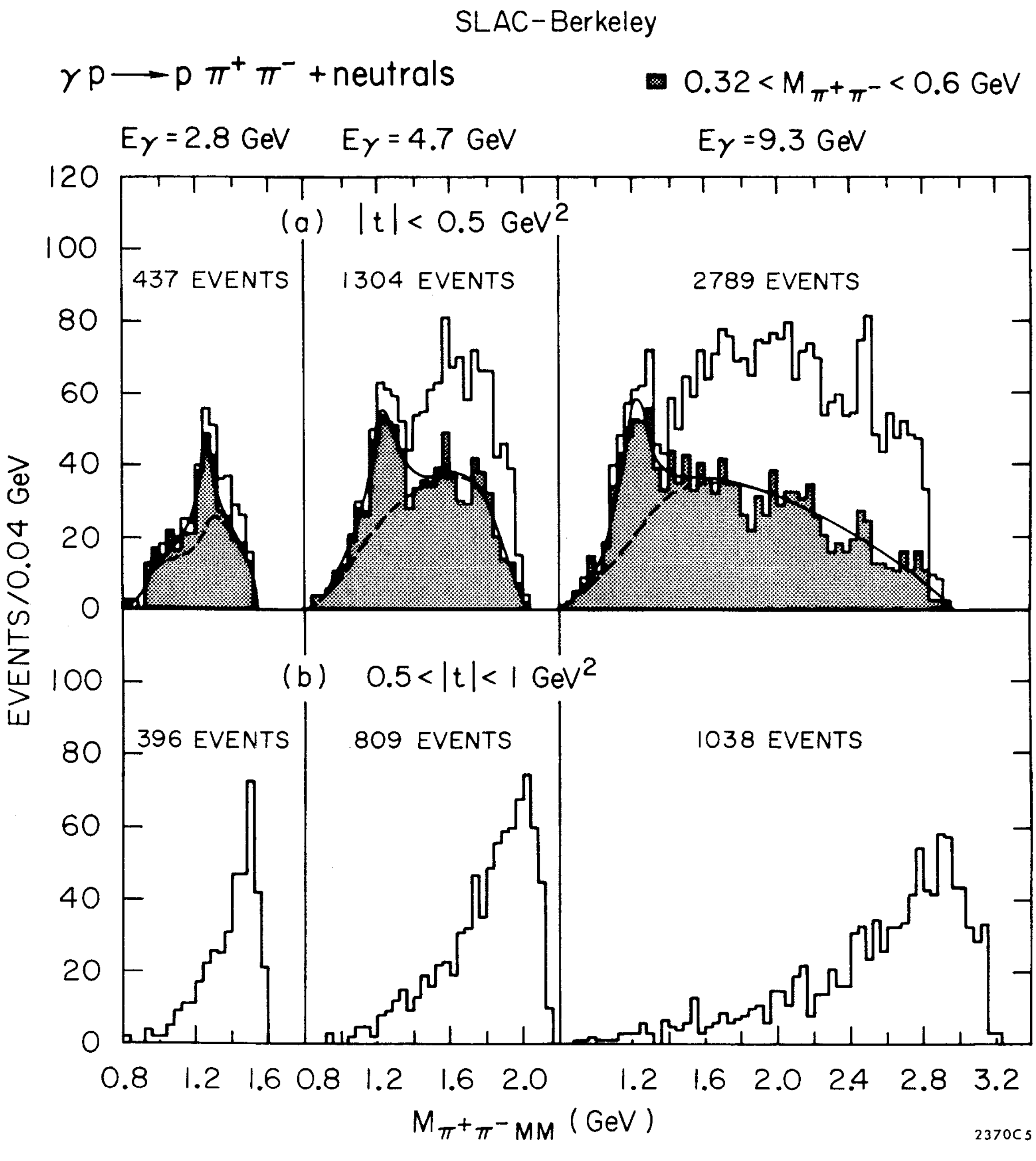
SLAC-Berkeley
$\gamma p \longrightarrow p\,\pi^+\pi^-$ + neutrals
$0.32 < M_{\pi^+\pi^-} < 0.6$ GeV
$E_\gamma = 2.8$ GeV
$E_\gamma = 4.7$ GeV
$E_\gamma = 9.3$ GeV
(a) $|t| < 0.5$ GeV^2
437 EVENTS
1304 EVENTS
2789 EVENTS
(b) $0.5 < |t| < 1$ GeV^2
396 EVENTS
809 EVENTS
1038 EVENTS
EVENTS/0.04 GeV
$M_{\pi^+\pi^-MM}$ (GeV)
2370C5

Fig. 10

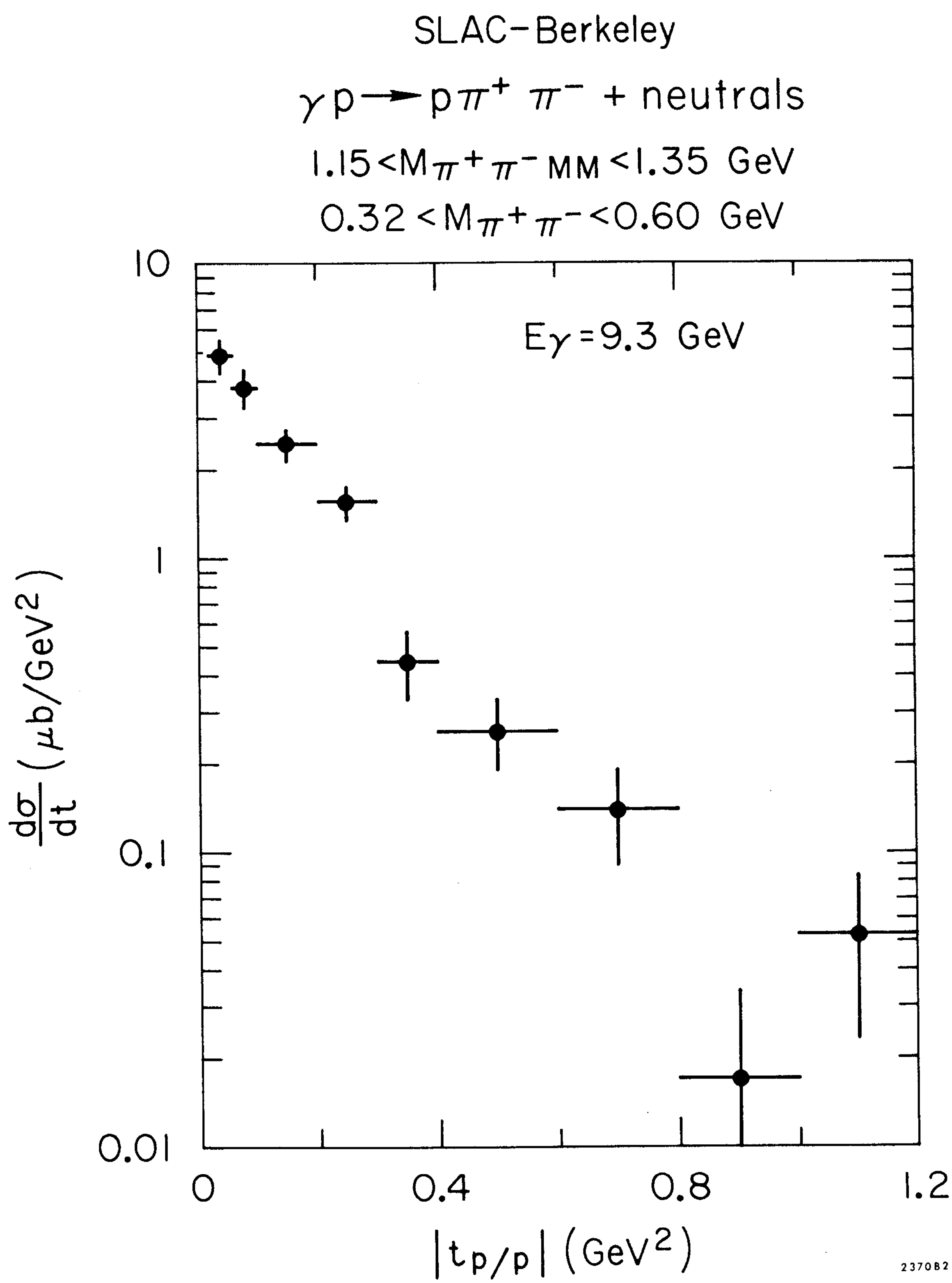

SLAC-Berkeley
$\gamma p \to p\pi^+ \pi^- +$ neutrals
$1.15 < M_{\pi^+\pi^- MM} < 1.35$ GeV
$0.32 < M_{\pi^+\pi^-} < 0.60$ GeV
$E\gamma = 9.3$ GeV
$\frac{d\sigma}{dt}$ (μb/GeV^2)
10
1
0.1
0.01
0
0.4
0.8
1.2
$|t_{p/p}|$ (GeV^2)
2370B2

Fig. 11

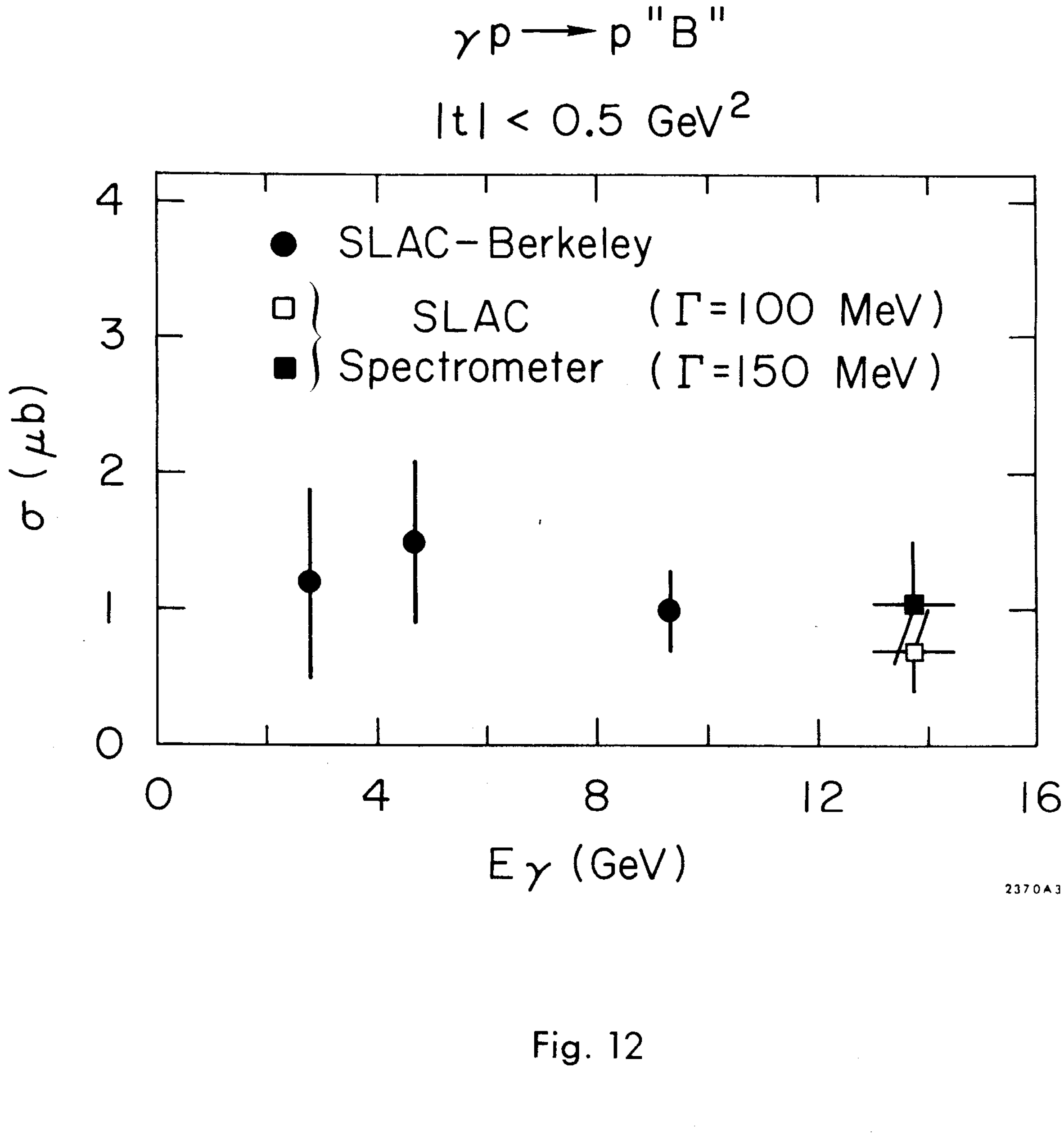

$\gamma p \longrightarrow p$ "B"
$|t| < 0.5$ GeV^2
SLAC-Berkeley
SLAC Spectrometer
(Γ=100 MeV)
(Γ=150 MeV)
σ (μb)
0
1
2
3
4
0
4
8
12
16
Eγ (GeV)
2370A3

Fig. 12

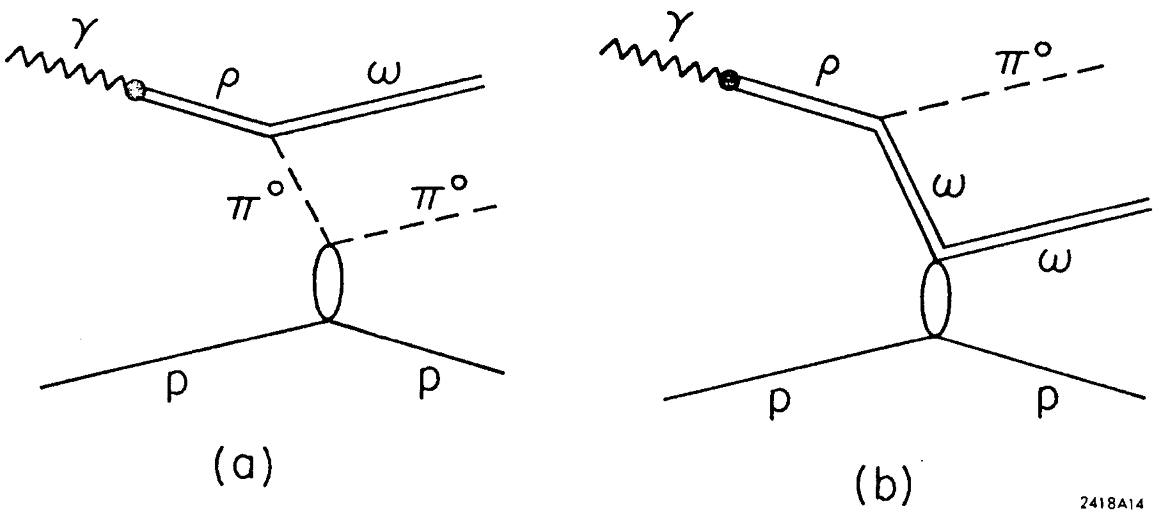

Fig. 13

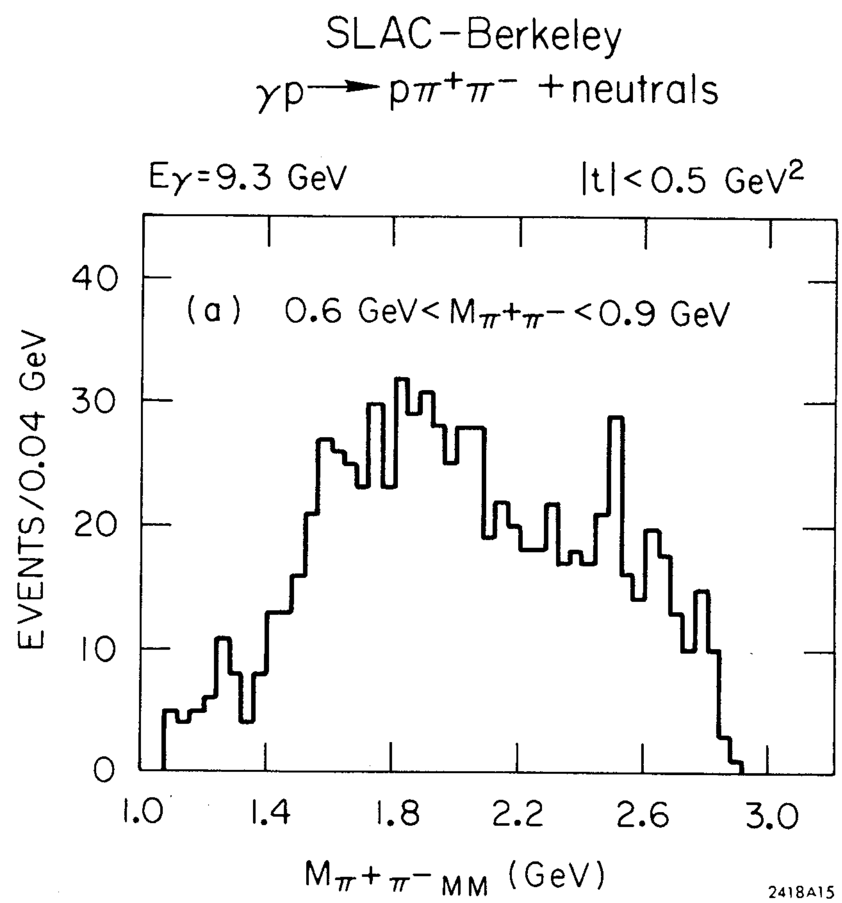
SLAC-Berkeley
$\gamma p \rightarrow p\pi^+\pi^-$ +neutrals
$E\gamma$=9.3 GeV
$|t|<0.5$ GeV^2
(a) 0.6 GeV< $M_{\pi^+\pi^-}$ <0.9 GeV
EVENTS/0.04 GeV
0
10
20
30
40
1.0
1.4
1.8
2.2
2.6
3.0
$M_{\pi^+\pi^-MM}$ (GeV)
2418A15

Fig. 14

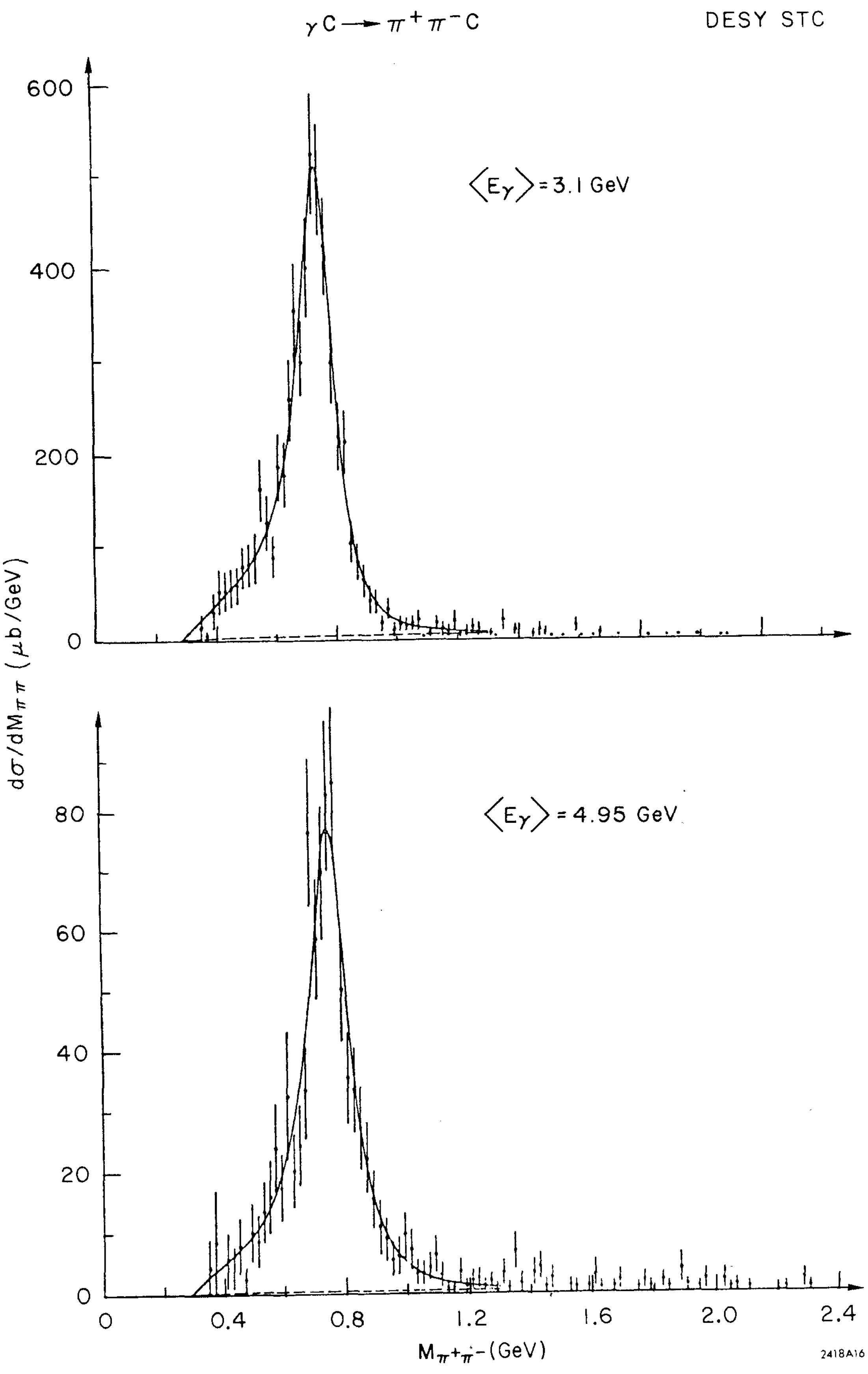

$\gamma C \rightarrow \pi^+ \pi^- C$
DESY STC
$\langle E_\gamma \rangle = 3.1$ GeV
$\langle E_\gamma \rangle = 4.95$ GeV
$d\sigma/dM_{\pi\pi}$ (μb/GeV)
600
400
200
0
80
60
40
20
0
0
0.4
0.8
1.2
1.6
2.0
2.4
$M_{\pi^+\pi^-}$ (GeV)
2418A16

Fig. 15

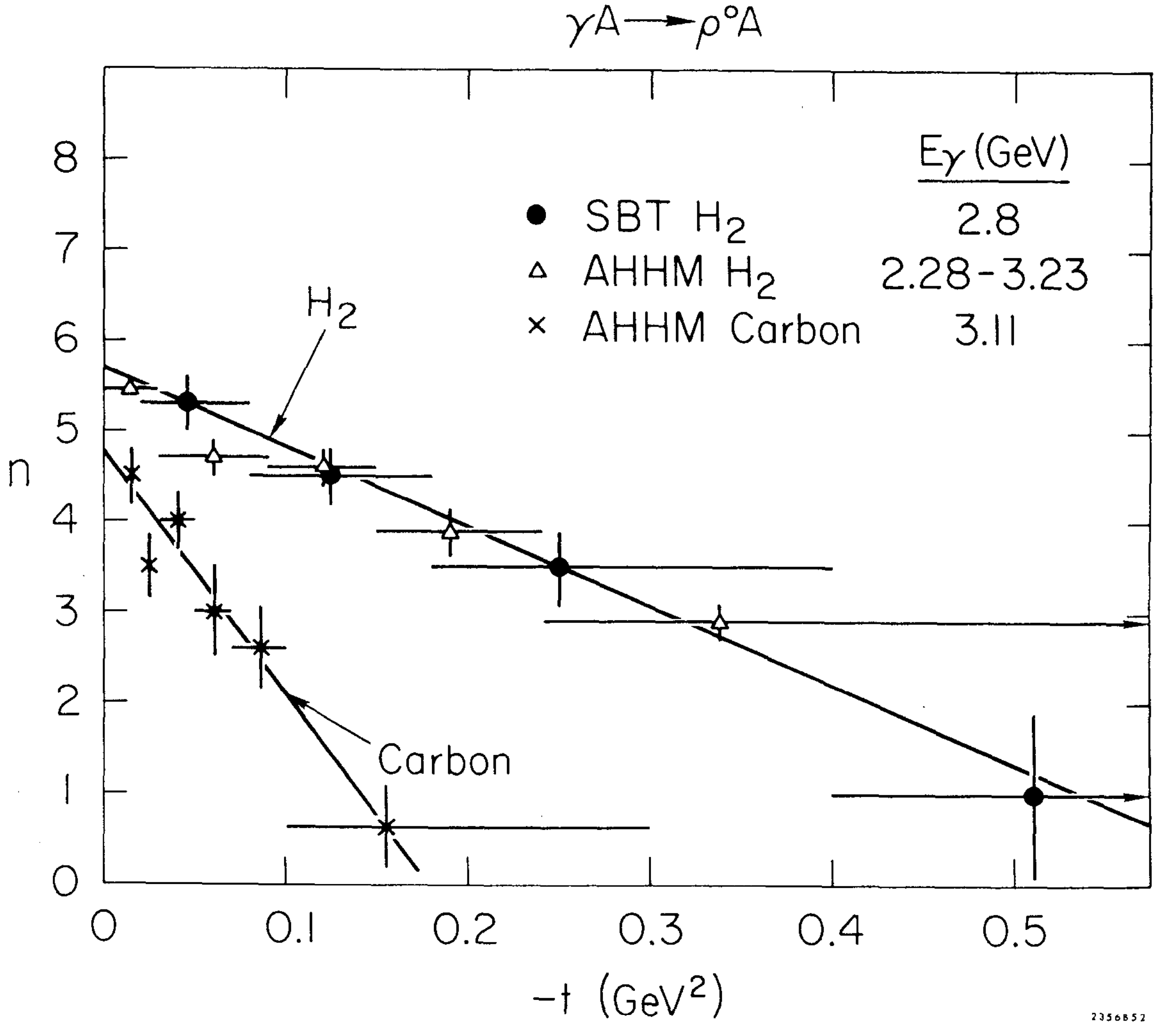

$\gamma A \longrightarrow \rho^{\circ} A$
n
E_γ (GeV)
SBT H_2 2.8
AHHM H_2 2.28-3.23
AHHM Carbon 3.11
H_2
Carbon
0
1
2
3
4
5
6
7
8
0
0.1
0.2
0.3
0.4
0.5
$-t$ (GeV^2)
2356B52

Fig. 16

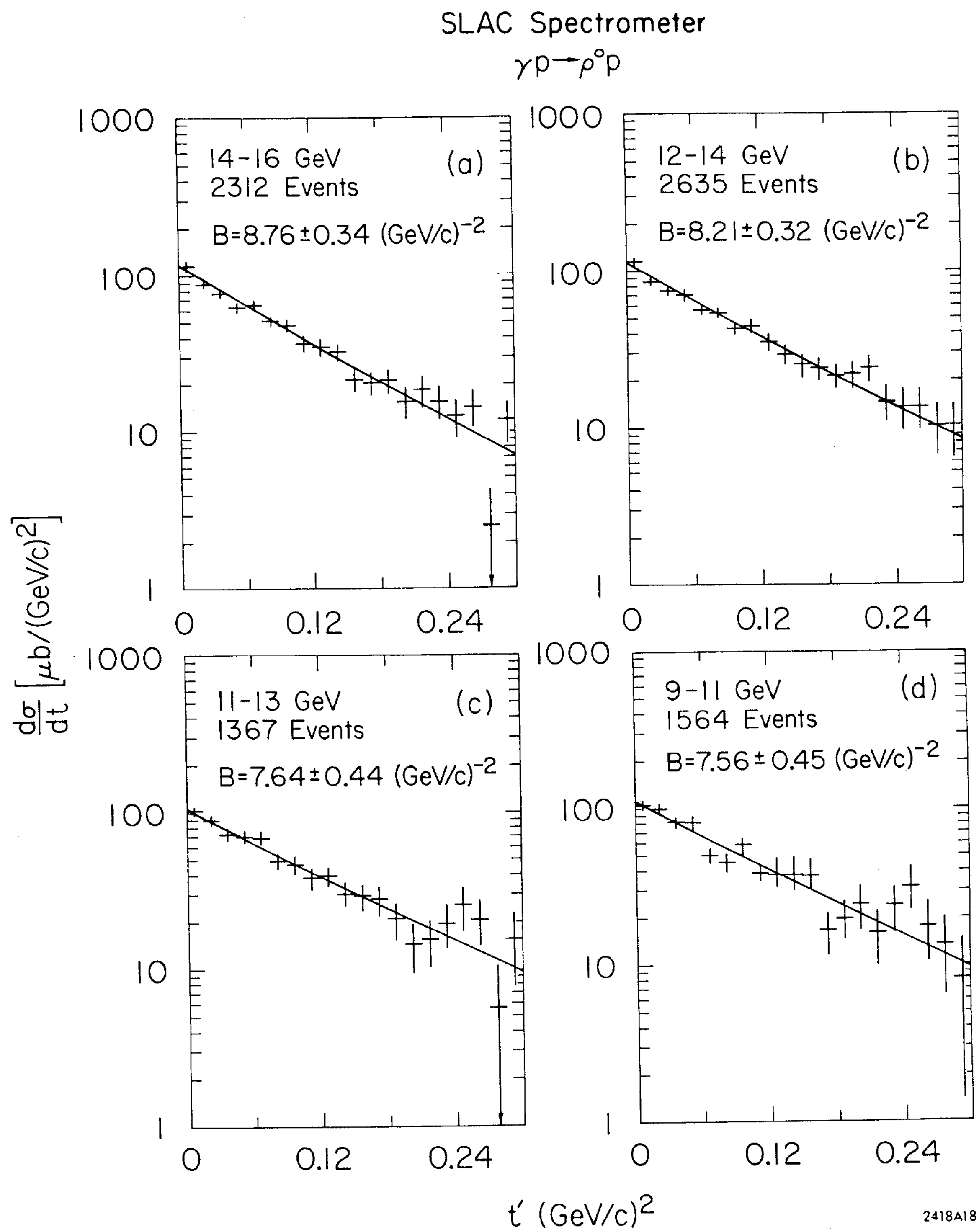
SLAC Spectrometer
γp→ρ°p
14-16 GeV
2312 Events
(a)
B=8.76±0.34 (GeV/c)^-2
12-14 GeV
2635 Events
(b)
B=8.21±0.32 (GeV/c)^-2
11-13 GeV
1367 Events
(c)
B=7.64±0.44 (GeV/c)^-2
9-11 GeV
1564 Events
(d)
B=7.56±0.45 (GeV/c)^-2
1000
100
10
1
0
0.12
0.24
dσ/dt [μb/(GeV/c)^2]
t′ (GeV/c)^2
2418A18

Fig. 17

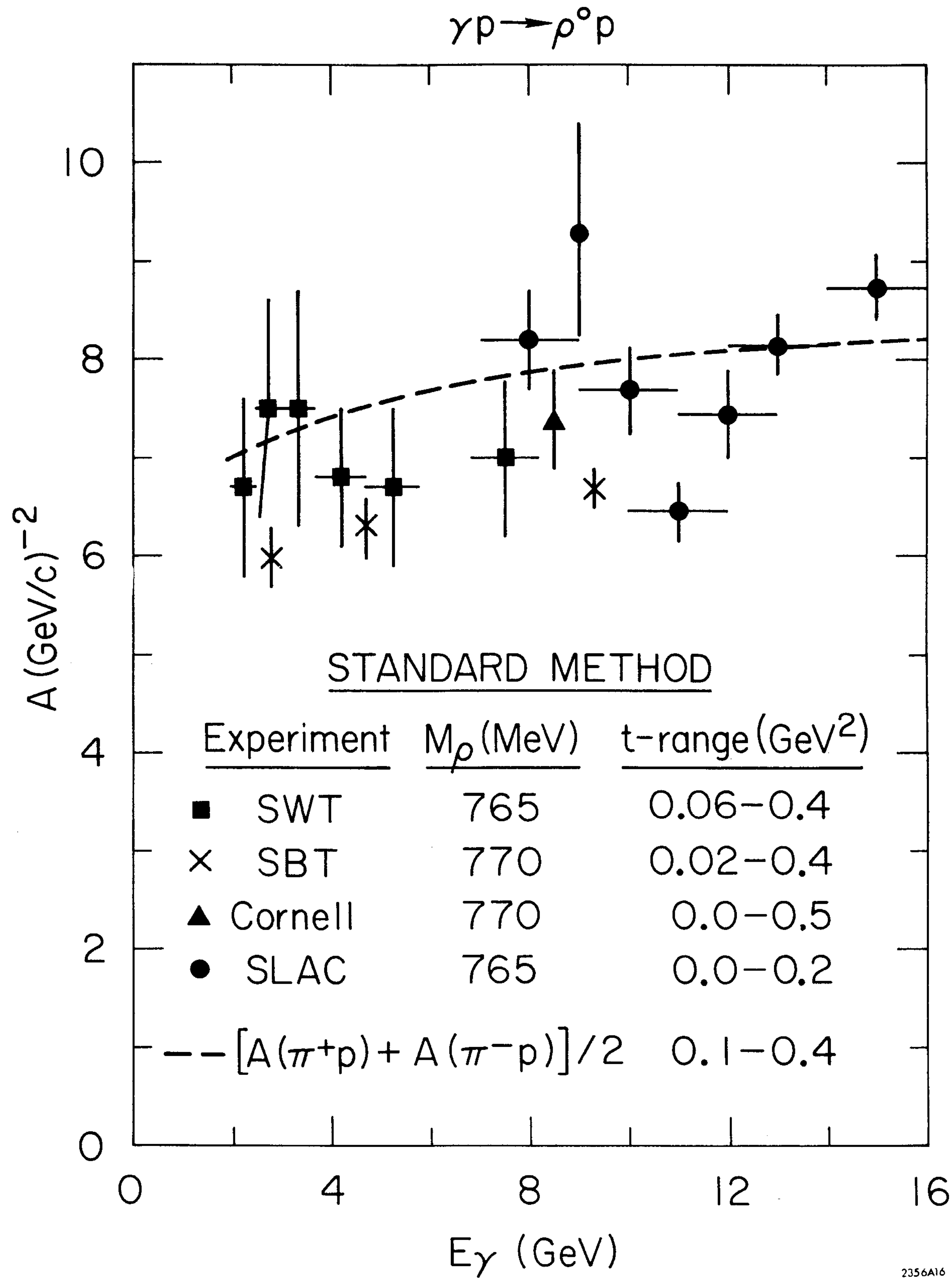

$\gamma p \rightarrow \rho^\circ p$
A $(\text{GeV/c})^{-2}$
0
2
4
6
8
10
0
4
8
12
16
E_γ (GeV)
STANDARD METHOD
Experiment
M_ρ (MeV)
t-range (GeV^2)
SWT 765 0.06–0.4
SBT 770 0.02–0.4
Cornell 770 0.0–0.5
SLAC 765 0.0–0.2
$[A(\pi^+p) + A(\pi^-p)]/2$ 0.1–0.4
2356A16

Fig. 18

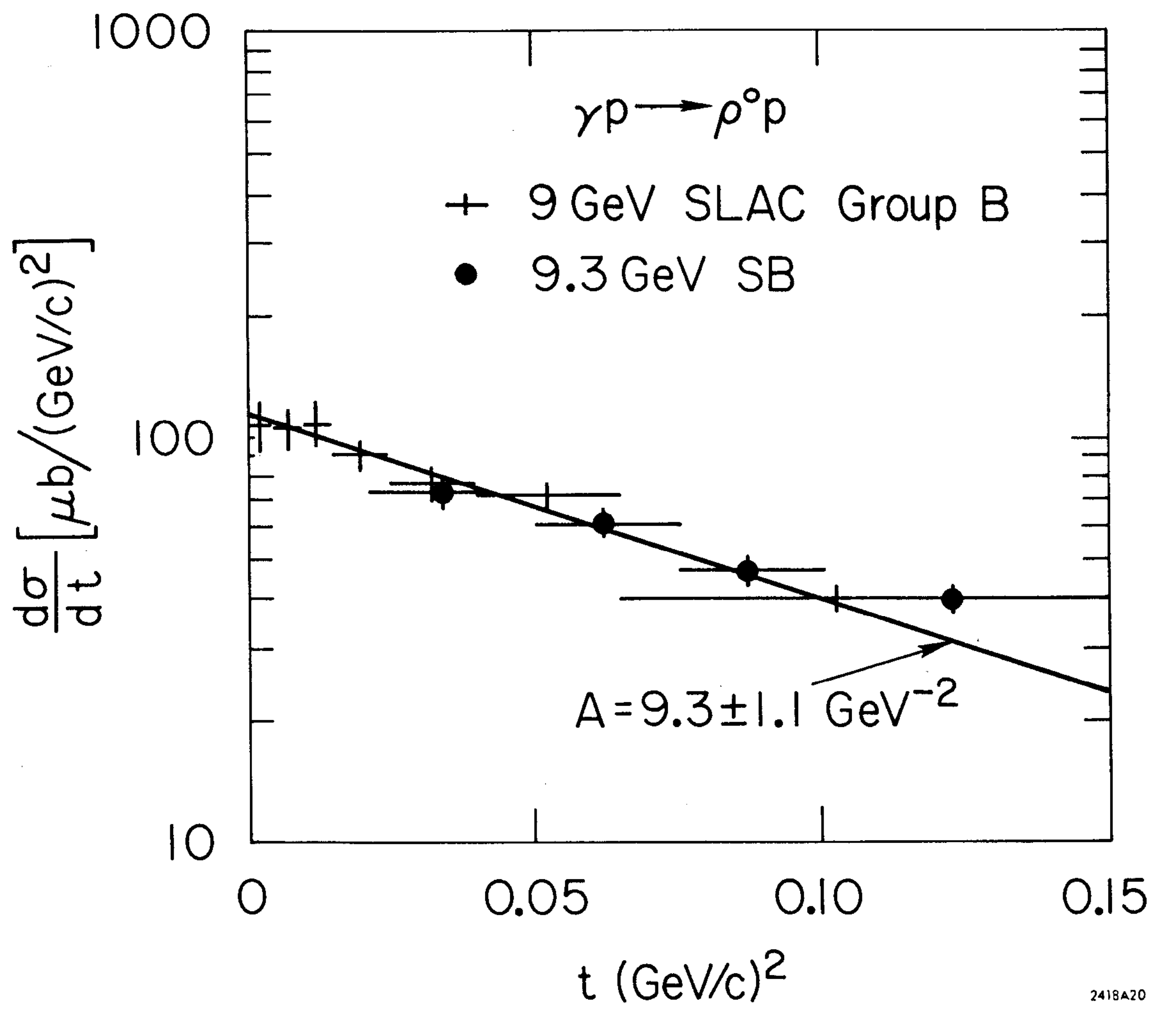

$\gamma p \longrightarrow \rho^{\circ} p$
+ 9 GeV SLAC Group B
● 9.3 GeV SB
$A = 9.3 \pm 1.1$ GeV^{-2}
1000
100
10
0
0.05
0.10
0.15
$\frac{d\sigma}{dt}\left[\mu b/(GeV/c)^2\right]$
t (GeV/c)^2
2418A20

Fig. 19

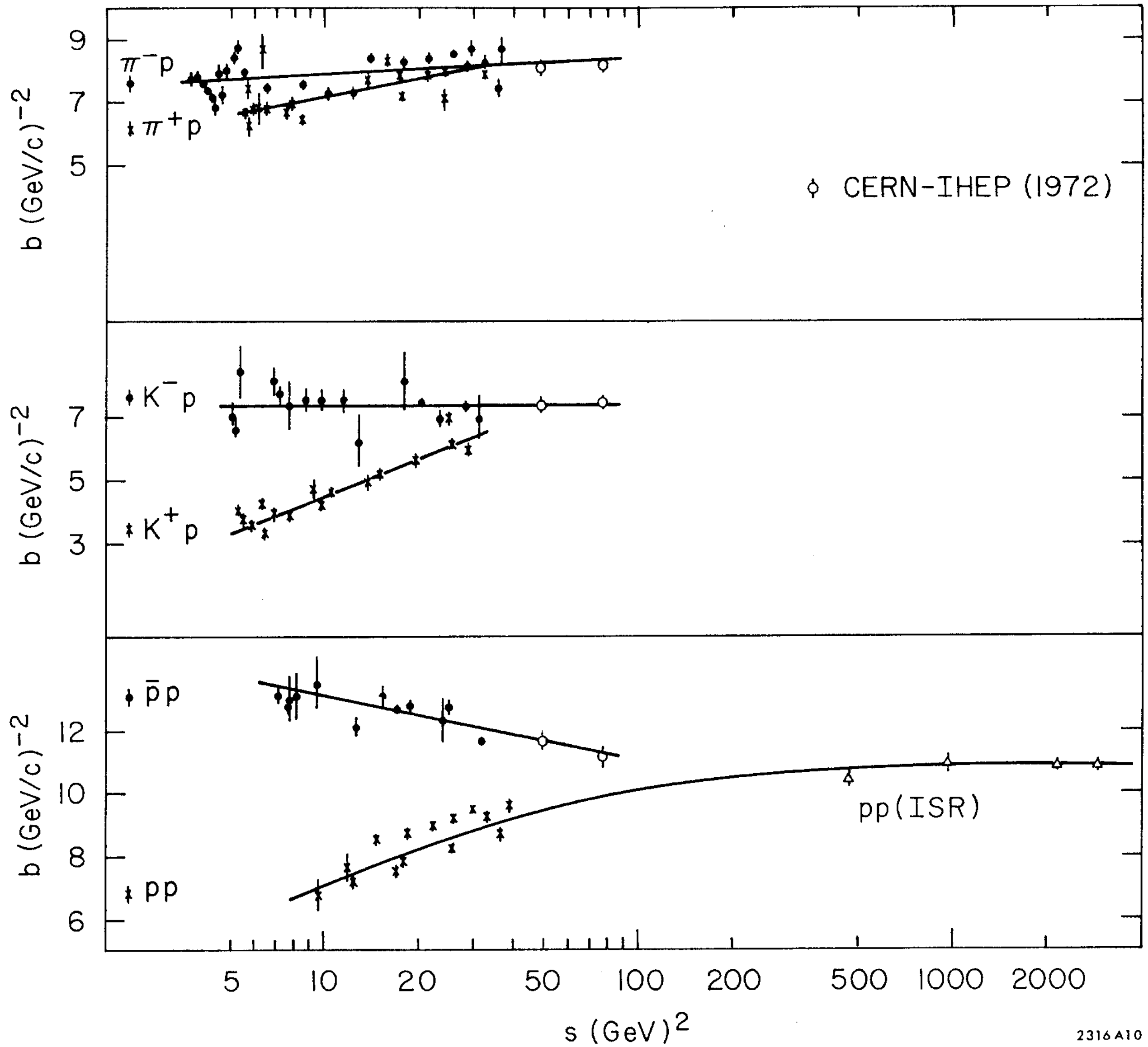

π^-p
π^+p
CERN-IHEP (1972)
b (GeV/c)$^{-2}$
9
7
5
K^-p
K^+p
7
5
3
$\bar{p}p$
pp
pp(ISR)
12
10
8
6
5
10
20
50
100
200
500
1000
2000
s (GeV)^2
2316A10

Fig. 20

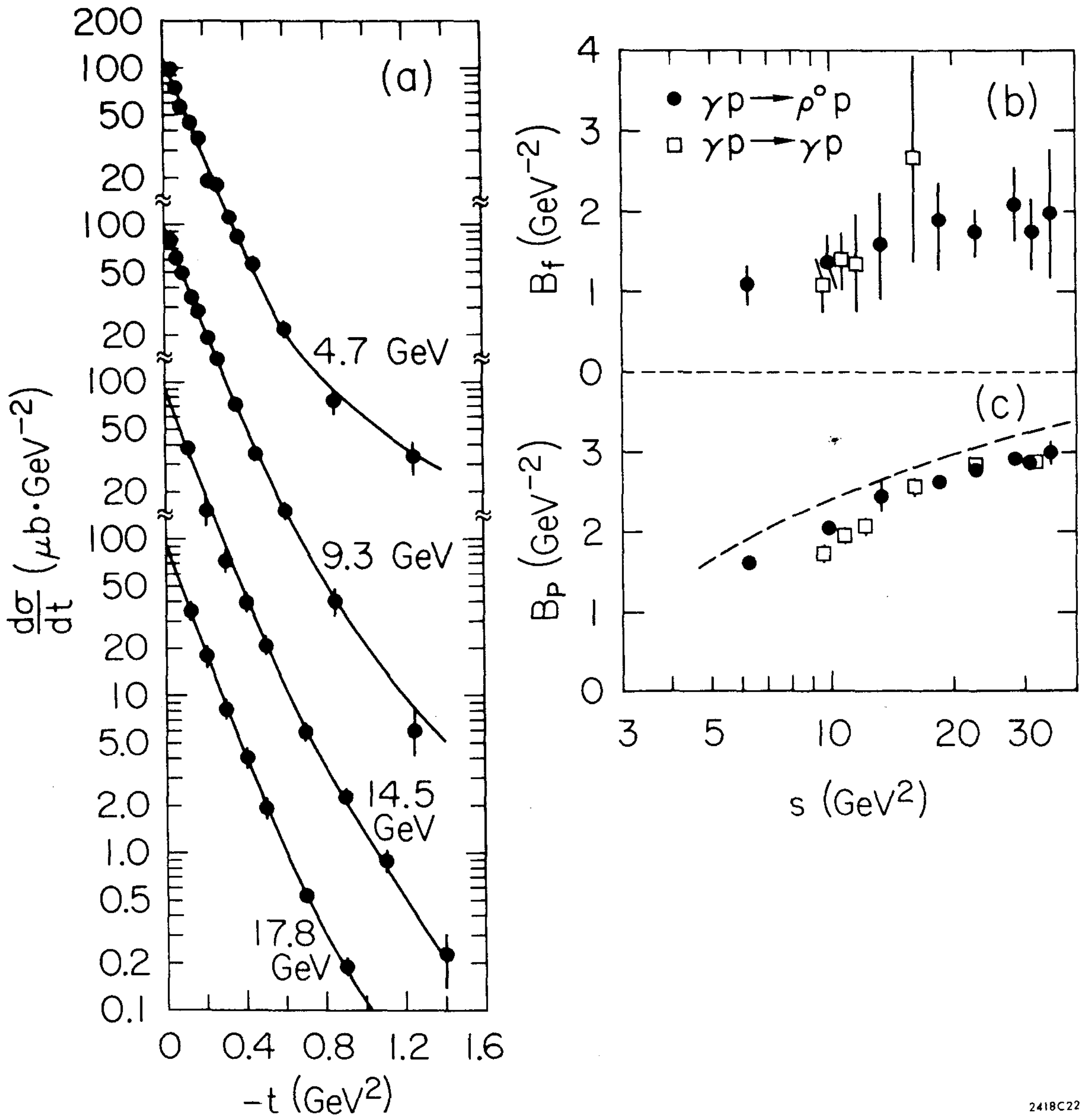

(a)
4.7 GeV
9.3 GeV
14.5 GeV
17.8 GeV
$\frac{d\sigma}{dt}$ (μb·GeV^{-2})
−t (GeV^2)
(b)
$\gamma p \rightarrow \rho^\circ p$
$\gamma p \rightarrow \gamma p$
B_f (GeV^{-2})
(c)
B_p (GeV^{-2})
s (GeV^2)
2418C22

Fig. 21

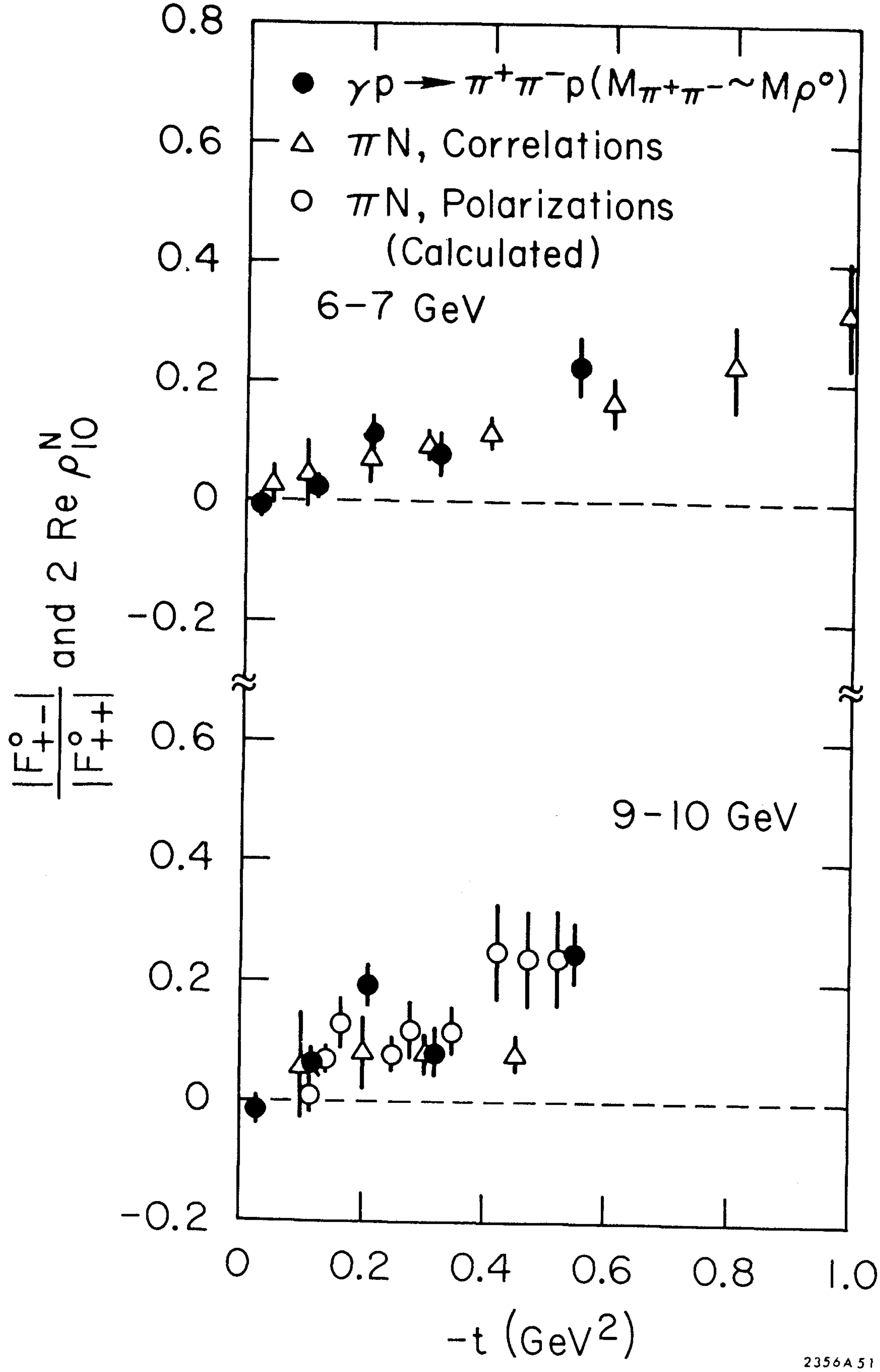

$\gamma p \rightarrow \pi^+\pi^- p (M_{\pi^+\pi^-} \sim M\rho^\circ)$
πN, Correlations
πN, Polarizations (Calculated)
6-7 GeV
9-10 GeV
$\frac{|F^\circ_{+-}|}{|F^\circ_{++}|}$ and $2 \text{ Re } \rho^N_{10}$
$-t$ (GeV^2)
2356A51

Fig. 22

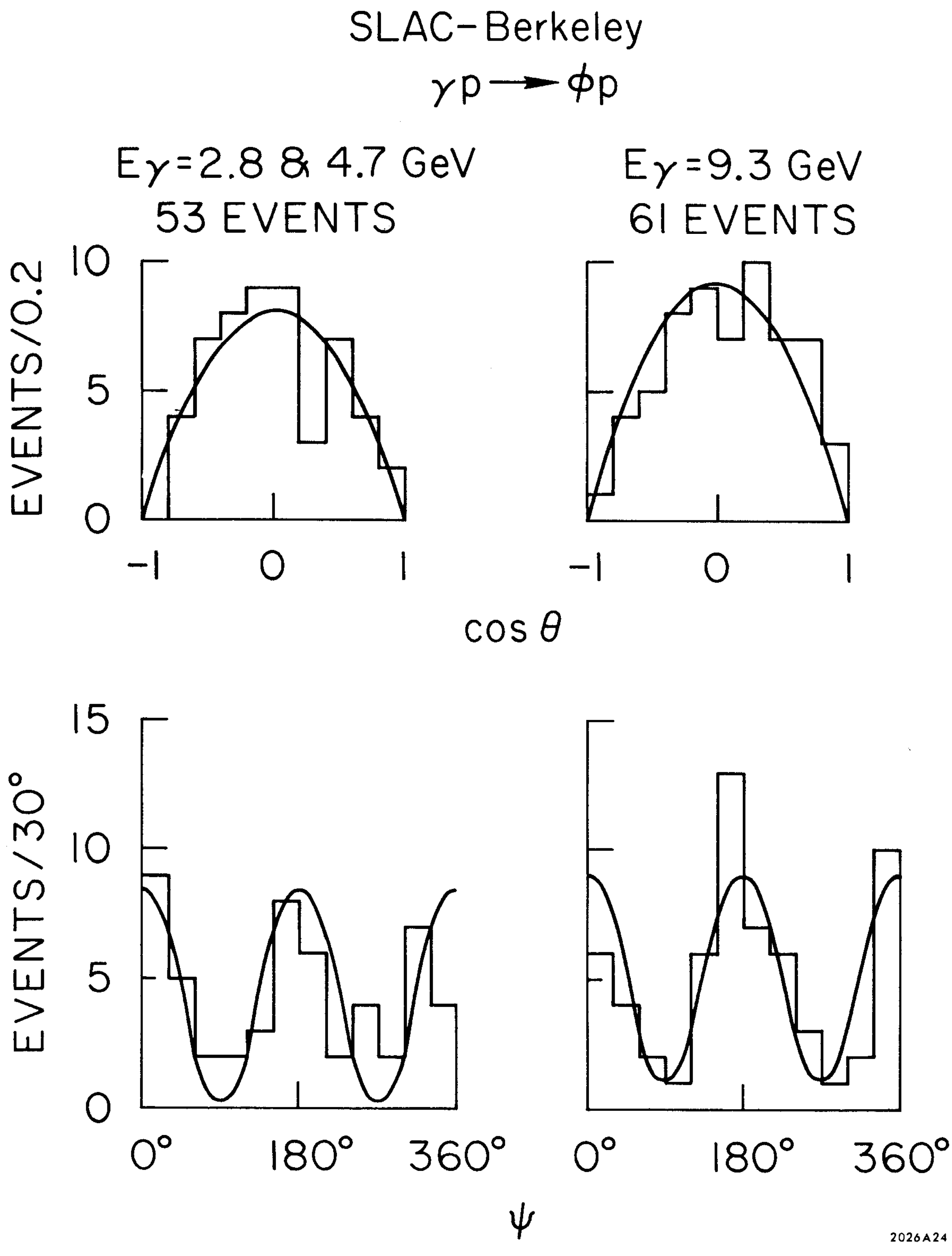

SLAC-Berkeley
$\gamma p \rightarrow \phi p$
$E\gamma$=2.8 & 4.7 GeV
53 EVENTS
$E\gamma$=9.3 GeV
61 EVENTS
EVENTS/0.2
10
5
0
-1
0
1
-1
0
1
cos θ
EVENTS/30°
15
10
5
0
0°
180°
360°
0°
180°
360°
ψ
2026A24

Fig. 23

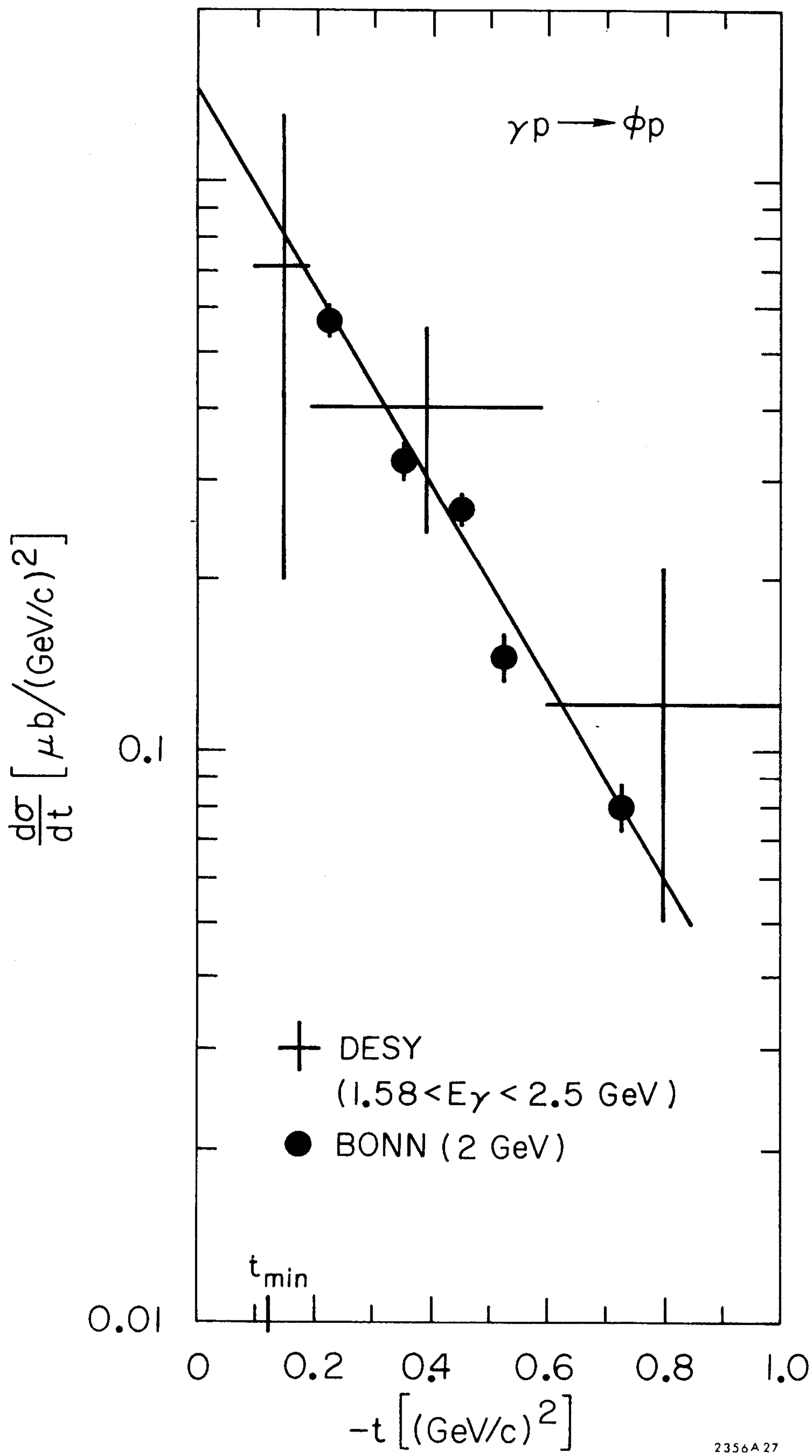

γp ⟶ φp
0.1
0.01
dσ/dt [μb/(GeV/c)²]
DESY
(1.58 < Eγ < 2.5 GeV)
BONN (2 GeV)
t_min
0
0.2
0.4
0.6
0.8
1.0
−t [(GeV/c)²]
2356A27

Fig. 24

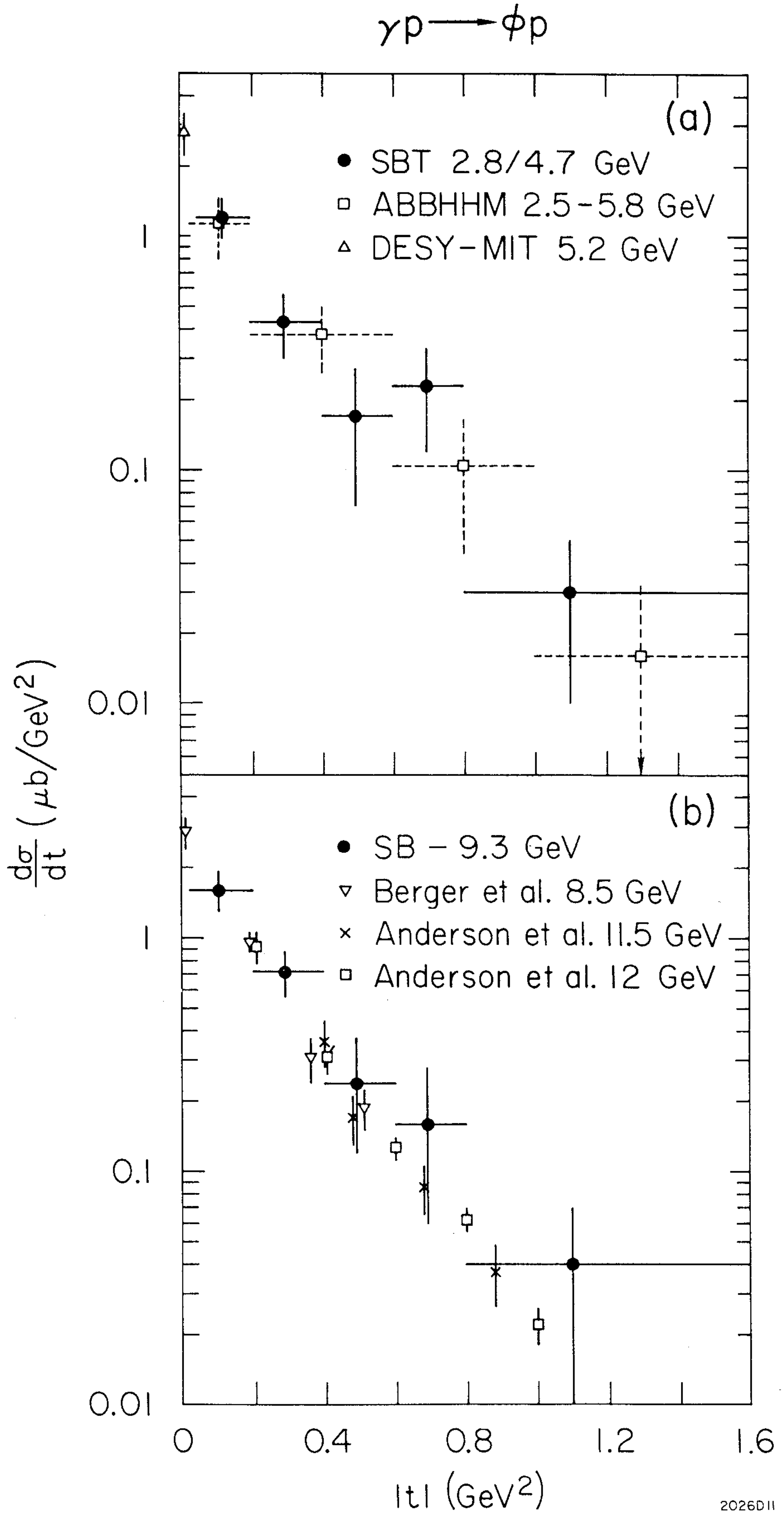

γp ⟶ φp
(a)
SBT 2.8/4.7 GeV
ABBHHM 2.5-5.8 GeV
DESY-MIT 5.2 GeV
(b)
SB – 9.3 GeV
Berger et al. 8.5 GeV
Anderson et al. 11.5 GeV
Anderson et al. 12 GeV
dσ/dt (μb/GeV²)
1
0.1
0.01
0
0.4
0.8
1.2
1.6
|t| (GeV²)
2026D11

Fig. 25

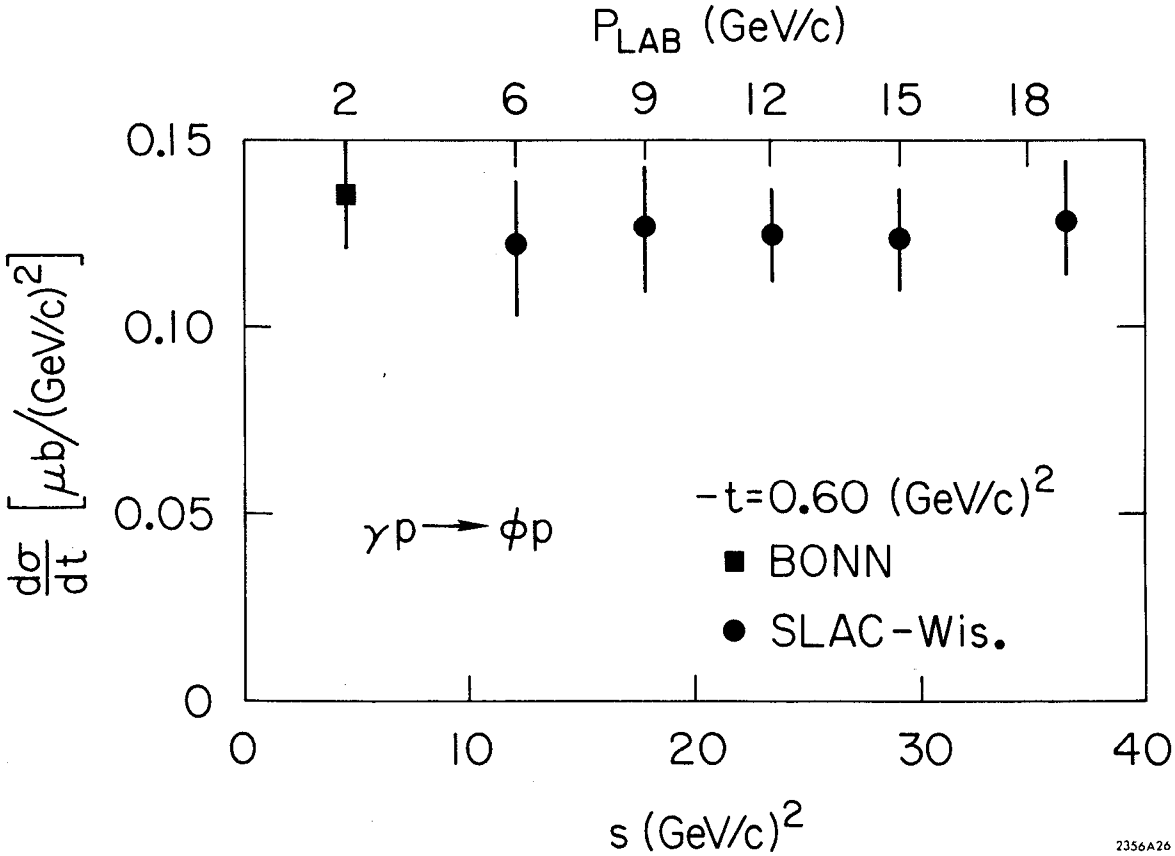

P_{LAB} (GeV/c)
2
6
9
12
15
18
0.15
0.10
0.05
0
$\frac{d\sigma}{dt}$ $[\mu b/(GeV/c)^2]$
$\gamma p \longrightarrow \phi p$
$-t=0.60$ $(GeV/c)^2$
BONN
SLAC-Wis.
0
10
20
30
40
s $(GeV/c)^2$
2356A26

Fig. 26

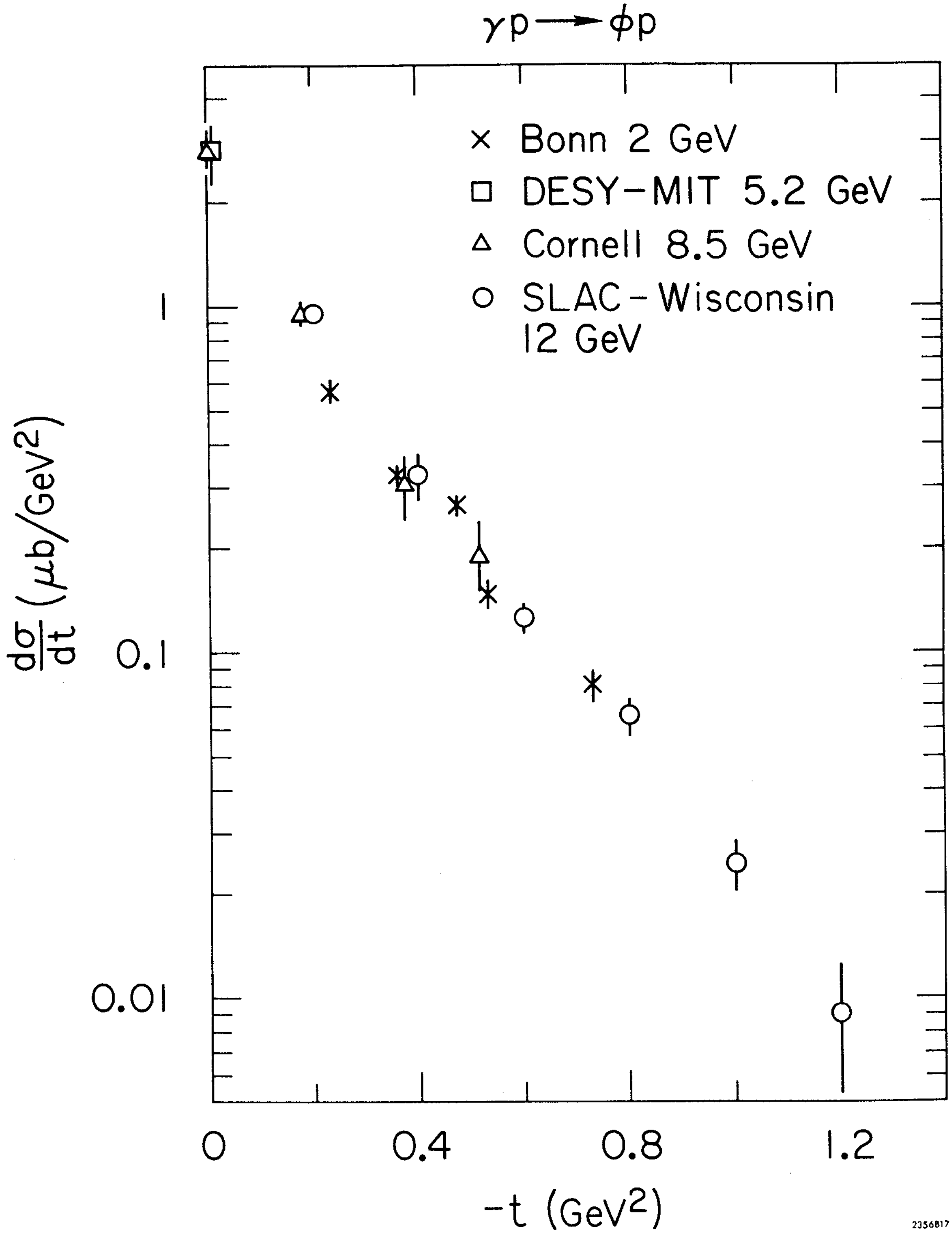

$\gamma p \longrightarrow \phi p$
× Bonn 2 GeV
□ DESY-MIT 5.2 GeV
△ Cornell 8.5 GeV
○ SLAC-Wisconsin 12 GeV
$\frac{d\sigma}{dt}$ (μb/GeV^2)
1
0.1
0.01
0
0.4
0.8
1.2
$-t$ (GeV^2)
2356B17

Fig. 27

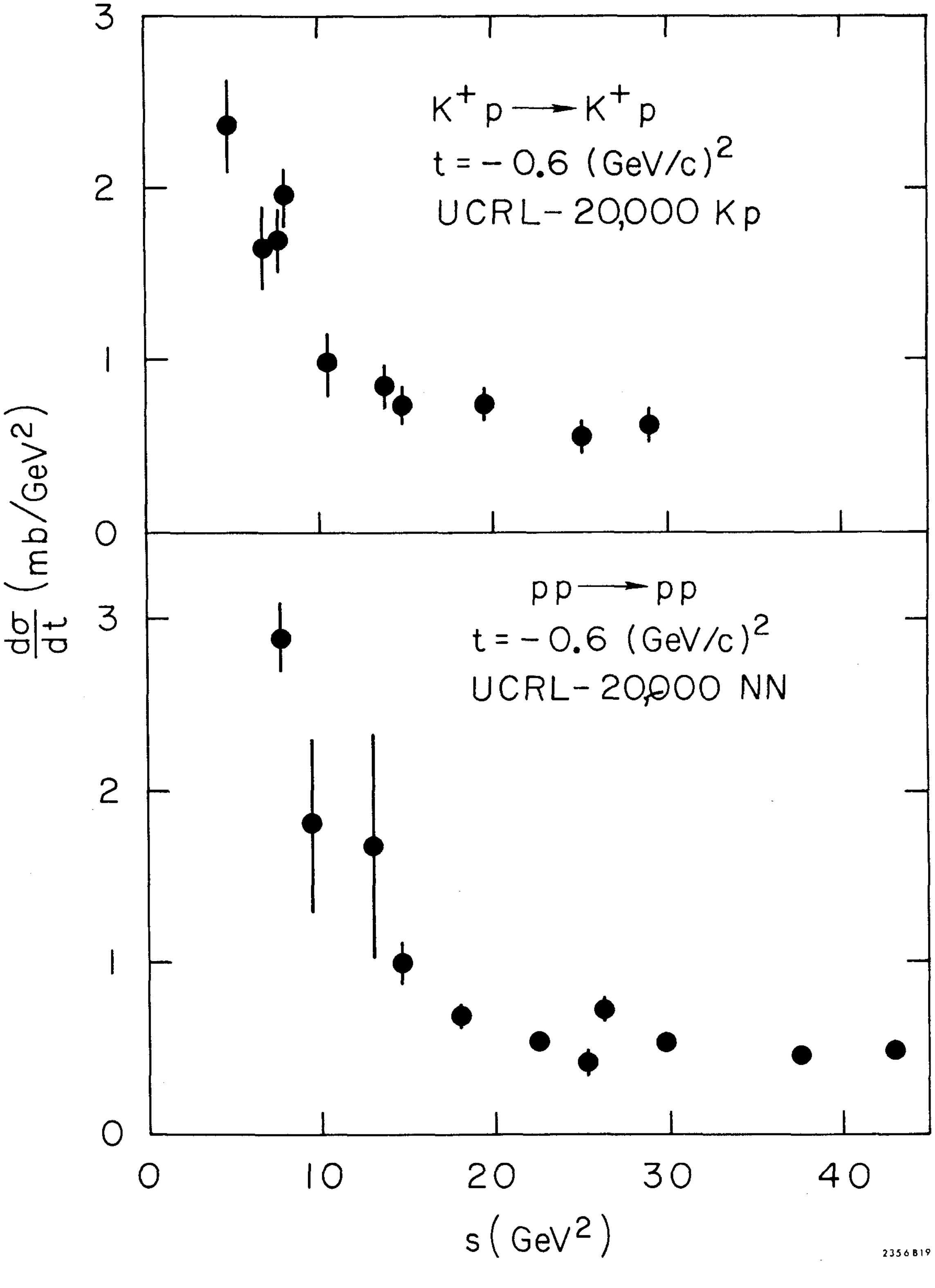

3
2
1
0
3
2
1
0
$K^+ p \longrightarrow K^+ p$
$t = -0.6\ (\mathrm{GeV}/c)^2$
UCRL-20,000 Kp
$pp \longrightarrow pp$
$t = -0.6\ (\mathrm{GeV}/c)^2$
UCRL-20,000 NN
$\frac{d\sigma}{dt}\ (\mathrm{mb}/\mathrm{GeV}^2)$
0
10
20
30
40
$s\ (\mathrm{GeV}^2)$
2356B19

Fig. 28

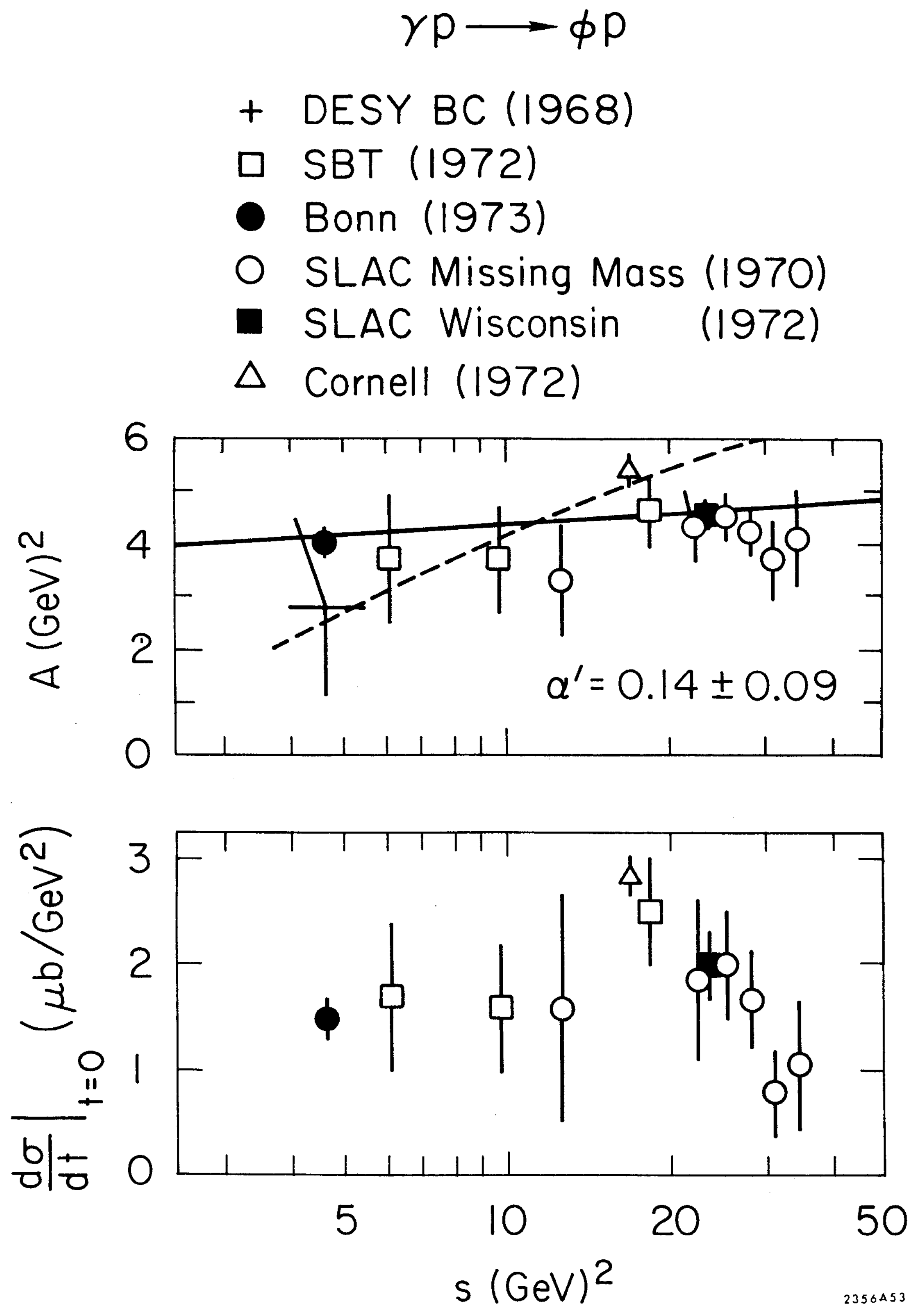
γp ⟶ φp
+ DESY BC (1968)
□ SBT (1972)
● Bonn (1973)
○ SLAC Missing Mass (1970)
■ SLAC Wisconsin (1972)
△ Cornell (1972)
A (GeV)²
α′ = 0.14 ± 0.09
dσ/dt |t=0 (μb/GeV²)
s (GeV)²
0
2
4
6
0
1
2
3
5
10
20
50
2356A53

Fig. 29

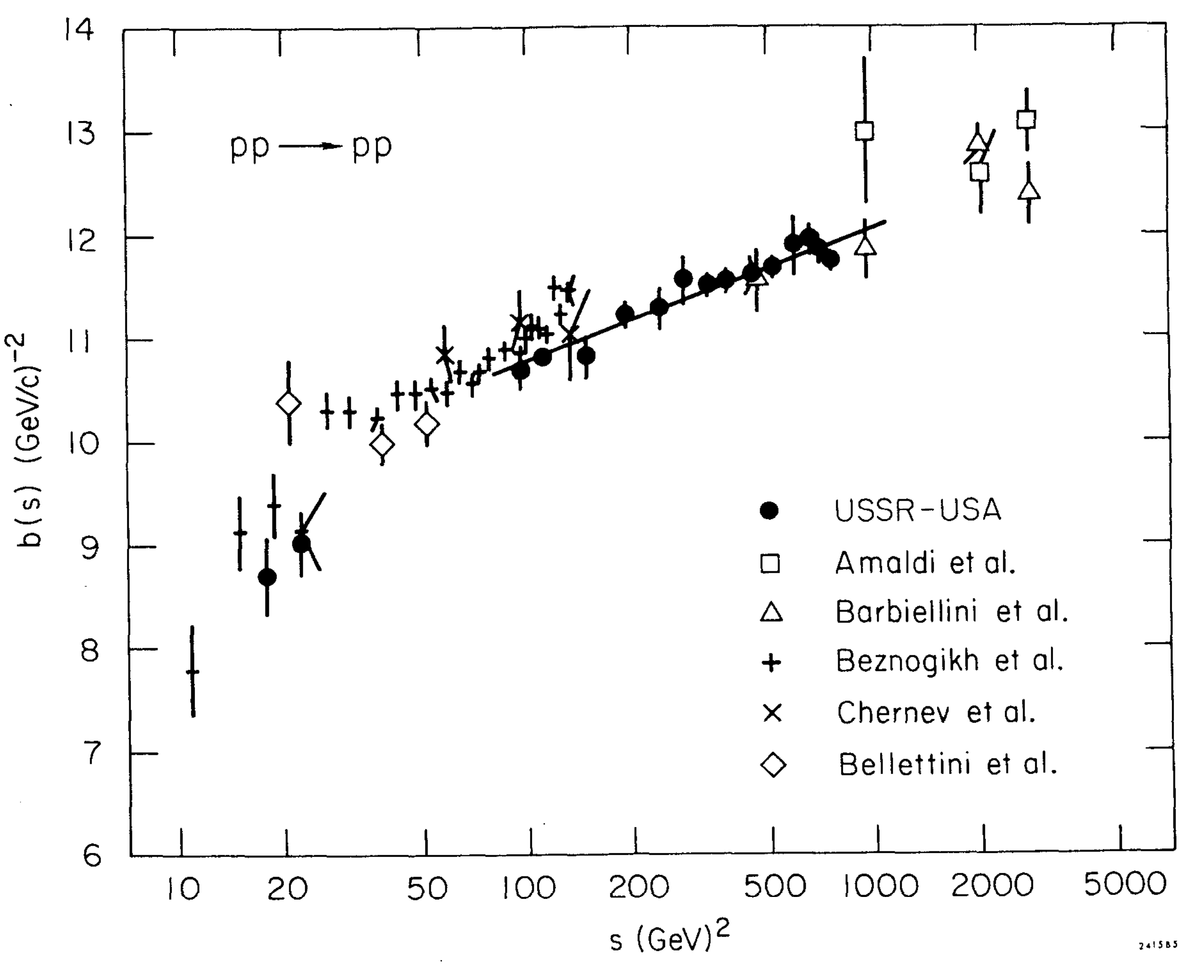

pp → pp
USSR-USA
Amaldi et al.
Barbiellini et al.
Beznogikh et al.
Chernev et al.
Bellettini et al.
b(s) (GeV/c)$^{-2}$
s (GeV)^2
6
7
8
9
10
11
12
13
14
10
20
50
100
200
500
1000
2000
5000

Fig. 30

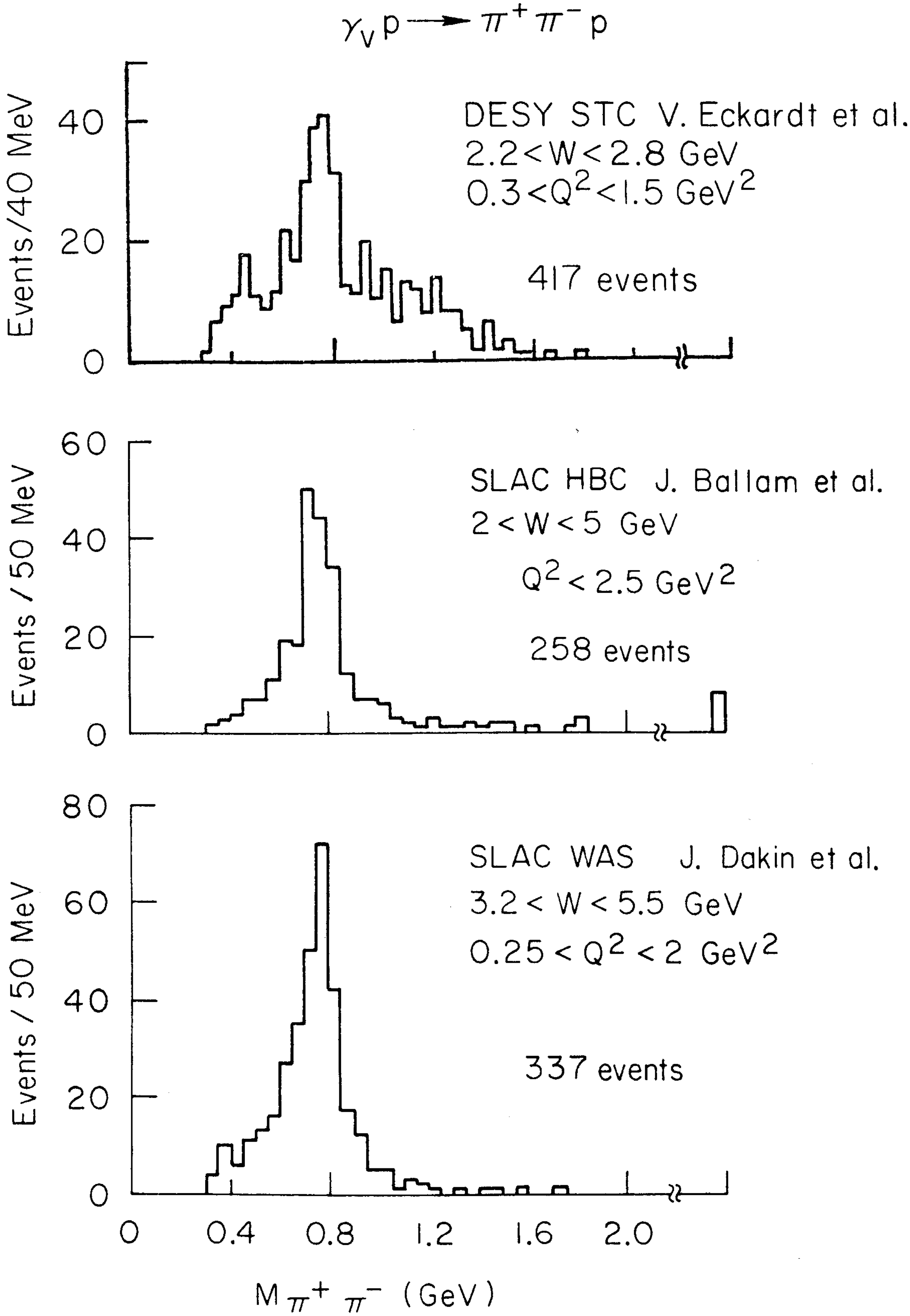

$\gamma_V p \longrightarrow \pi^+ \pi^- p$
Events/40 MeV
40
20
0
DESY STC V. Eckardt et al.
2.2<W<2.8 GeV
0.3<Q²<1.5 GeV²
417 events
Events / 50 MeV
60
40
20
0
SLAC HBC J. Ballam et al.
2 < W < 5 GeV
Q² < 2.5 GeV²
258 events
Events / 50 MeV
80
60
40
20
0
SLAC WAS J. Dakin et al.
3.2 < W < 5.5 GeV
0.25 < Q² < 2 GeV²
337 events
0
0.4
0.8
1.2
1.6
2.0
$M_{\pi^+\pi^-}$ (GeV)

Fig. 31

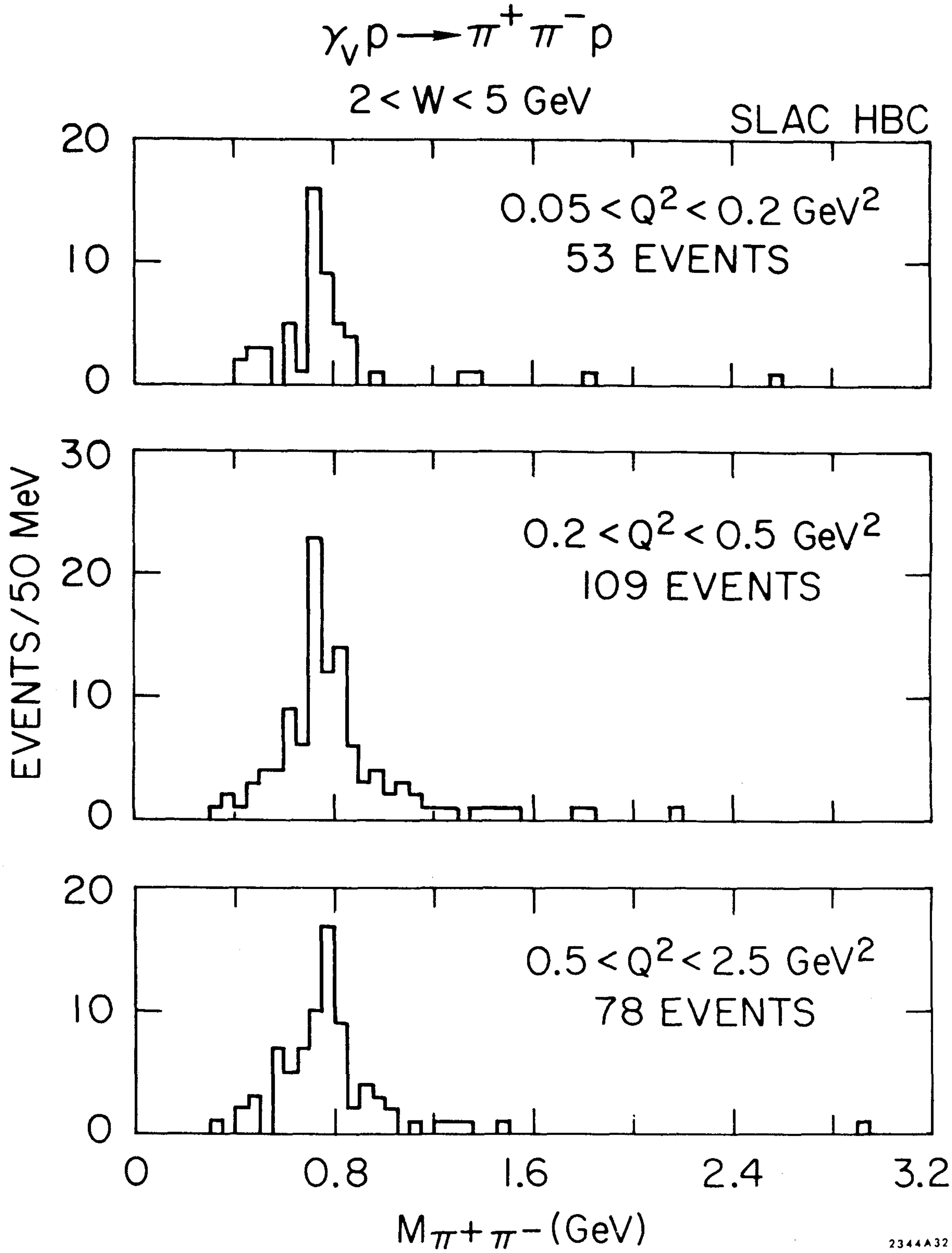

$\gamma_V p \rightarrow \pi^+ \pi^- p$
$2 < W < 5$ GeV
SLAC HBC
$0.05 < Q^2 < 0.2$ GeV^2
53 EVENTS
$0.2 < Q^2 < 0.5$ GeV^2
109 EVENTS
$0.5 < Q^2 < 2.5$ GeV^2
78 EVENTS
EVENTS/50 MeV
$M_{\pi^+\pi^-}$ (GeV)
0
10
20
30
0.8
1.6
2.4
3.2
2344A32

Fig. 32

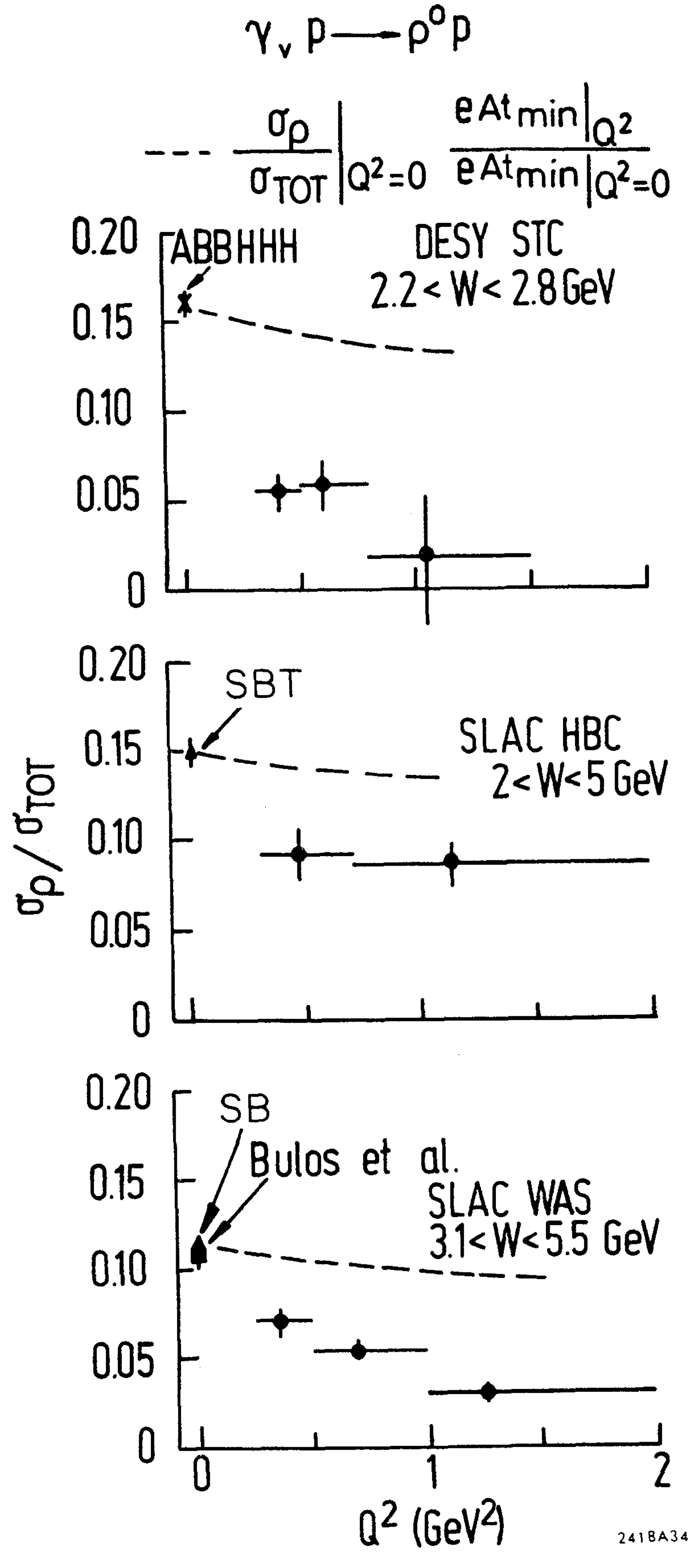

$\gamma_v\, p \longrightarrow \rho^0 p$
$\frac{\sigma_\rho}{\sigma_{TOT}}\Big|_{Q^2=0} \frac{e^{At_{min}}|_{Q^2}}{e^{At_{min}}|_{Q^2=0}}$
ABBHHH
DESY STC
2.2 < W < 2.8 GeV
SBT
SLAC HBC
2 < W < 5 GeV
SB
Bulos et al.
SLAC WAS
3.1 < W < 5.5 GeV
σ_ρ/σ_{TOT}
Q^2 (GeV^2)
0.20
0.15
0.10
0.05
0
1
2
2418A34

Fig. 33

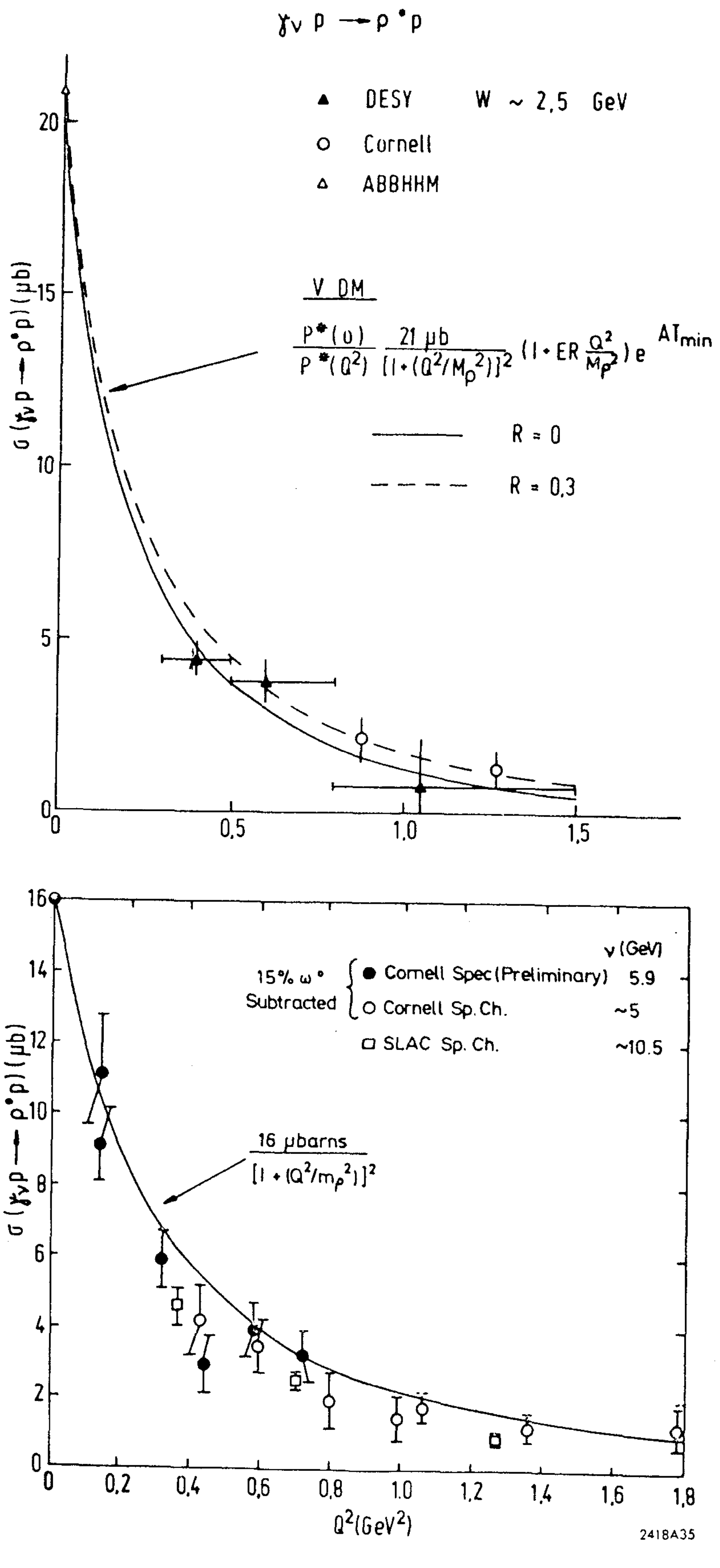

γv p → ρ° p
DESY W ~ 2,5 GeV
Cornell
ABBHHM
σ (γv p → ρ° p) (μb)
V DM
$\frac{P^*(0)}{P^*(Q^2)} \frac{21\ \mu b}{[1+(Q^2/M_\rho^2)]^2} (1+ER\frac{Q^2}{M_\rho^2})\, e^{AT_{min}}$
R = 0
R = 0,3
ν (GeV)
15% ω° Subtracted
Cornell Spec (Preliminary) 5.9
Cornell Sp. Ch. ~5
SLAC Sp. Ch. ~10.5
$\frac{16\ \mu barns}{[1+(Q^2/m_\rho^2)]^2}$
$Q^2 (GeV^2)$
2418A35

Fig. 34

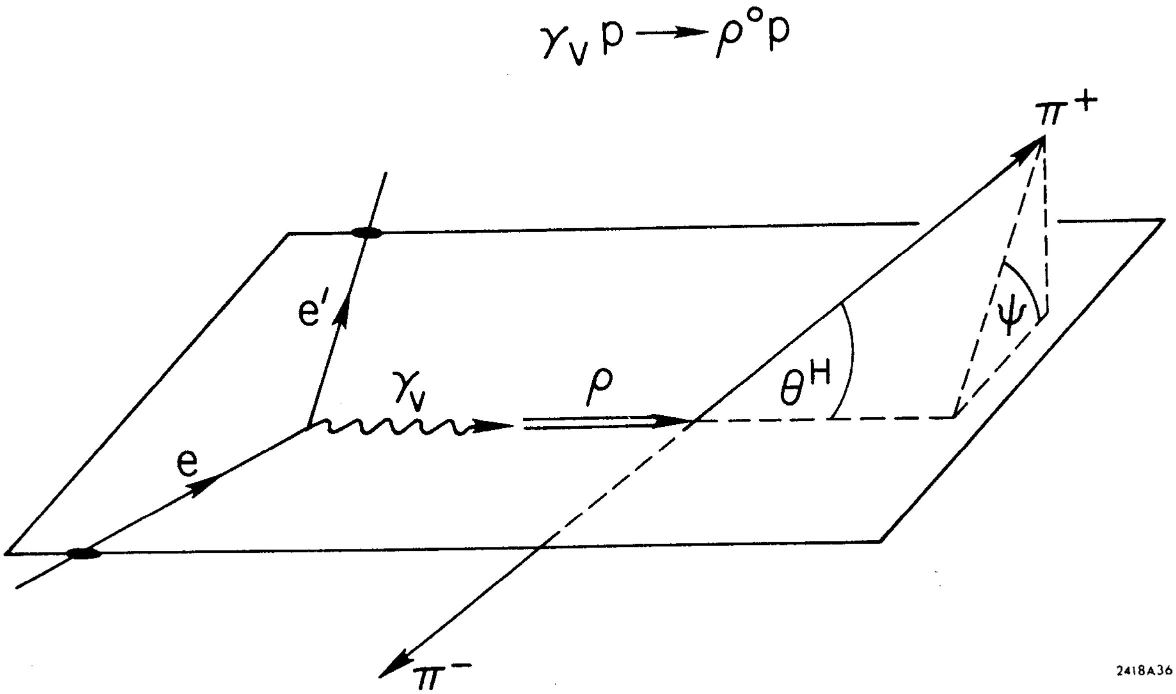

$\gamma_V p \longrightarrow \rho^\circ p$
π^+
e'
γ_V
ρ
θ^H
ψ
e
π^-
2418A36

Fig. 35

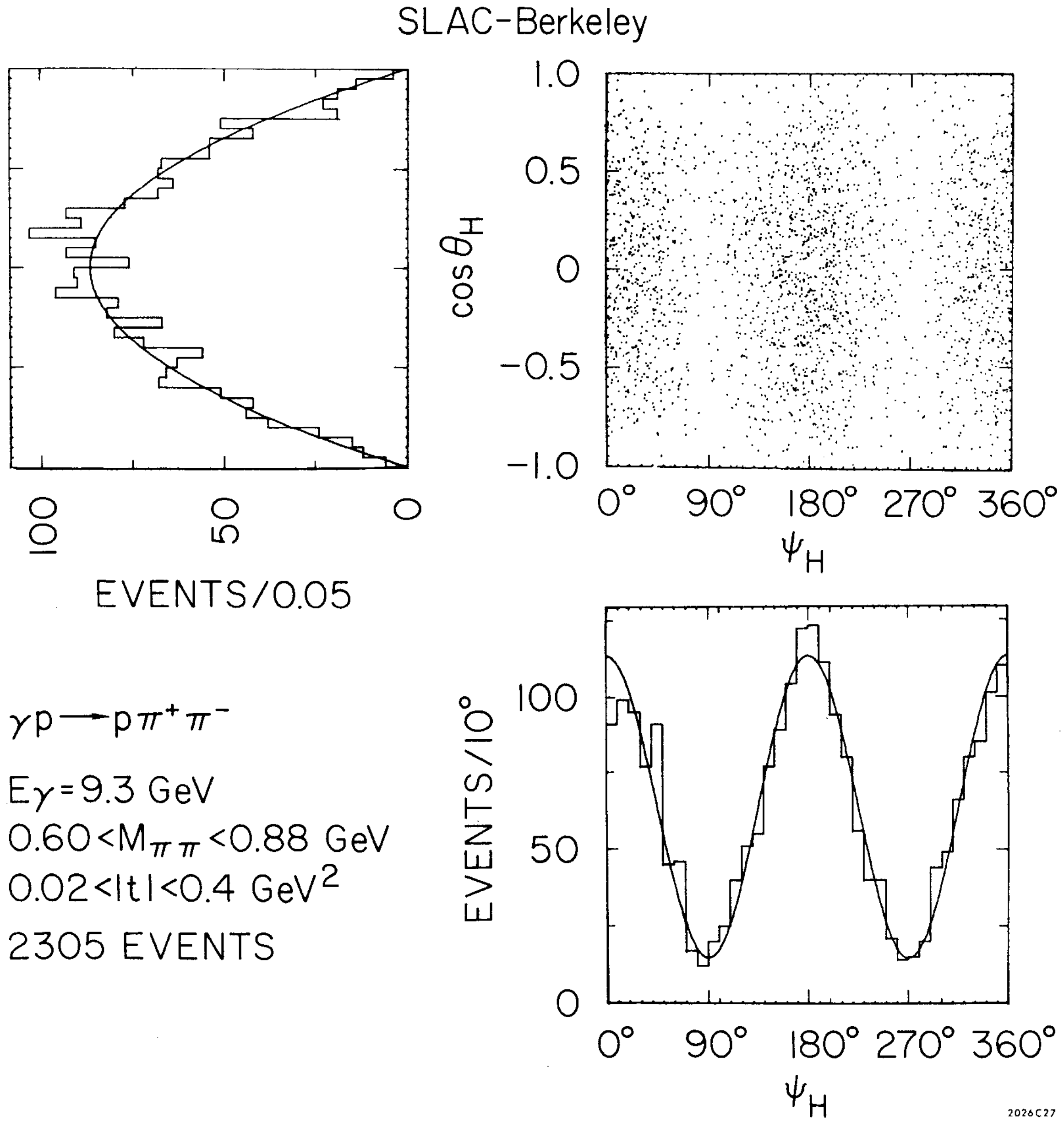

SLAC-Berkeley
1.0
0.5
0
−0.5
−1.0
$\cos\theta_H$
0° 90° 180° 270° 360°
ψ_H
100
50
0
EVENTS/0.05
$\gamma p \rightarrow p\pi^+\pi^-$
$E\gamma$=9.3 GeV
$0.60 < M_{\pi\pi} < 0.88$ GeV
$0.02 < |t| < 0.4$ GeV^2
2305 EVENTS
100
50
0
EVENTS/10°
0° 90° 180° 270° 360°
ψ_H
2026C27

Fig. 36

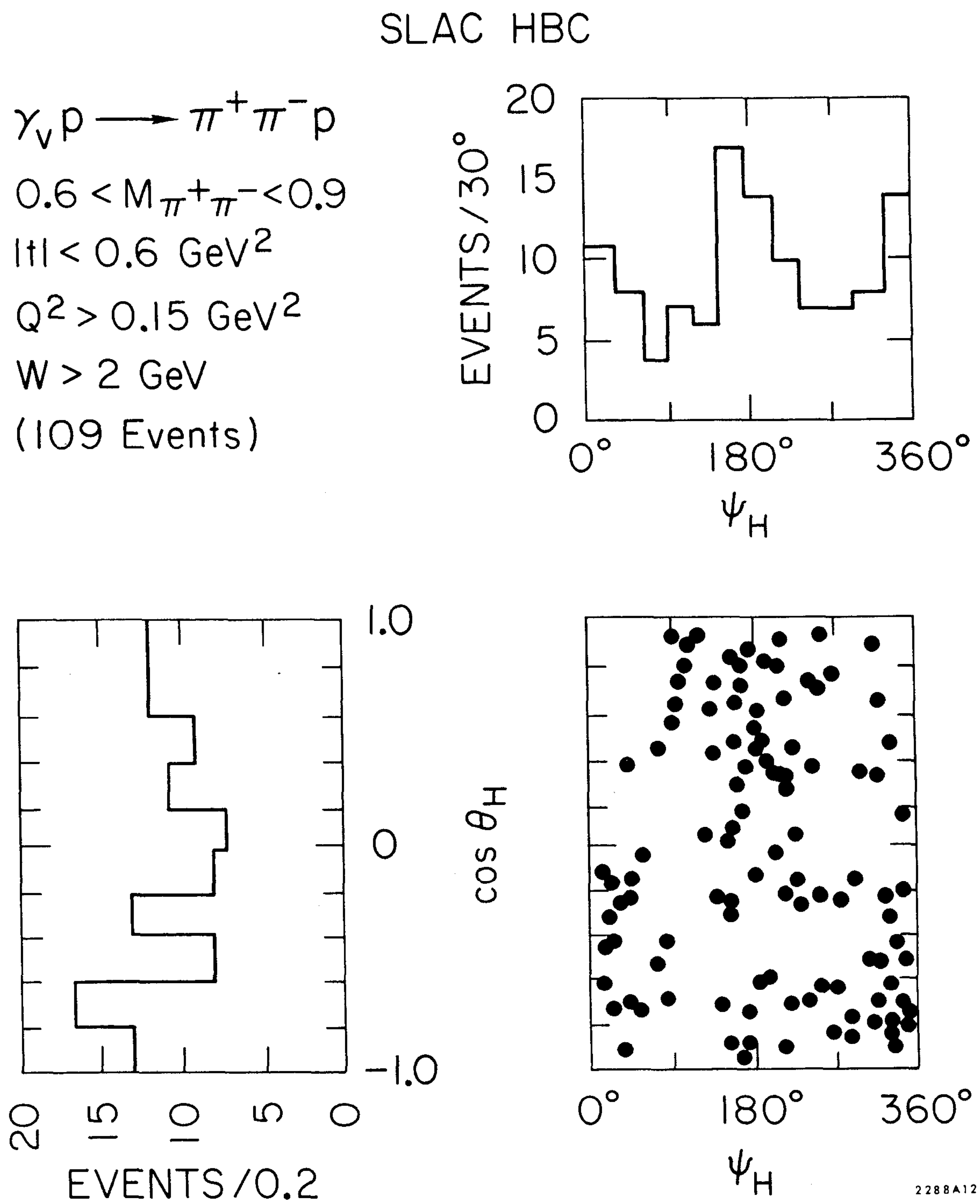
SLAC HBC
$\gamma_V p \longrightarrow \pi^+\pi^- p$
$0.6 < M_{\pi^+\pi^-} < 0.9$
$|t| < 0.6$ GeV^2
$Q^2 > 0.15$ GeV^2
W > 2 GeV
(109 Events)
EVENTS/30°
20
15
10
5
0
0°
180°
360°
ψ_H
1.0
0
−1.0
$\cos\theta_H$
EVENTS/0.2
2288A12

Fig. 37a

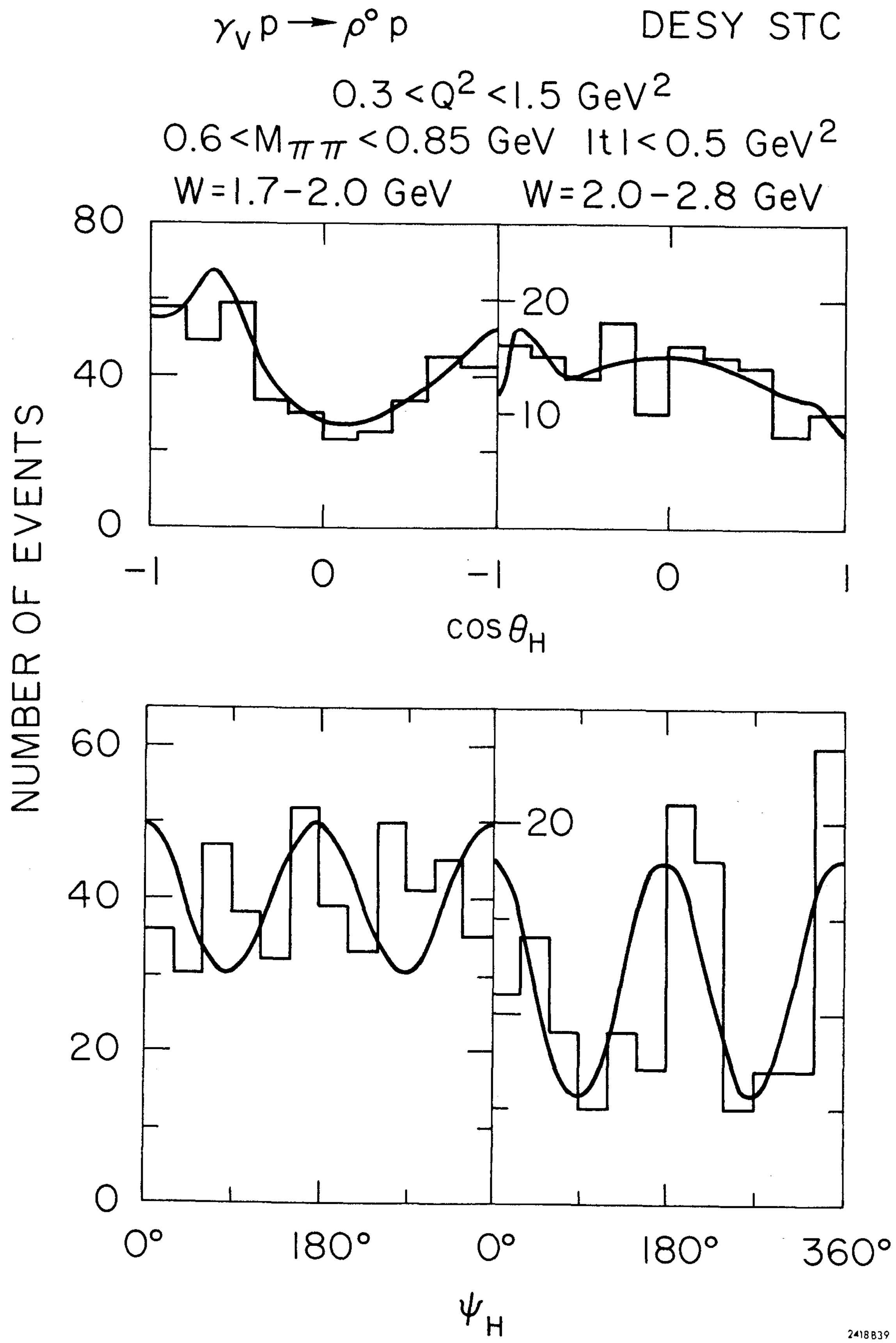

$\gamma_V p \to \rho^\circ p$
DESY STC
$0.3 < Q^2 < 1.5$ GeV^2
$0.6 < M_{\pi\pi} < 0.85$ GeV $|t| < 0.5$ GeV^2
W=1.7–2.0 GeV
W=2.0–2.8 GeV
NUMBER OF EVENTS
80
40
0
20
10
-1
0
-1
0
1
$\cos\theta_H$
60
40
20
0
20
0°
180°
0°
180°
360°
ψ_H
2418B39

Fig. 37b

SLAC WAS

$\langle W \rangle = 4.5$ GeV

$\gamma^* + p \to \rho^\circ + p$ RAW DATA

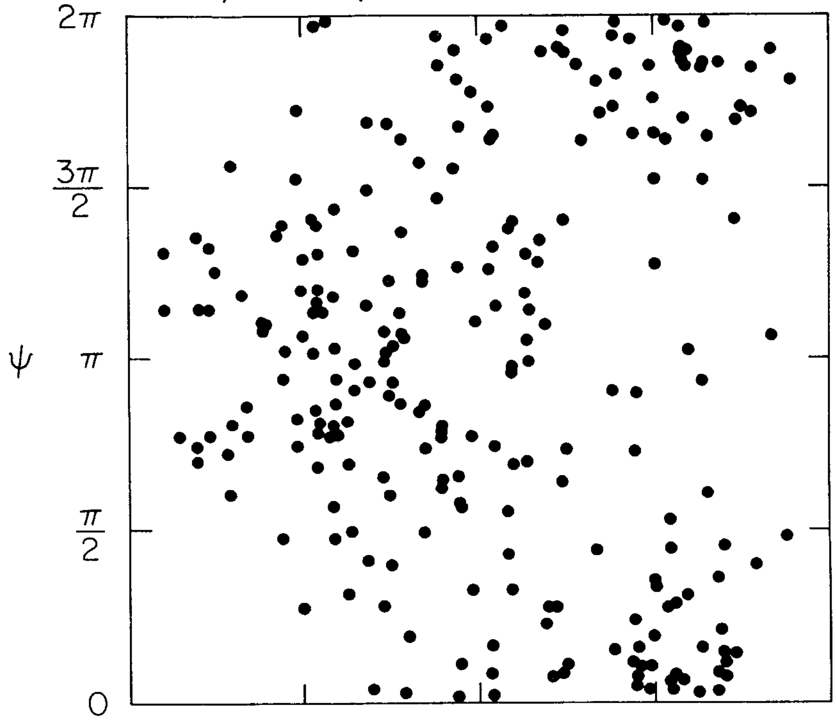

DATA CORRECTED FOR ACCEPTANCE

0	0	3.4	4.1	6.3	3.9	10.4	9.5
0	1.5	2.4	2.6	0.8	3.3	2.4	4.4
0	2.3	0	2.1	1.3	2.8	2.3	0
2.6	1.7	2.6	1.3	2.7	0	1.2	0
7.0	2.3	3.2	2.2	4.0	1.1	0	0
6.2	3.6	6.2	3.4	6.2	0	2.4	5.4
0	1.4	6.2	2.6	3.7	3.2	2.4	0
9.4	3.8	5.2	3.6	3.6	1.1	0	0
0	0.9	2.0	3.1	1.4	0	2.4	0
0	1.2	3.2	0.6	0.6	1.4	2.3	5.5
0	1.5	2.4	1.7	3.0	2.1	3.2	0
0	0	1.7	4.1	6.3	6.5	11.2	0

ψ: 0, π/2, π, 3π/2, 2π

1.0 0.5 0 −0.5 −1.0

$\cos\theta$

2418A40

Fig. 37c

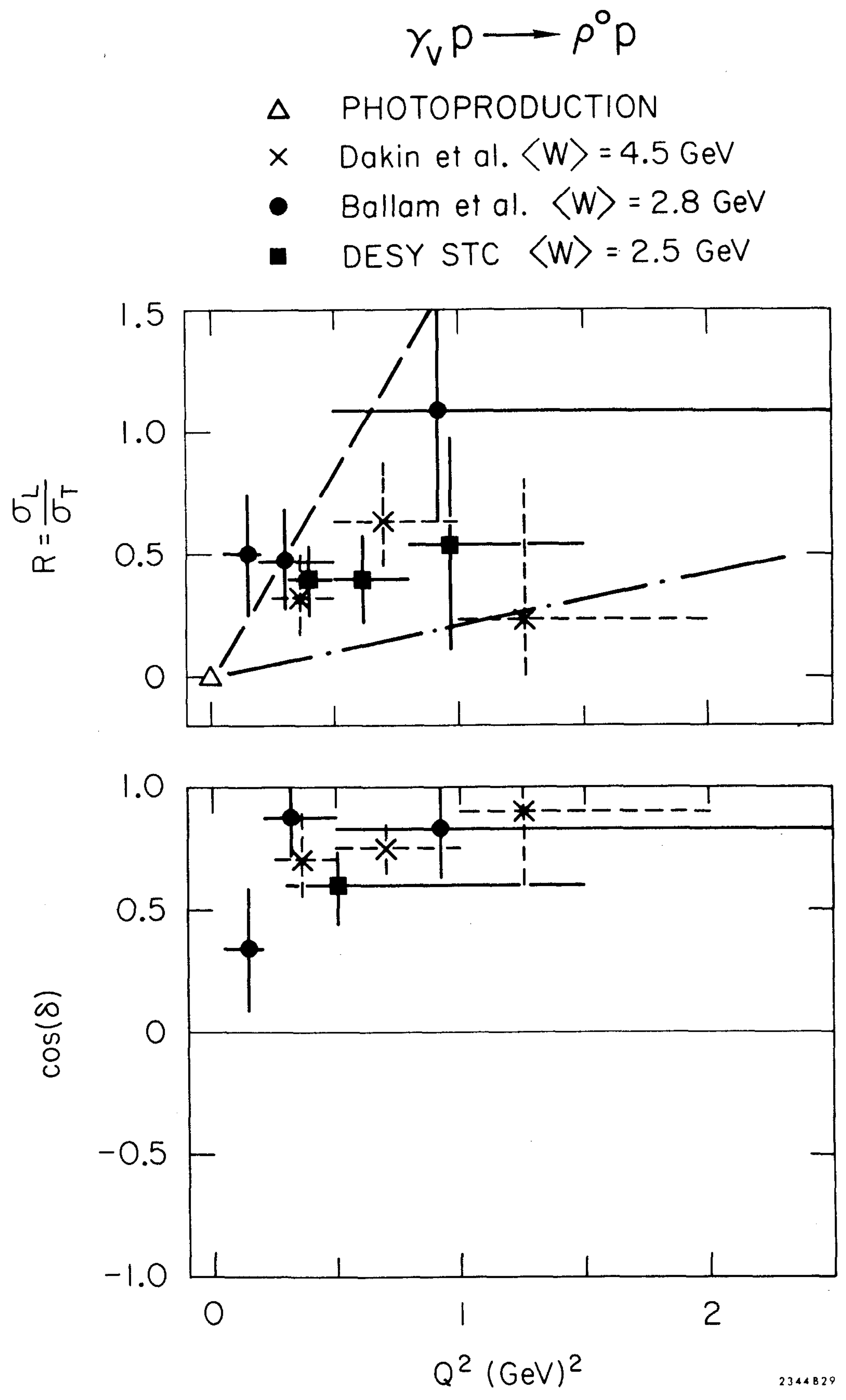
$\gamma_V p \longrightarrow \rho^\circ p$
PHOTOPRODUCTION
Dakin et al. ⟨W⟩ = 4.5 GeV
Ballam et al. ⟨W⟩ = 2.8 GeV
DESY STC ⟨W⟩ = 2.5 GeV
$R = \frac{\sigma_L}{\sigma_T}$
1.5
1.0
0.5
0
$\cos(\delta)$
1.0
0.5
0
−0.5
−1.0
0
1
2
Q^2 (GeV)^2
2344B29

Fig. 38

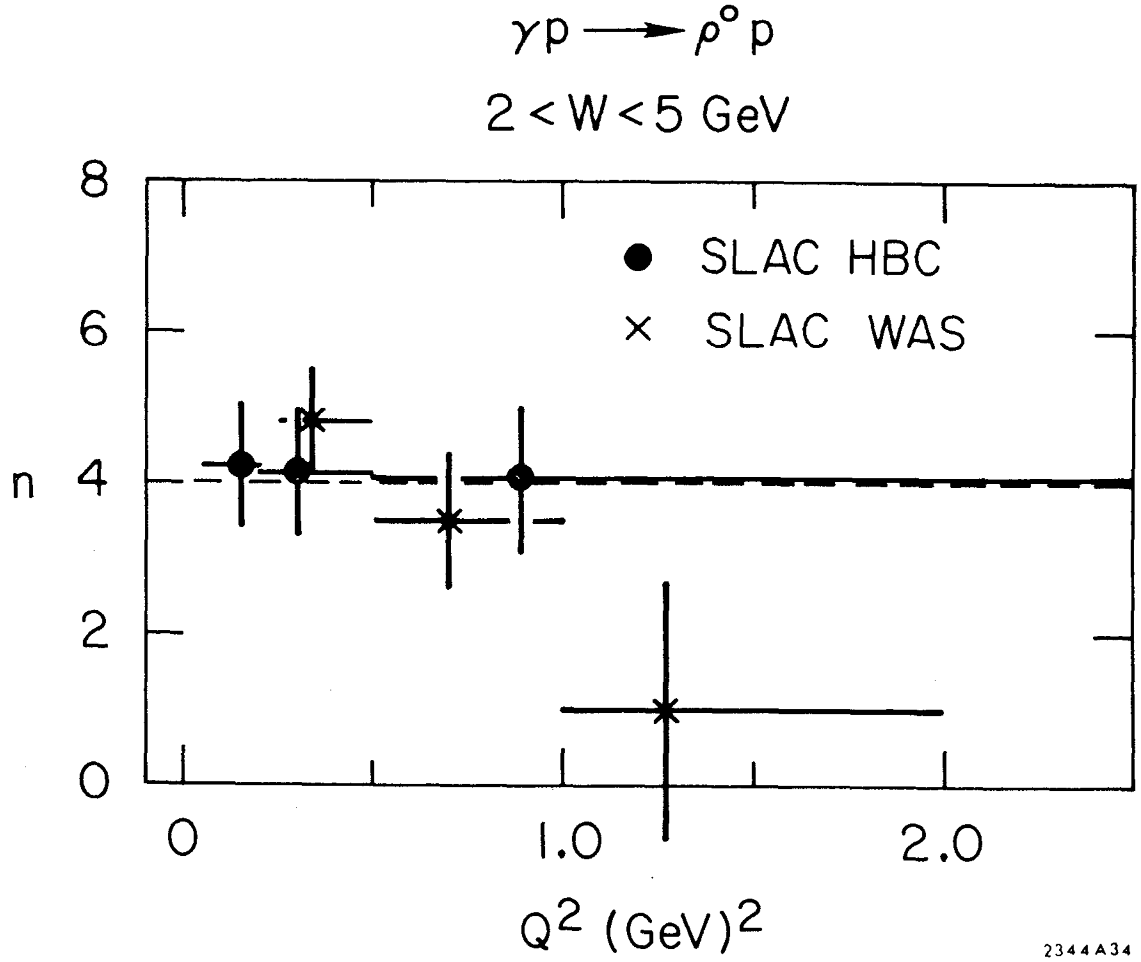

$\gamma p \longrightarrow \rho^\circ p$
2 < W < 5 GeV
SLAC HBC
SLAC WAS
n
8
6
4
2
0
0
1.0
2.0
Q^2 (GeV)^2
2344A34

Fig. 39

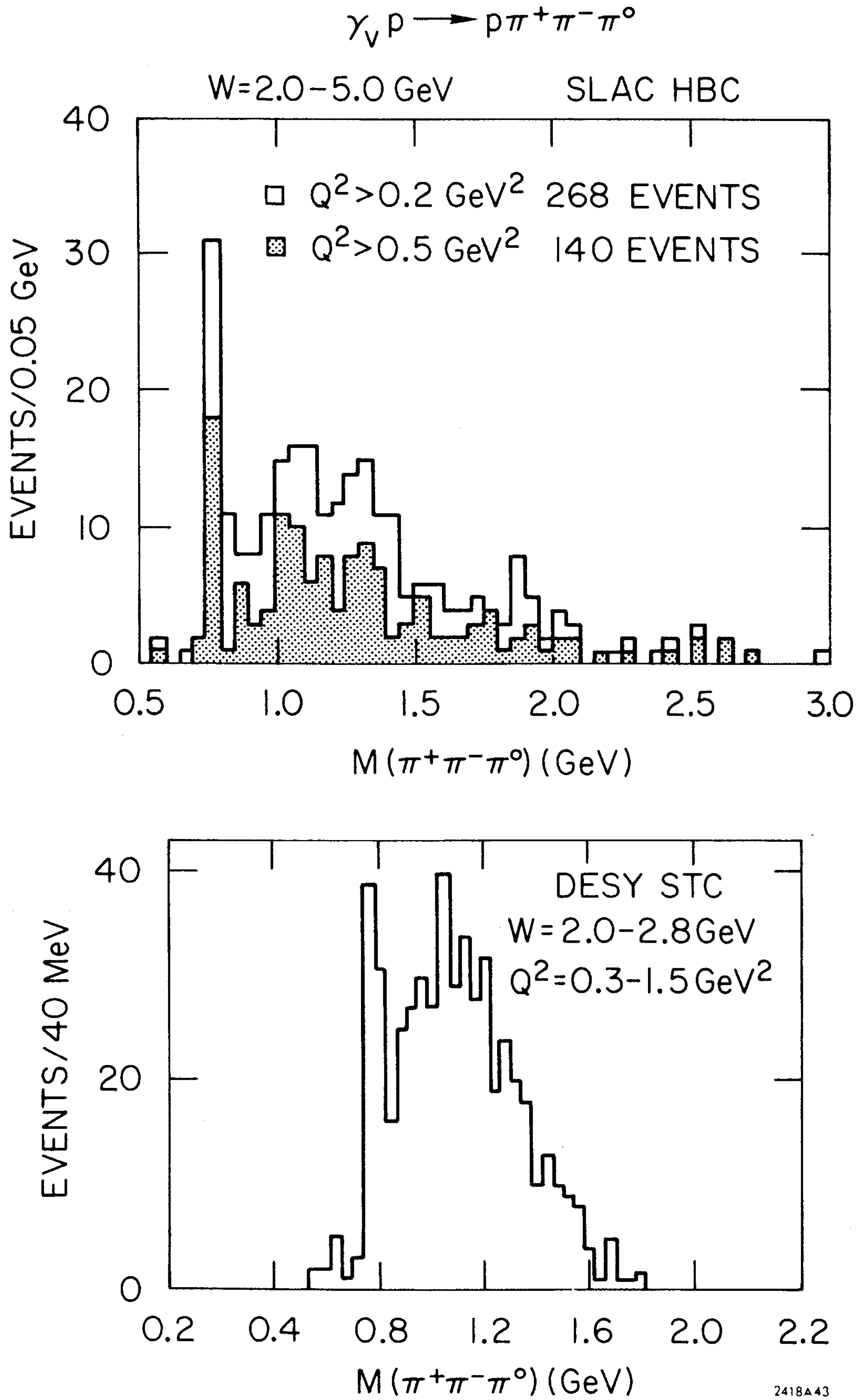
$\gamma_V p \longrightarrow p\pi^+\pi^-\pi^\circ$
W=2.0–5.0 GeV
SLAC HBC
$Q^2 > 0.2\ GeV^2$ 268 EVENTS
$Q^2 > 0.5\ GeV^2$ 140 EVENTS
EVENTS/0.05 GeV
0
10
20
30
40
0.5
1.0
1.5
2.0
2.5
3.0
$M(\pi^+\pi^-\pi^\circ)$ (GeV)
DESY STC
W=2.0–2.8 GeV
Q^2=0.3–1.5 GeV^2
EVENTS/40 MeV
0
20
40
0.2
0.4
0.8
1.2
1.6
2.0
2.2
$M(\pi^+\pi^-\pi^\circ)$ (GeV)
2418A43

Fig. 40

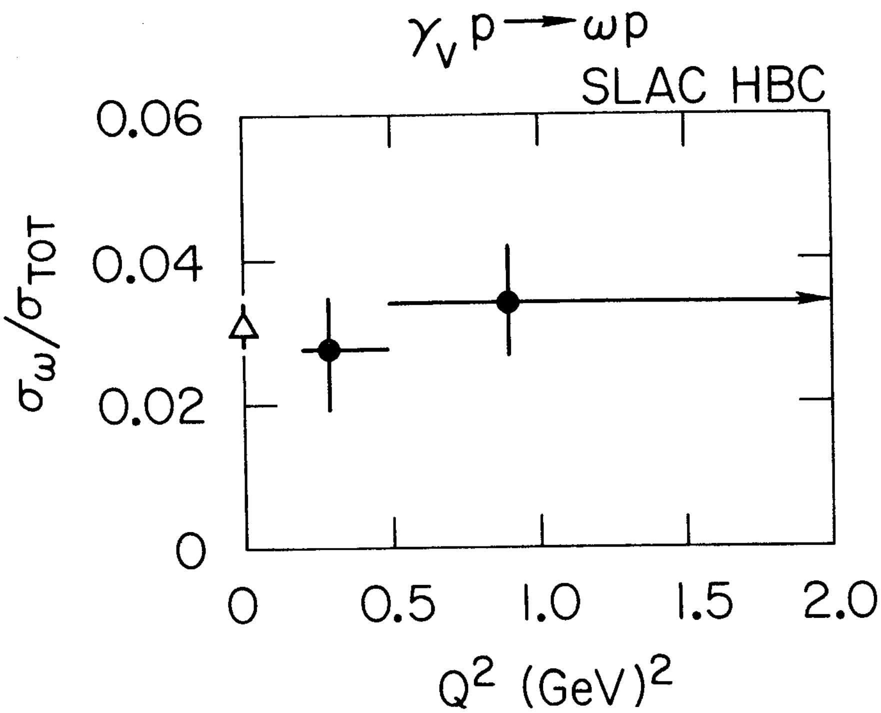

$\gamma_V p \to \omega p$
SLAC HBC
0.06
0.04
0.02
0
$\sigma_\omega/\sigma_{TOT}$
0
0.5
1.0
1.5
2.0
Q^2 (GeV)^2

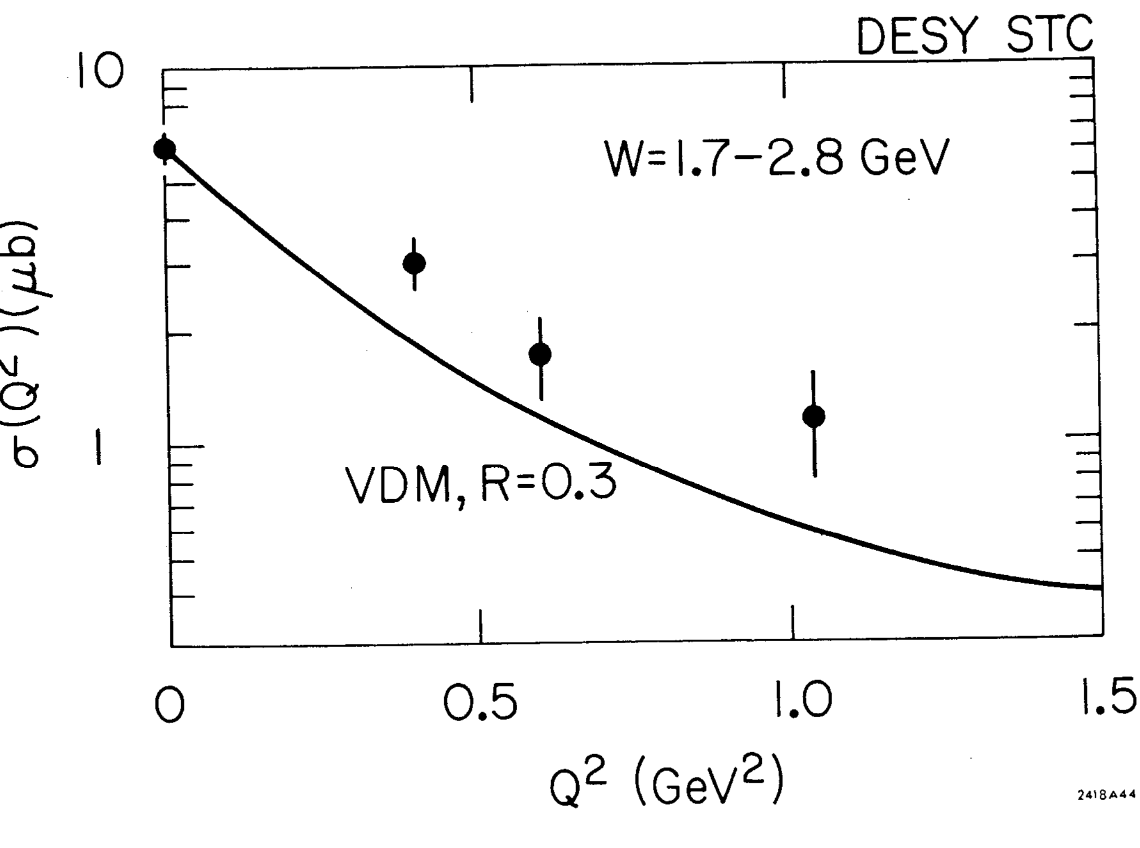

DESY STC
10
1
W=1.7–2.8 GeV
VDM, R=0.3
$\sigma(Q^2)(\mu b)$
0
0.5
1.0
1.5
Q^2 (GeV^2)
2418A44

Fig. 41